VOLUME III

FATIGUE TESTS AND STRAIN MEASUREMENTS ON GRID DECKS

by

Karl H. Klippstein, P.E.

Department of Civil Engineering
University of Pittsburgh

1993

for

Western Pennsylvania Advanced Technology Center

and

IKG Industries

ACKNOWLEDGEMENTS

Most valuable input and cooperation of several colleagues and co-workers have contributed significantly to the successful completion of Phase III of the project described in this report.

Dr. C. P. Mangelsdorf provided the necessary continuity between the static-test studies conducted mainly by him during previous phases and the fatigue study under Phase III. Assisted through special efforts by technician R. E. Bartlett, Dr. Mangelsdorf painstakenly assembled the hydraulic portions of the test setup and persistently kept them going despite many unexpected equipment problems that always seem to occur during fatigue testing.

Student J. J. Ream and technician R. E. Bartlett also extended strenuous efforts to assist in putting up the structural test setup. Both contributed vitally supportive late-hour and week-end efforts to keep the tests going and to collect the valuable data recorded in this report. The extra-ordinary cooperation of Technician Supervisor F. L. Kowatch to support these efforts is also gratefully acknowledged.

Dr. A. K. Ahmadi provided very valuable input for the determination of work related to test planning and evaluation. Dr. Ahmadi also conducted the finite element analysis of the Test #3 specimen.

The relentless cooperative efforts by D. R. Jurkovic of co-sponsor IKG Industries are especially noteworthy. His labors for financial support, coverage of unexpected expenditures, and assistance in providing technical support and input were vital to all accomplishments reported.

TABLE OF CONTENTS

TABLE OF CONTENTS, continued

STATIC AND FATIGUE STRENGTH DETERMINATION OF DESIGN PROPERTIES FOR GRID BRIDGE DECKS

VOLUME III - FATIGUE TESTS AND STRAIN MEASUREMENTS ON GRID DECKS

1.0 INTRODUCTION

Volume III is part of a project that was conceived to develop the static and fatigue strength properties of open or concrete-filled steel grid bridge deck. The project was jointly funded by the Ben Franklin Partnerships (Commonwealth of Pennsylvania) as represented by the Western Pennsylvania Technology Center of Pittsburgh, Pennsylvania (BF); by IKG Industries of Cheswick, Pennsylvania (IKG); and the University of Pittsburgh (UoP). The project was initiated 1 March 1989 and, so far, was carried through three phases. An additional phase is intended.

1.1 Phase I - March 1, 1989 - August 31, 1989

During Phase I of the project the theoretical basis for the orthotropic action of the panels was formulated, the testing strategy for the static tests was developed, and the test setup was designed. The objective for the static tests was to determine the physical constants suitable for computer evaluation of the panel performances under service conditions. The chosen test specimens consisted of 10 square panels which were 7'-8" on each side.

Efforts extended during Phase I were recorded in quarterly progress reports. In addition, some of the works and findings of this phase were also documented in the report issued under Phase II.

1.2 Phase II - September 1, 1989 - December 31, 1990

During Phase II, orders were placed for the test frame components, for the chosen test panels, and for some additional equipment required for the static tests. In January of 1990 the first components were received and the assembly of the test setup began. The test frame was completed in March of 1990. Static testing commenced immediately on the unfilled grid specimens (without concrete in the interstices).

Testing the different geometries for the open panels included up to five different test conditions for each test panel. A uniformly distributed line load along the mid-span was used with the panel spanning in the parallel and transverse direction to the main bars. These loads were applied with the test panels in their regular and in their upside-down position. The fifth condition consisted of a concentrated corner-point load and supports at the remaining three corners to produce twisting.

The results of the Phase and Phase II efforts were included in two previous reports.[1,2*]

1.3 Phase III - September 1, 1991 - December 31, 1992

The objectives for Phase III were to supplement the static properties developed in Phase I and II with fatigue design information on three concrete filled steel grid decks. Although current field performance of open and concrete filled deck does not suggest that there are imminent fatigue problems when the steel grid is designed in accordance with current industry and AASHTO design provisions[3,4], it was felt vitally important to develop such information in case the AASHTO design specifications would be relaxed and more liberal provisions would allow increased spans that would result in higher stresses. Therefore, it was planned to conduct fatigue tests of three grid decks with the objective to obtain more knowledge about the behavior of steel grid decks under controlled fatigue conditions, and what current fatigue design provisions should be used under various traffic volume conditions. To develop such information, and try to simulate the actual field conditions as much as possible, it was agreed to use steel grid deck specimens that were approximately 6'-6" wide and 20 foot long such that they could be fatigue tested at UoP's U-PARC (University of Pittsburgh Applied Research Center) facilities under positive and negative moment conditions.

Other objectives were to utilize the findings of the Phase I and II efforts and to verify their application to the static conditions encountered during the research process of Phase III. It was intended to document the findings such that they could be used in

---

* See References

the future for an improved prediction of the stress distribution within concrete-filled steel-grid bridge-deck assemblies.

The results of these efforts are described in this report, which mainly covers the Phase III efforts. In its conclusions, this report draws on the findings of the Phase I and Phase II reports.

1.4 Potential Phase IV Study

It is intended to conduct a Phase IV study under Ben Franklin sponsorship. A proposal has been drafted to test a least two more full-size panels and to open up some of the fatigue cracks developed under the Phase III efforts to determine the crack initiation sites in the main longitudinal steel bars. This will provide the opportunity for possible improvements of the present designs.

Also, a proposal has been drafted to test small-scale specimens (2 by 8 feet) with and without concrete fill to determine the applicable fatigue categories and demonstrate geometrical improvements resulting in better fatigue categories. It is anticipated that either the National Science Foundation or the Bridge Grid Flooring Manufacturers Association will sponsor such efforts.

2.0 TEST SETUPS

An erector-type steel frame was used to conduct the three fatigue tests described in this report. The frame was previously donated to UoP by the United States Steel Division, a subsidiary of USX Corporation, and is now located at U-PARC in Harmarville, Pennsylvania, approximately 12 miles east of the main university campus.

All main features of the steel frame are shown in Figure 1. As seen from the figure, main cross frames that support hydraulic loading jacks may be arranged at 6-inch increments anywhere along the length of the test frame. Also, three reaction beams may be located similarly. The elevation of the hydraulic actuators (jacks) and load cells is also adjustable in increments.

The test frame provides a self-contained closed-loop system that is supported by the concrete floor of the test building without any attachment to the floor, or any special foundation. Individual test setup arrangements for the three fatigue tests are

described in detail in Appendix A, B, and C, for Test #1, #2, and #3, respectively. All loads applied had a stationary position which is not as critical for the entire deck as a moving load that may traverse a bridge deck in the field, however it is considered equally critical for the main longitudinal bar below the applied loads.

Load setups and constant-amplitude fatigue-load ranges for Test #1, #2, and #3 are summarized in elevations shown in Figure 2. The load setup and the chosen load range for Test #1 was totally arbitrary. It had nothing to do with actual field conditions but was merely chosen to provide a check on the hydraulic functioning of the system with the additional benefit of obtaining fatigue test data for the stress-vs-cycle (log S-N) plots. Since actual truck and trailer axles were used for Test #2 and Test #3, the load setups and load ranges used for these tests were more closely related to actual field conditions.

3.0 SPECIMEN DETAILS

Of the many configurations of steel bridge decks available, the four of six basic types of deck systems represented in Figure 3 were chosen for static tests described in the Phase I and II reports of this project. However, only deck types (a) and (d) shown in Figure 2 (4-1/4 Inch Interlock and ArmaDek 3 Inch T decks) were selected for the three fatigue tests described in this report.

Details of each of the three specimens tested (Test #1, #2, and #3) are given in the respective appendices (Appendix A, B, and C). This includes main bar spacings, cross bar sizes and spacings, reinforcing bar sizes and spacings, etc. All steel deck material conformed to ASTM A588 with a minimum yield point of 50 ksi.

As seen from Figure 3 and from the associated figures in the appendices, the specimens included punch-outs in the web of the major steel bars, tack welds that connected some main bars with cross bars at the top surface of their intersections, and tack welds that connected concrete form pans to the bottom flange of the main steel bars. Detailed geometrical parameters for the web punch-outs in the main bar may be obtained directly from the manufacturer (IKG) and/or from the descriptive product literature available.[3]

All concrete used in the test specimens was ordered to conform with PennDot's specifications, i.e. PennDot Mix AAA, having a minimum specified strength of 4,500 psi. Slump tests and compressive strength tests conducted on each batch of concrete delivered indicated that all mechanical requirements were met, as described in the relevant appendices for the described tests.

4.0 TEST PROCEDURES AND DATA ACQUISITION

Discussions provided in Appendix A, B, and C enumerate the details of the test procedures and data acquisition efforts conducted for each of the three tests described. In general, static calibration tests were made prior to the commencement of the fatigue tests, as well as at many opportune intermittent times during the fatigue tests.

Often, the fatigue tests were interrupted and stalled by equipment problems, as so frequently is the case with fatigue studies. However, the most important details that highlight the test and data acquisition procedures are contained in the tables and figures of the appendices. Additional details are available and could be furnished upon request if deemed important for future investigations.

As described in Appendix A, the loads for the first fatigue test were applied by two hydraulic actuators through 2-inch-thick steel plates, below which were located 1/2-inch-thick rubber conveyor-belt pads. For the second and third test, a truck and a trailer axle was used to introduce a single actuator load through one of the spring-leaf brackets into the wheels of the axle assembly, and through the wheels into the deck.

For all tests, an O. I. Rhiele console and pulsator (pump) were connected to appropriate hydraulic actuators. The minimum and maximum actuator loads differed for each test to produce the desired stress ranges.

The first axle used for Test #2 was a rear truck axle, which soon developed a crack within the differential housing at an approximate cycle count of 500,000. A trailer axle without a differential housing was then used as a replacement for this and the subsequent testing process. At the same time, a lower-capacity 40-kip actuator was installed to replace the previously used 80 kip actuator. The lower-capacity actuator had a smaller diameter and did not interfere with the side of the tires. However, most

importantly, its smaller diameter required less oil displacement per inch of deflection and accelerated the speed of testing. Thus, the test speed of 2 cycles per second could be maintained even though the total deflection was much greater than for Test #1.

Dial gages were used below the deck at both mid-spans. The type and location of the strain and dial gages employed are summarized in the appropriate tables of the appendices. The strain gage locations are also shown in the appropriate appendix figures.

5.0 STATIC AND FATIGUE TEST RESULTS

Detailed results of the strain gage and deflection data, and of the concrete and steel bar cracks, are made in the appendices that describe the results of each test made in detail. Also, for each test conducted, a S-N fatigue comparison is made with the 1991 AASHTO[4] fatigue provisions. The results contained in Figure A-12 of Appendix A, Figure B-14 of Appendix B, and Figure C-33 of Appendix C for Test #1, #2, and #3, respectively, are summarized in Figure 4.

As seen from Figure 4, squares were used to plot the fatigue results for Test #1, i.e. the number of fatigue cycles versus the effective stress range that was measured at the commencement of the fatigue test. Similarly, diamonds were used for Test #2, and right-pointed triangles were used for Test #3. At a given effective stress range these symbols enhance a range of fatigue cycles depicted by a horizontal bar. The symbol at the left end of the bars indicates the number of cycles at which the first fatigue crack was observed in one of the major longitudinal steel bars of the deck specimen. The symbols at the right end of the horizontal bars, with an arrow pointed upward and to the right, indicate the number of fatigue cycles at which the test was discontinued.

Also shown are the 1991 AASHTO fatigue design curves for the various fatigue fabrication details covered by the specification. This provides a comparison of the fatigue tests with currently categorized fabrication details. As seen from the figure, and as described in detail in the appendices, the fabrication details encountered within the steel decks tested are considered to classify as Category C and B' details but could

possibly be upgraded. A summary of the findings is provided under the conclusions described below.

6.0 FINITE ELEMENT ANALYSIS FOR TEST #3

One of the most formidable tasks of this research project was to determine the load/moment/strain/stress/deflection relationships for the concrete-filled steel-grid specimens investigated, and especially for the specimens with a concrete overfill. For all tests, analytical correlations with the test results were attempted by hand and/or finite-difference analysis. Although the finite difference calculations provided considerably improved correlations with the test results, it was felt by all co-investigators that a finite element analysis (FEA) should also be performed. The deck properties of the specimen utilized in fatigue Test #3 were used to conduct the finite element analysis.

A detailed description of the assumptions and results of the FEA are provided in Appendix D of this report. As seen from this appendix, the deck was modeled in three different ways and compared with statically derived test results. The basic model details and assumptions were as follows:

(1) using an isotropic model with constant plate thickness,

(2) use of an isotropic model with varying plate thickness,

(3) utilizing an orthotropic model with plate stiffness parameters derived from previous phases of this study.

As the results in Appendix D indicate, the first way of modeling the deck provided the least correlation between the analytical stress analysis and the stresses resulting from the test data. That is, the stress or correlation ratios (analytical divided by test values of stresses) at significant locations of the test specimens ranged from 0.16 to 2.74. The best correlation was achieved by utilizing the second model.

An attempt was also made in Appendix D (Section D-6) to utilize and modify the test results so that the actual neutral axes could be determined and more realistic section moduli could then be used for the stress determination. This attempt resulted in the stress correlation values presented in Table D-2 of this report with stress

correlation values that ranged from 0.93 through 1.53. The results show that the stress correlation is much better than directly obtained from the FEA analysis. However, if further studies could be made, it is anticipated that the most precise stress conditions necessary for the fatigue life determination could be predicted if the neutral axis, or the effective section moduli in the positive and negative bending moment regions, were established by tests.

In retrospect, and based on the evidence collected, any attempts to represent the concrete-filled deck as a single material and using the finite-element (or finite difference) results to calculate stresses from moments is doomed to failure. Recent research evidence obtained by Dr. C. P. Mangelsdorf, and soon to be published, suggests that significant membrane stresses are generated under the concentrated load, which would normally be insignificant in small deflection theory. These membrane stresses alter the stress intensities and affect the resulting fatigue-initiation and fatigue-propagation lives, significantly.

Also, neither the hand, spread sheet, finite difference, or FEA calculation approaches utilized did adequately predict the actual stress conditions in the steel grid or concrete for the chosen test setups. Even more difficulties are expected for actual field conditions when wheel loads move across the deck, or environmental effects causing re-bonding between steel and concrete. Also, partial fixity at girders or stringers caused by welds between their top flanges and the steel deck, and the use of welded studs, provide stress effects in the steel grid which presently are not accounted for. A future study is recommended to not only predict the extreme conditions, as essentially done by using the current AASHTO provisions , but also allow for load conditions that may not represent the extreme loading conditions such as those used in the three tests described in this report.

7.0 FORMATION OF ADVISORY PANEL AND PROMOTIONAL ACTIONS

Eighteen renown engineering experts were contacted and asked if they would volunteer to review the progress of this project as conducted so far, make comments on the past efforts, and provide input on the remaining and future work. Following

is a list of experts who were contacted, some of whom responding positively, as noted by an asterisk:

Victor Bertolini, P.E., SAI Consulting Engineers
Jim Cooper, P.E., FHWA
Tom Dugan, P.E., Middle States Steel Construction
John Gilligan, P.E., Consultant*
John (Fred) Graham, P.E., Allegheny County*
Geerhard Haaijer, Ph.D., P.E., AISC
Art Hedgren, Ph.D., P.E., HDR - Richardson/Gordon*
Herbert Higgenbotham II, P.E., Allegheny County*
John Kulicki, Ph.D., P.E., Modjeski & Masters
Bob Nickerson, P.E., AISI/FHWA*
Henry Nutbrown, P.E., PENN-DOT
Dean Palmer, P.E., Richland Engineering*
Mehandra Patel, P.E., PENN-DOT*
Chuck Schilling, P.E., Structural Engineer
Chuck Schubert, P.E., Michael Baker Corporation
William Williams, P.E., FHWA - Penna Division
William Wright, P.E., FHWA
Chris S.C. Yiu, P.E., Steinman Engineering

A copy of this report will be forwarded to the advisory panel members for their review and comments. Also, a copy of the proposal for Phase VI will be forwarded to them for their comments.

Because of the budget cuts explained above, the traveling budget included in the original proposal for this phase of the project was eliminated. Therefore, the activities of the advisory members will be conducted by correspondence only, and travels by the investigators for intended presentations of the results will not be possible.

8.0 CONCLUSIONS AND RECOMMENDATIONS

Detailed conclusions and recommendations derived from the three fatigue tests conducted under Phase III of this study are enumerated in Appendix A, B, and C. Similarly, detailed conclusions and recommendations for the finite element analyses attempts conducted to determine design stresses are contained in Appendix D. Briefly, these and other conclusions and recommendations are summarized as follows.

* Although no fatigue failures of open or concrete-filled steel-grid bridge deck have come to the attention of the principal investigator, three full-scale fatigue tests were conducted to provide a better insight for future fatigue considerations and possible AASHTO fatigue design provisions.
* Neither hand, spread sheet, finite difference, or FEA calculation approaches utilized could adequately predict the actual stress conditions in the steel grid or concrete for the chosen test setups. Even more difficulties are expected for actual field conditions when wheel loads move across the deck or when environmental effects cause re-bonding between steel and concrete. Also, partial fixity at girders or stringers caused by welds between their top flanges and the steel deck, and the use of welded studs, provide stress effects in the steel grid which presently are not accounted for. A future study specifically addressing this conditions is recommended.
* The fatigue design of IKG's 4-1/4 Inch Interlock grid deck, with 6- or 8-inch main bar spacing, filled with concrete, including an overfill of 1-5/8 inch as manufactured in accordance with IKG's material specifications, is recommended to be conducted by utilizing the 1991 AASHTO fatigue design provisions for redundant load structures conditions defined in Table 10.3.1A under Category C for positive and negative moments.
* The fatigue design of IKG's ArmaDek 3 Inch T grid deck, filled flush with concrete as specified and manufactured in accordance with IKG's specifications, is recommended to be conducted by utilizing the 1991 AASHTO fatigue design provisions for redundant load structures conditions defined in Table 10.3.1A under Category B' for positive and negative moments. Since no cracks were found in the negative bending moment region when the fatigue test was terminated, the deck has the potential of being upgraded to Category B for negative bending. This would have to be confirmed by proposed small-scale tests.

* Fatigue crack initiation sites of the three specimens tested should be investigated in a future study to find out what manufacturing detail is critical, i.e. where in the steel bars the crack initiation occurred. A proposal for such work is under preparation and will be submitted to Ben Franklin in the near future.
* The IKG 4-1/4 Inch Interlock grid deck and the IKG ArmaDek 3 Inch T grid deck could probably qualify for Category B if the tack welds could be eliminated in critical moment and stress regions.
* The fatigue design of concrete-filled steel-grid bridge decks, with or without overfill, is recommended to be based on the nominal stresses derived from the use of section properties that result from the current AASHTO specification transformed area method until more representative long-term design parameters or procedures are established. Such procedures may result in non-linear log-log S-N curves and render the above-mentioned procedures overconservative.
* Further small-scale fatigue tests of this type of floor deck are recommended, without concrete fill. A proposal has been prepared and submitted to NSF but funding was not yet obtained.
* Further full-scale fatigue tests of other types of floor deck are recommended. A proposal to Ben Franklin is in preparation and will be submitted, soon.
* An Advisory Panel has been established. Members will be consulted on further testing details if further work is sponsored and prior to when testing details will be finalized.
* Because of budget cuts an intended meeting of the advisory panel members had to be scratched. If the proposed Phase IV of the project is sponsored, interaction with advisory panel members will most likely be conducted by correspondence only.
* For the same reason, intended travels for possible presentations of the results at engineering conferences could not be conducted.

9.0 REFERENCES

1. Baker, Tod H., "Static And Fatigue Strength Determination Of Design Properties For Grid Bridge Decks, Volume I - Plate Stiffness Constants For Concrete Filled Steel Grid Decks," Research Report ST-9, August 1991, Department of Civil Engineering, University of Pittsburgh,

2. Mangelsdorf, C. P., "Static And Fatigue Strength Determination Of Design Properties For Grid Bridge Decks, Volume II - Plate Stiffness Summary And Strain Measurements On Grid Decks," Research Report ST-10, December 1991, Department of Civil Engineering, University of Pittsburgh.

3. "Bridge Flooring Systems," IKG Greulich, R.D. 2, Route 910, Cheswick, Pennsylvania 15024.

4. American Association of State Highway and Transportation Officials (AASHTO), STANDARD SPECIFICATION FOR HIGHWAY BRIDGES, Washington, D.C., Interim Specification, 1991.

Table 1 - Summary Of Fatigue Data

Test #	Deck Description[1]	Stress[2] Range, ksi[2]	Location	No. Of Cycles	
				First[3]	Disc.[4]
1	**4-1/4 Inch Interlock,**	21.0	East Span	557,200	900,000
	6" main bar spacing,	18.7	Center Sup.	n.o.[5]	900,000
	1-5/8" concrete overfill,	18.0	West Span	801,800	900,000
	3/4" max. gravel size				
2	**ArmaDek 3 Inch T,**	13.1	West Span	4,562,300	6,024,010
	no concrete overfill,	11.0	Center Sup.	(none)	6,024,010
	3/8" max. gravel size				
3	**4-1/4 Inch Interlock,**	10.5	West Span	3,590,050	5,350,000
	8" main bar spacing,	9.3	Center Sup.	n.o.[5]	5,350,000
	1-5/8" concrete overfill,				
	3/4" max. gravel size				

Notes:

1. All steel grid material conformed to ASTM A588, with a specified minimum yield point of 50 ksi. Concrete was specified to PennDot Mix AAA, with minimum ultimate strength of 4,500 psi.

2. Stresses at beginning of fatigue test. Initial load settings were maintained throughout the tests although local stress levels changed due to cracks in concrete and steel.

3. Number of applied load cycles after which the first crack in steel bars was observed, as indicated in the respective tables of Appendix A, B, and C providing highlight of inspection recordings.

4. Number of applied load cycles after which the respective tests were discontinued.

5. n.o. = not observable

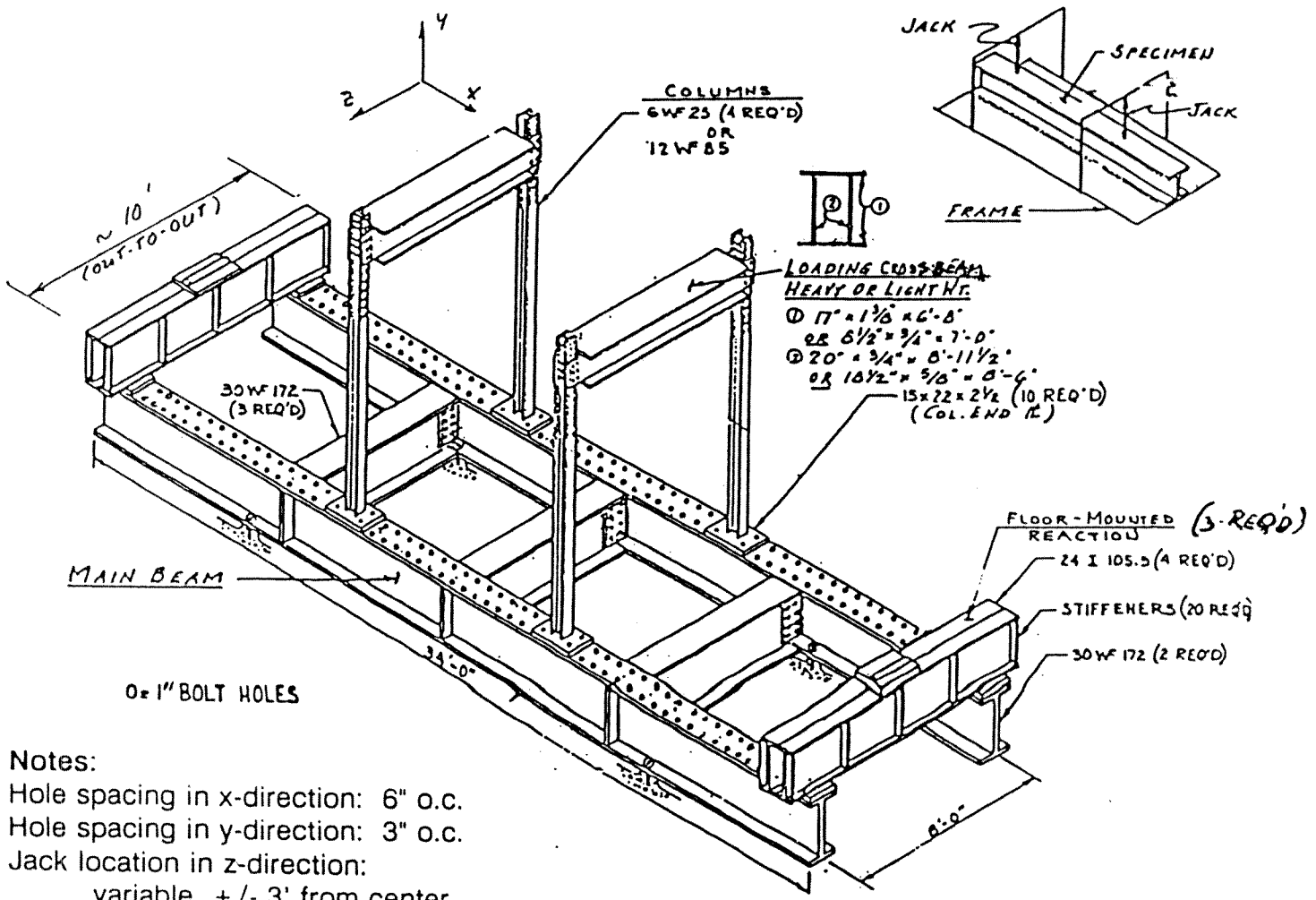

Fig. 1 - Structural Loading Frame

Notes:
Hole spacing in x-direction: 6" o.c.
Hole spacing in y-direction: 3" o.c.
Jack location in z-direction:
variable, +/- 3' from center

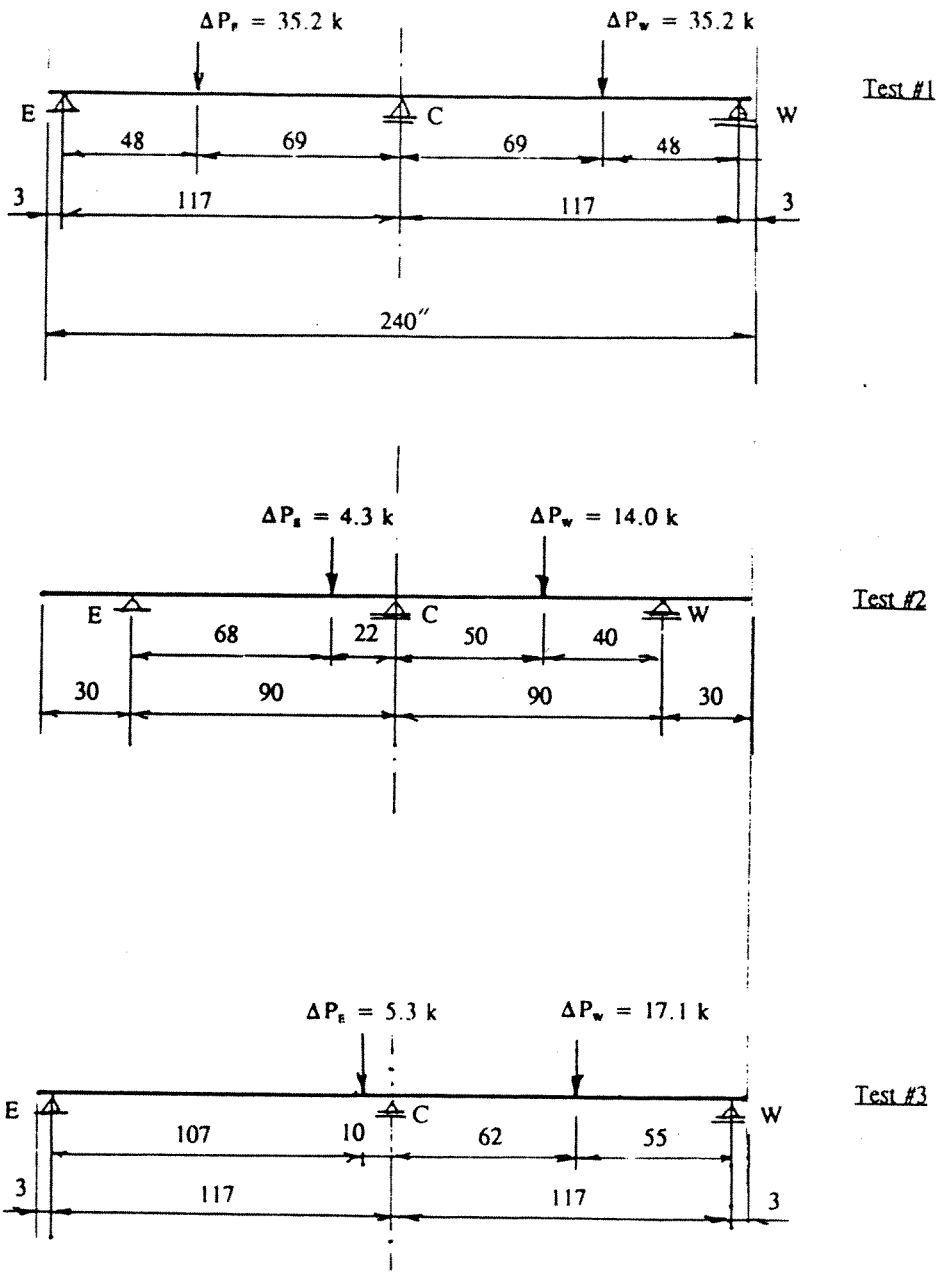

Fig. 2 - Test Setups And Fatigue-Load Ranges For Test #1, #2, And #3

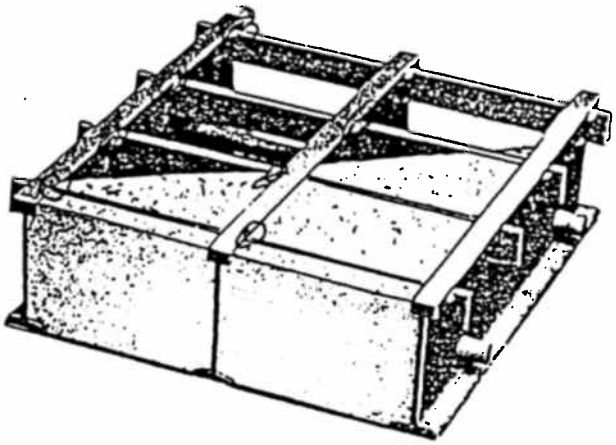

(a) 4-1/4 Inch Interlock

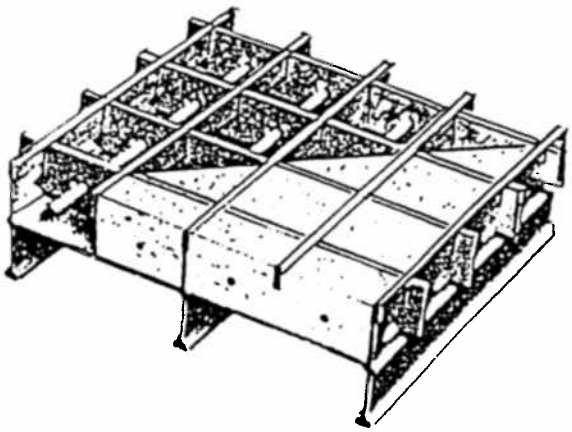

b) 5 Inch RB/Half Depth
(Full Depth not shown)

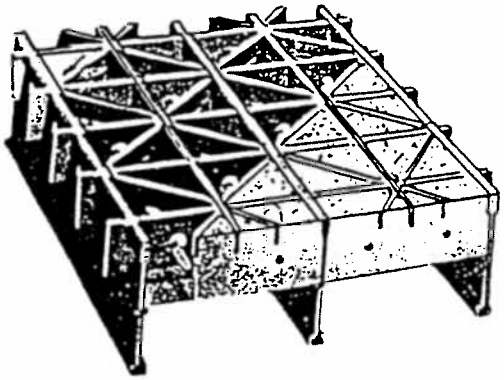

(c) 5 Inch Four Way/Half Depth

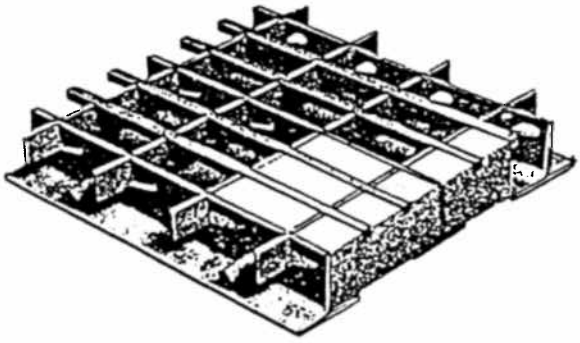

(d) ArmaDeck 3 Inch T

Fig. 3 - Grid Decks Considered For Static And Fatigue Tests

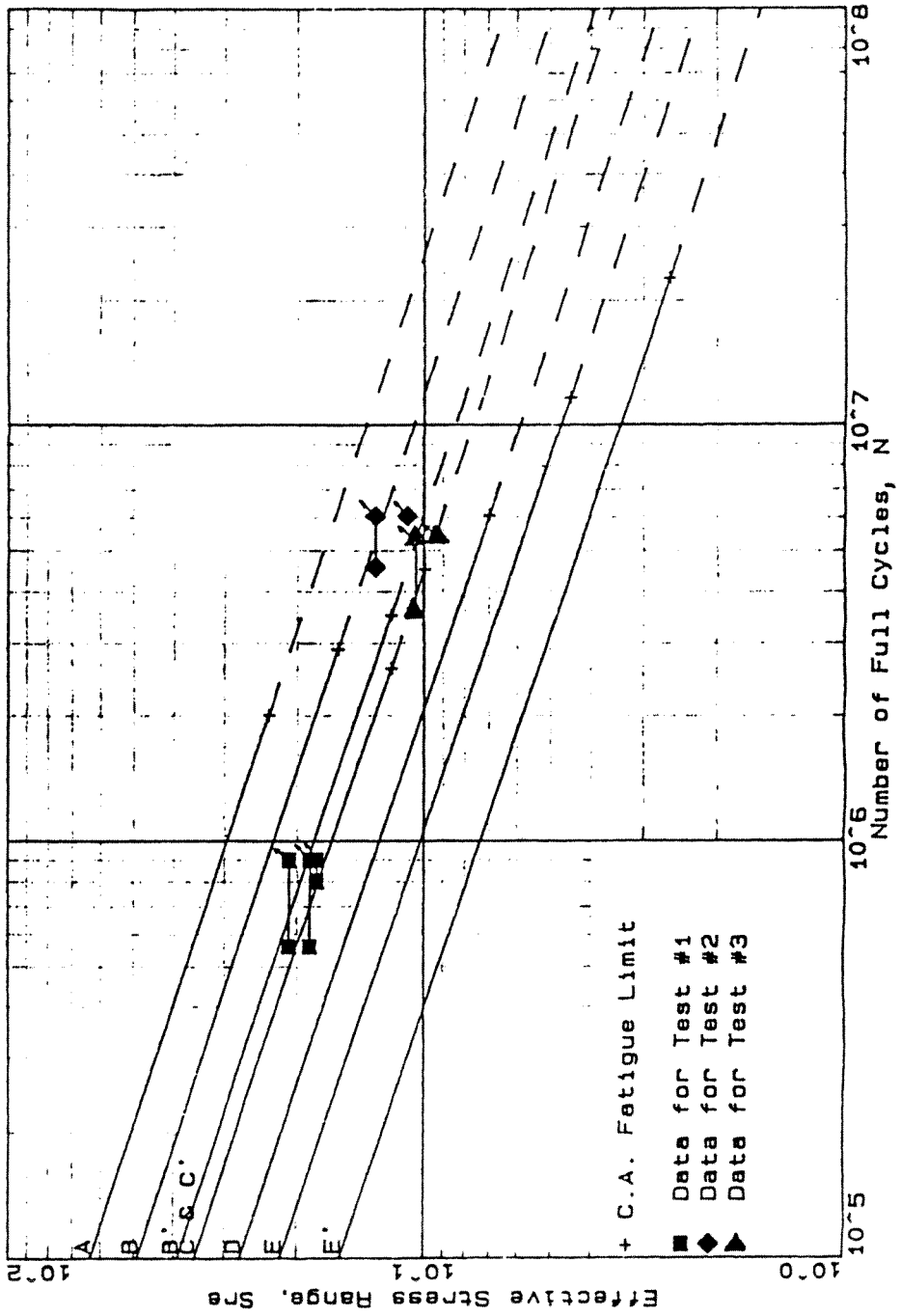

Fig. 4 - Fatigue Endurance Of Main Steel Bars For All Tests Compared With 1991 AASHTO Fatigue Categories

APPENDIX A - FATIGUE TEST #1

A-1 OBJECTIVES

For Test #1, IKG's most economical and most applied steel-grid bridge flooring system was chosen, i.e. a 4-1/4 Inch Interlock grid deck with a 1-5/8-inch concrete overfill. The material selection, spans and load locations for this test were chosen with the objective that the tensile stresses in the bottom fiber of the main steel bars below the applied concentrated loads were approximately the same as the tensile stresses in the top fiber of the main steel bars above the interior support of the two-span continuous slab setup. Specifically, the span and load conditions were chosen because it was not apparent at that time whether or not the weldments at the top of the steel grid (main and transverse bar connections), or at the bottom (tack welds connecting form pans to bottom flange of main bars), would represent the most critical fatigue details under positive versus negative bending moment conditions, respectively.

Secondary objectives for Test #1 were to verify the performance of the test system, including the possible speed of testing for the chosen hydraulic and structural test set-up and details. This information was deemed very important for the planning and timing of future tests.

A-2 TEST SETUP

A longitudinal cross section of the test frame and the test specimen along the center plane of the setup is shown in Figure A-1. The support and load arrangements are symmetrical to this plane and about the center support (except for the 34-foot-long beams of the test frame. An end view of the test setup is shown in Figure A-2. Further details of the load and support conditions are shown in Figure A-3. Also, general strain gage and crack locations are shown in Figure A-3. Specific types of strain gages (steel & concrete) and their locations are described in Table A-1.

The load transfer from the actuators to the specimen was accommodated through 12-by-12-inch steel bearing plates, 2 inches thick. The plates are shown in the Plan

View and the Elevation of Figure A-3. As seen from Figure A-3, the centers of the bearing plates were located 69 inches from the center support within a span of 9'-9" (or 69 + 48 = 117 in.), and along the longitudinal centerline of the specimen and the test frame. Dial gages were used below each load point, marked East and West for the corresponding spans. (In all plan views and elevations the east span is shown to the left.) The type and location of the strain and dial gages employed are summarized in Table A-1. Strain gage locations are also identified in Figure A-3.

A-3 ADDITIONAL SPECIMEN DETAILS

General physical and geometric details of the Test #1 specimen are shown in Figures A-3 and A-4 and are generally described in the main body of this report. The main bar spacing of the steel grid was 6 inches.

The concrete mix contained crushed rock gravel while the other specimens used river bed gravel. The maximum gravel size was 3/4 inch. While pouring the concrete, a slump of approximately 1 inch was measured. The average concrete strength after 42 days of curing, based on two 3-inch-diameter samples, was 4,591 psi, which meets the minimum strength requirements of 4,500 psi specified.

A-4 TEST PROCEDURE AND DATA ACQUISITION

The chosen load arrangement for this test was intended to provide approximately equal tensile stress ranges in the bottom fiber of the main steel bars below the applied concentrated loads and in the top fiber of the main steel bars above the center support. To monitor the response of the setup static load tests were made at the beginning of the test, and twice after the fatigue process had been initiated. During such static tests, recordings were made of all strain gages and dial gages. The loads were incremented from zero to a maximum of 41.7 kips in six steps.

At several occasions during the fatigue testing process, the test setup and test specimen were inspected. Detailed recordings were made of date, time, cycle count, and inspector. The inspection included the equipment (oscilloscope settings, oil

temperature, alignment, tie-downs, etc.) and the specimen (cracks in the main steel bars and in the concrete overfill near the center support).

A-5 RESULTS

The results of the static-load tests made at the beginning and during the testing process are displayed in strain-versus-load and deflection-versus-load graphs, Figures A-5 through A-10, and Figure A-11, respectively. The fatigue life (number of cycles versus stress range) is summarized in a log-log S-N graph, Figure A-12.

The strain-gage types and locations, and the dial gage locations, are described in detail in Table A-1. Highlights of the inspection recordings are given in Table A-2. This table also provides a record of the number of cycles at which fatigue cracks were observed in the various steel bars. The location of the cracks is also denoted in Figure A-3.

The speed of testing was approximately 2 cycles per second. More details are discussed below.

A-5.1 Strain-Gage Data

A static-test strain-load record made near the beginning of testing, after the static loads had been increased and decreased in the above-mentioned increments during four preceding load cycles (runs). The results for Run 5 are presented in Figure A-5. The plotted strain-vs-load traces for almost all gages are nearly linear, except for Gage 5, which is a concrete gage that was located at the center support, between main steel Bars 7 and 8, near the top of the steel grid elevation. Gage 12, which was attached to the top of the steel grid (main Bar 7) above the center support, showed the most significant non-linearity for the steel gages.

One of the original goals for Test #1 was to locate the hydraulic actuators such that the magnitude of the tensile stresses in the outer steel fibers of the steel grid within the positive and negative bending moments were approximately equal. The purpose was to find out which condition was more fatigue critical. As shown in Figure A-5, this goal was initially achieved. Steel strain Gages 11 and 15, spaced almost

symmetrically from the center support in the west and east span, respectively, and exposed to symmetrically applied loads, recorded strains that were nearly equal to each other (approximately within ± 7 percent of each other). Steel strain Gage 12, located above the center support, responded in the same direction (tension) and but recorded strains almost 40 percent higher in magnitude.

To more clearly identify the panel behavior during static test Run 5 in the west span, at the center support, and in the east span, the data shown in Figure A-5 were broken down into three respective graphs represented by Figures A-6, A-7, and A-8. For the west span, Figure A-6, concrete Gages 1, 2, and 3, as well as steel Gages 10 and 11 exhibited linear behavior. As seen from Figure A-7, concrete Gage 5 at the center support exhibited the least linear behavior, even though the fatigue loads had not yet been applied. Apparently, the gage readings reveal the fact that the concrete above the interior support had already cracked under the previously-applied static loads (4 runs). Figure A-7 also confirms that steel Gage 12 at the interior support already behaved in a non-linear fashion before the fatigue loads were applied. For the east span, Figure A-8, concrete Gages 7, 8, and 9, and steel Gages 14 and 15 behaved in a nearly linear fashion.

Similar to the data plotted in Figure A-5 for all gages at zero fatigue cycles, Figures A-9 and A-10 show the strain-versus-load relationship for all strain gages at 541,080 and 900,080 fatigue cycles, respectively. At 541,080 cycles (Figure A-9), concrete Gage 4 (at top surface above center support) did not function any more. Also, concrete Gages 5 and 12 showed irregular behavior. At 900,080 cycles (Figure A-10) Gages 4, 8, and 12 did not function any more, and Gages 5 and 7 showed irregular behavior.

Since the strain gages in the east and west span were not located directly below the loads where the fatigue cracking of the steel bars eventually became visible in the extreme bottom fibers of the main longitudinal bars, a manual inter-polation/extrapolation of the stresses was made so that the observed bar failures could be plotted against the number of cycles at which cracks were, or were not, observed.

This resulted in the stated stress ranges for the east span (21.0 ksi) and the west span (18.0 ksi) as stated in Figure A-12 and Table 1, and as used for the plot in Figure 3.

The reason for the difference in the stress ranges between the east and west spans can only be explained by possible initial unsymmetrical un-bonding between concrete and steel grid in the vicinity of the negative bending moment region straddling the center support. It is also possible that such unsymmetrical un-bonding may have occurred in the positive bending moment regions of the east and west spans. As noticed from the maximum readings for Gage 11 and 15 (west and east spans, respectively), the strains after 541,080 cycles (Figure A-9) had remained nearly the same as recorded prior to the commencement of the fatigue test process (Run 5, Figure A-5).

Similarly, it was determined that the nominal initial fatigue stress range at the center support as used in Figure A-12, in Table 1, and in Figure 3, was best represented by a nominal stress range of 18.7 ksi even though the initial strain readings prior to the commencement of the fatigue tests (Figure A-5) suggested a higher stress range. However, the reliability of Gage 12, as evidenced by Figure A-9, can not be taken for granted.

A-5.2 Deflection Data

As part of the static-load tests, deflections were measured below the loads in the east and west spans before the fatigue loading began, and after 541,080 and 900,080 load cycles were applied. The results are shown in Figure A-11.

As seen from Figure A-11, the deflections increased with increasing number of fatigue-load cycles applied. This is indicative of the cracking that occurred in the concrete above the interior support as well as the cracking of the main steel bars in the east and west spans, which reduced the stiffness of the test specimen and caused increased deflections.

The displacements of the hydraulic actuators exceeded 2 inches. This includes the deflection of the test specimen and the test frame and is a useful measure in determining the potential speed of testing because the oil supply is limited.

A-5.3 Concrete Cracks

The first concrete crack was observed shortly after the fatigue test was started. As expected, the crack occurred above the interior support at the maximum negative bending moment.

While the fatigue testing continued, additional cracks occurred nearly parallel and near to the interior support line. At 95,000 cycles, three cracks were observed across the full floor slab width, and two additional cracks partially across the floor slab. At 146,040 cycles five cracks were observed across the floor slab width, and two additional partial cracks were noted. At 801,000 cycles, seven cracks extended across the floor slab width.

The concrete cracks did not follow the grid pattern, i.e. they were not exactly parallel to the interior support. At the mid-width of the floor slab the cracks were generally closer to the center support than along the edges of the slab.

A-5.4 Steel Bar Cracks

The first cracks in the main steel bars were observed after 557,200 fatigue cycles in steel Bars 7 and 8 at the bottom fibers in the east span (see Figure A-3 and Table A-2) below the east concentrated load. After 801,000 cycles, similar cracks were also found in Bars 5, 6, and 9 of the east span, and in Bars 6, 7, 8, and 9 of the west span. At the termination of the test (~900,000 cycles) six main bars in the east span had fully cracked across the bottom flange (Bars 5, 6, 7, 8 ,9, and 10), and five bars in the west span (Bars 5, 6, 7, 8 and 9).

It is not known at this time how many bars have cracked at the center support. From the strain gage data it is obvious that at least Bar 7 has cracked. Work has been proposed which would include funds to remove a 6-inch-wide deck at the center support and below the loads, remove the concrete, and open up the main steel bar cracks to determine the crack initiation sites in the bars.

A-5.5 S-N Fatigue Comparison

The fatigue-crack observations contained in Table A-2 were used to compare the crack occurrences in the floor slab tested with the present (1991) AASHTO fatigue

design provisions. Both, the AASHTO fatigue design lines and the fatigue-crack observations are shown in Figure A-12.

Specifically, Figure A-12 shows the straight S-N curves (stress range versus number of full cycles to fatigue failure) for various fabrication categories, identified as A, B, B', C, C', D, E, and E'. The slope of these lines is -3.0, as commonly accepted for welded fabrication details. The intercept of these lines was obtained from a regression analysis that utilized the data contained in AASHTO Specification Table 10.3.1A for the allowable fatigue stress ranges in redundant load path structures.

The solid lines in Figure A-12 represent the lower 95% confidence limit of the fatigue life for various fabrication details categorized as A, B, etc. The + symbol shown for each category line depicts the stress range defined as the constant-amplitude fatigue limit. Below the constant-amplitude fatigue limit, it is commonly accepted that any fatigue-stress range may cause crack propagation and fatigue failure defined by the dashed line S-N relationship.

The cycle ranges of the fatigue crack data obtained from Test #1 are shown in Figure A-12. At a given stress range (18.7, 21.0. or 18.0 ksi) the left symbol of the cycle range denotes the number of fatigue cycles at which a crack was first observed, and the right symbol denotes the number of fatigue cycles at which the fatigue test was stopped.

The 18.7 ksi stress range data plotted for the measured stress range at the top fiber of the main bars above the center support starts to the right of the Category D line and close to the left of the Category C line. This is indicative of the possible presence of Category D details in the negative bending moment region. Fatigue crack data recorded for the 21.0 ksi stress range in the east span at the bottom fiber of the main bars starts to the right of the Category C line and should thus be classified as fatigue Category C.

The horizontal bars plotted for the 18.7 ksi and 21.0 ksi stress ranges start at 557,200 cycles because no cracks were observed at the previous check of 541,080 cycles (see Table A-2). They end at 900,000 cycles when the test was terminated.

The cycle range for the measured 18.0 ksi stress range plotted in Figure A-12 is for the bottom fiber of the main steel bars in the west span, starts at 801,000 cycles and ends at 900,080 cycles. The start falls slightly to the right of the Category C line and complements the conclusions for the east span (21.0 ksi stress range).

A-6 CONCLUSIONS

Based on the results of the full-scale Test #1 conducted, it is concluded that the fatigue behavior of IKG's 4-1/4-Inch Interlock floor panel with 6-inch main bar spacing and 1-5/8-inch concrete overfill is controlled by the AASHTO-Category-C-stress-range limitations for positive bending (tension at the bottom), and possibly for negative bending (tension at the top). Although the first fatigue crack observed for the positive bending moment region suggests that Category D criteria are applicable, the closeness of the results to the Category C criteria, and the performance of the other decks, suggest that assuming Category C for positive bending moment regions is warranted.

Table A-1 - Strain Gage Types And Locations For Test #1

Gage Number	Type	Location
1	Concrete	Top of concrete overfill, west span, 60 inch from center support, along centerline of slab.
2	Concrete	Level with top of steel grid, west span, 60 inch from center support, along centerline of slab.
3	Concrete	Bottom of concrete (steel pan locally removed), west span, 60 inch from center support, along centerline of slab.
4	Concrete	Top of concrete overfill, at center support, along centerline of slab.
5	Concrete	Level with top of steel grid, at center support, along centerline of slab.
6	Concrete	Bottom of concrete (steel pan locally removed), 4 inch east of center support, along centerline of slab.
7	Concrete	Top of concrete overfill, east span, 58 inch from center support, along centerline of slab.
8	Concrete	Level with top of steel grid, east span, 58 inch from center support, along centerline of slab.
9	Concrete	Bottom of concrete (steel pan locally removed), east span, 58 inch from center support, along centerline of slab.
10	Steel	Top of steel grid, west span, 60 inch from center support, on Bar 7.
11	Steel	Bottom of steel grid, west span, 60 inch from center support, on Bar 7.
12	Steel	Top of steel grid, at center support, on Bar 7.
13	Steel	Bottom of steel grid, at center support, on Bar 7.

Table A-1, continued

Gage Number	Type	Location
14	Steel	Top of steel grid, east span, 58 inch from center support, on Bar 7.
15	Steel	Bottom of steel grid, east span, 58 inch from center support, on Bar 7.

Table A-2 - Highlights Of Inspection Recordings For Test #1

Number of Cycles	Notes
95,000	3 concrete cracks all across slab, 2 over partial width, straddling center support;
146,040	5 concrete cracks all across slab, 2 over partial width, straddling center support;
366,350	7 concrete cracks all across slab, cracks are not straight;
557,200	bottom flange of Bar 7 cracked, east span, 72-7/8 inch from center support;
	bottom flange of Bar 8 cracked, east span, 72-1/2 inch from center support;
804,000	bottom flange of Bar 5 cracked, east span, 72-7/8 inch from center support;
	bottom flange of Bar 6 cracked, east span, 72-7/8 inch from center support;
	bottom flange of Bar 9 cracked, east span, 70-1/2 inch from center support;
	bottom flange of Bar 6 cracked, west span, 71-3/4 inch from center support;
	bottom flange of Bar 7 cracked, west span, 68 inch from center support;
	bottom flange of Bar 8 cracked, west span, 68-1/8 inch from center support;
	bottom flange of Bar 9 cracked, west span, 67-3/4 inch from center support;
895,500	bottom flange of Bar 10 cracked, east span, 65-3/4 inch from center support;
	bottom flange of Bar 5 cracked, west span, 65-3/4 inch from center support;
900,000	fatigue test was terminated

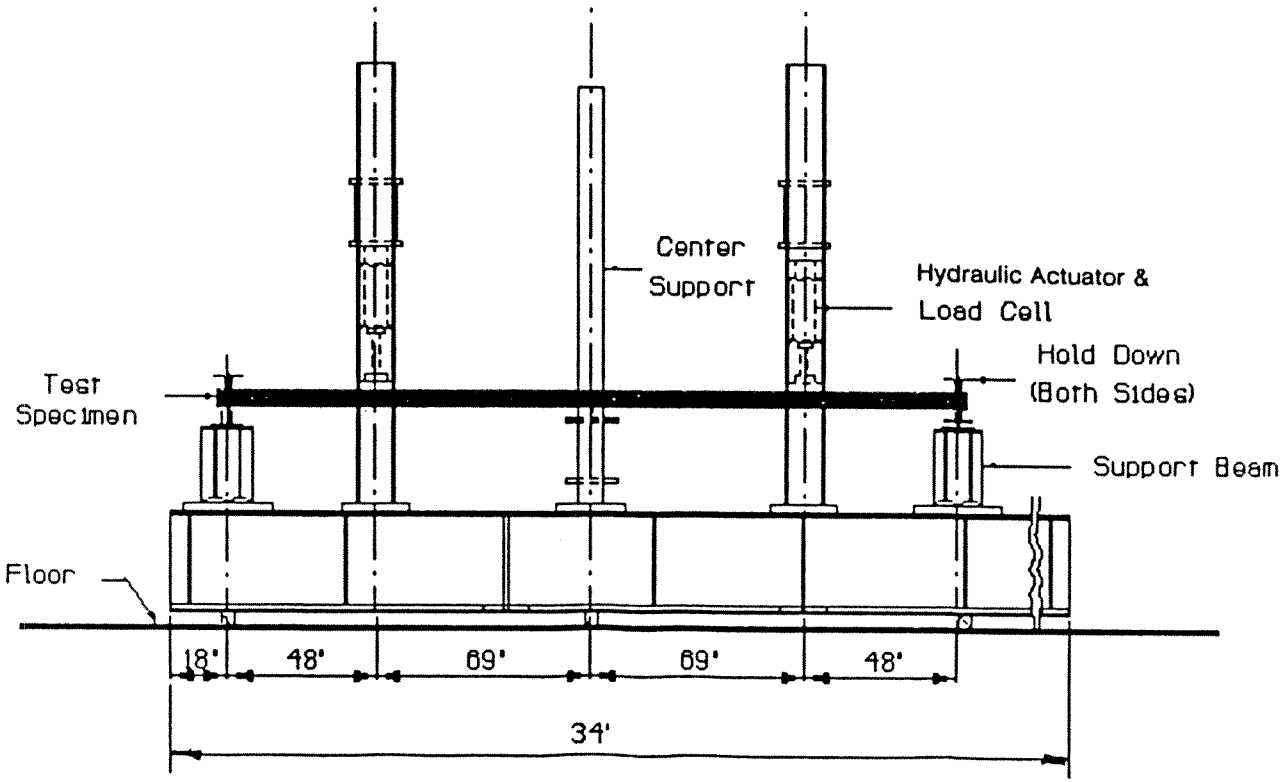

Fig. A-1 - Test Frame Setup For Test #1 - Section Along Centerline, Viewing South

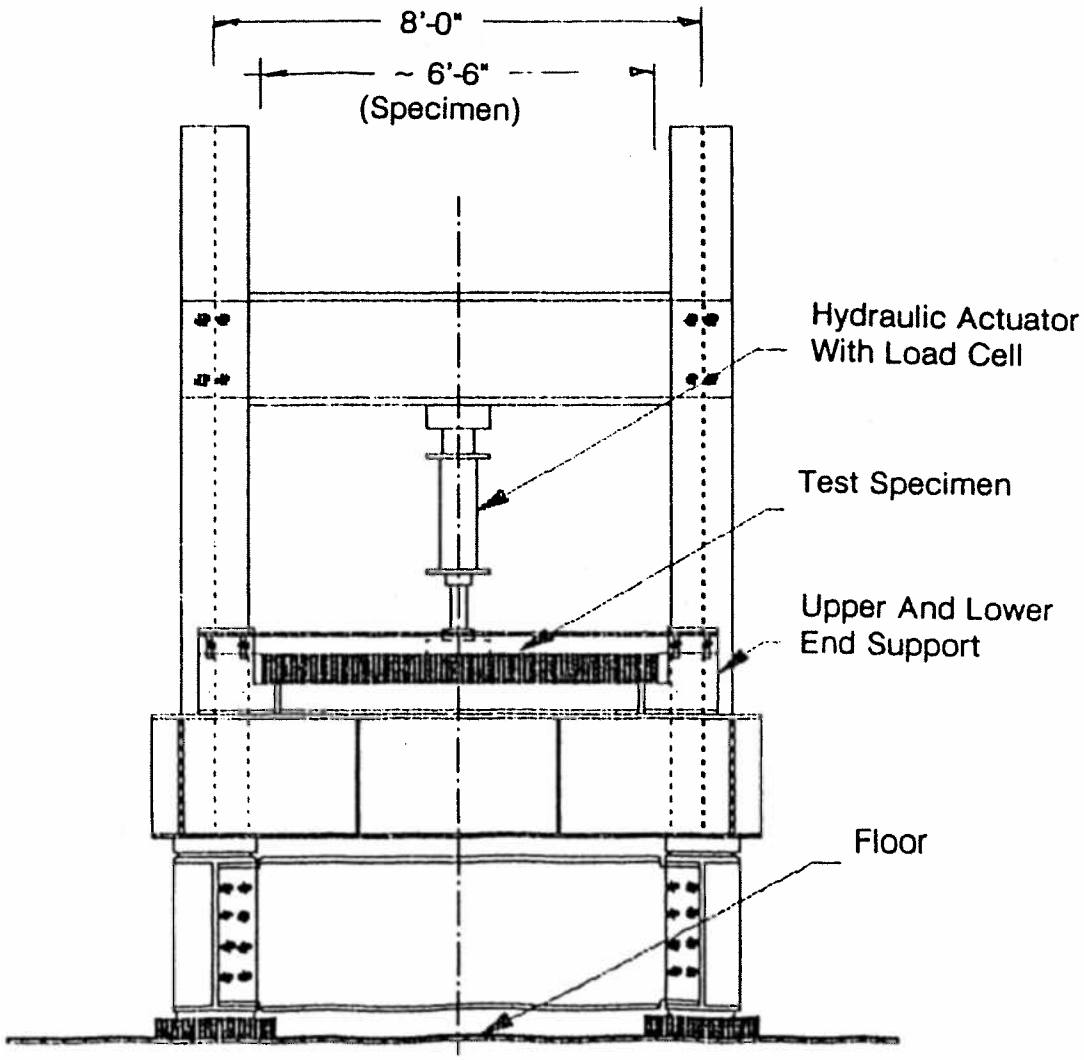

Fig. A-2 - Test Frame Setup For Test #1 - End View

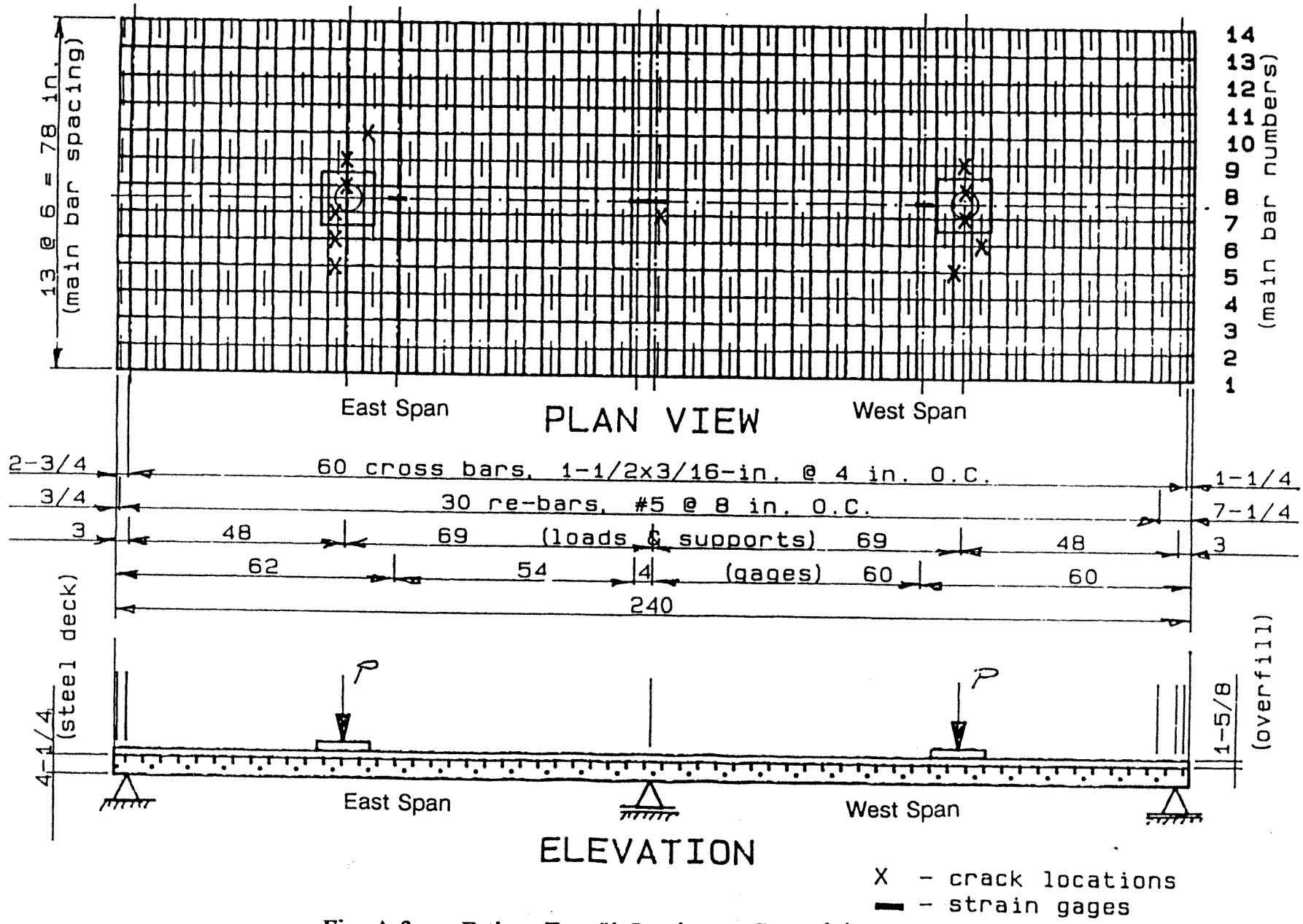

Fig. A-3 - Fatigue Test #1 Specimen - General Arrangement, Including Gage And Crack Locations

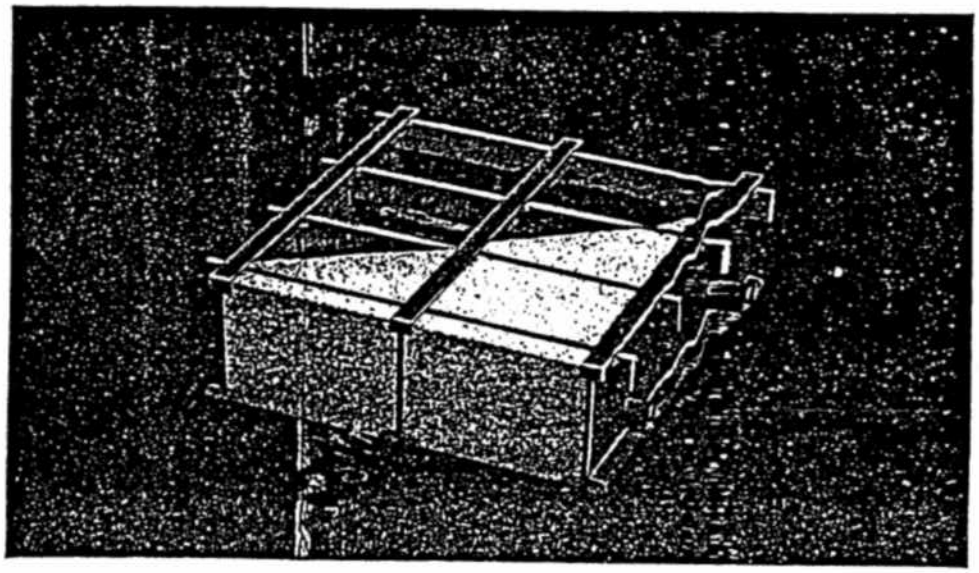

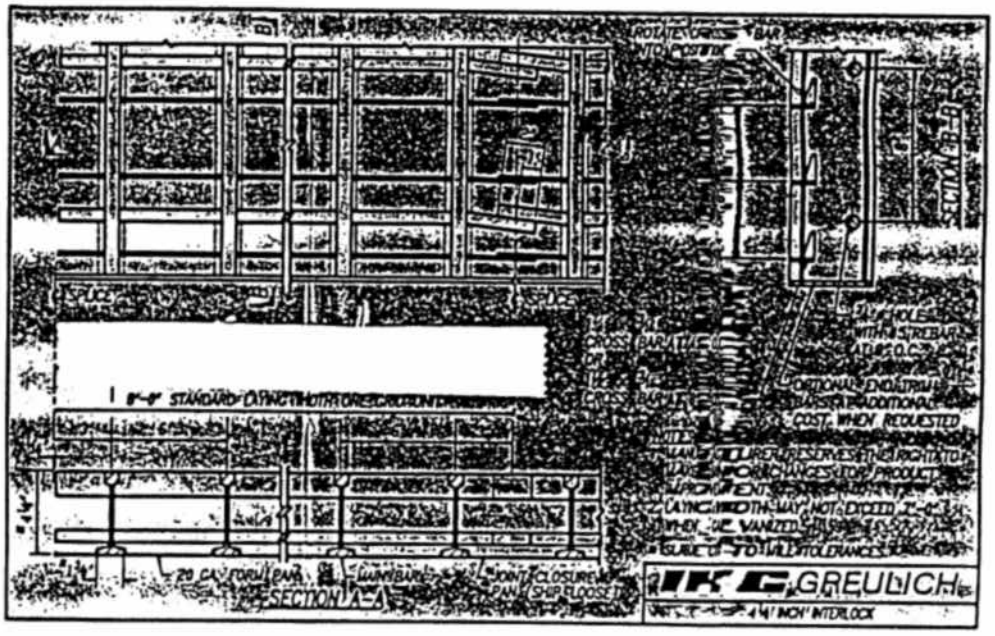

Fig. A-4 - 4-1/4-Inch Interlock Panel Details For Test #1 With 1-5/8-Inch Overfill

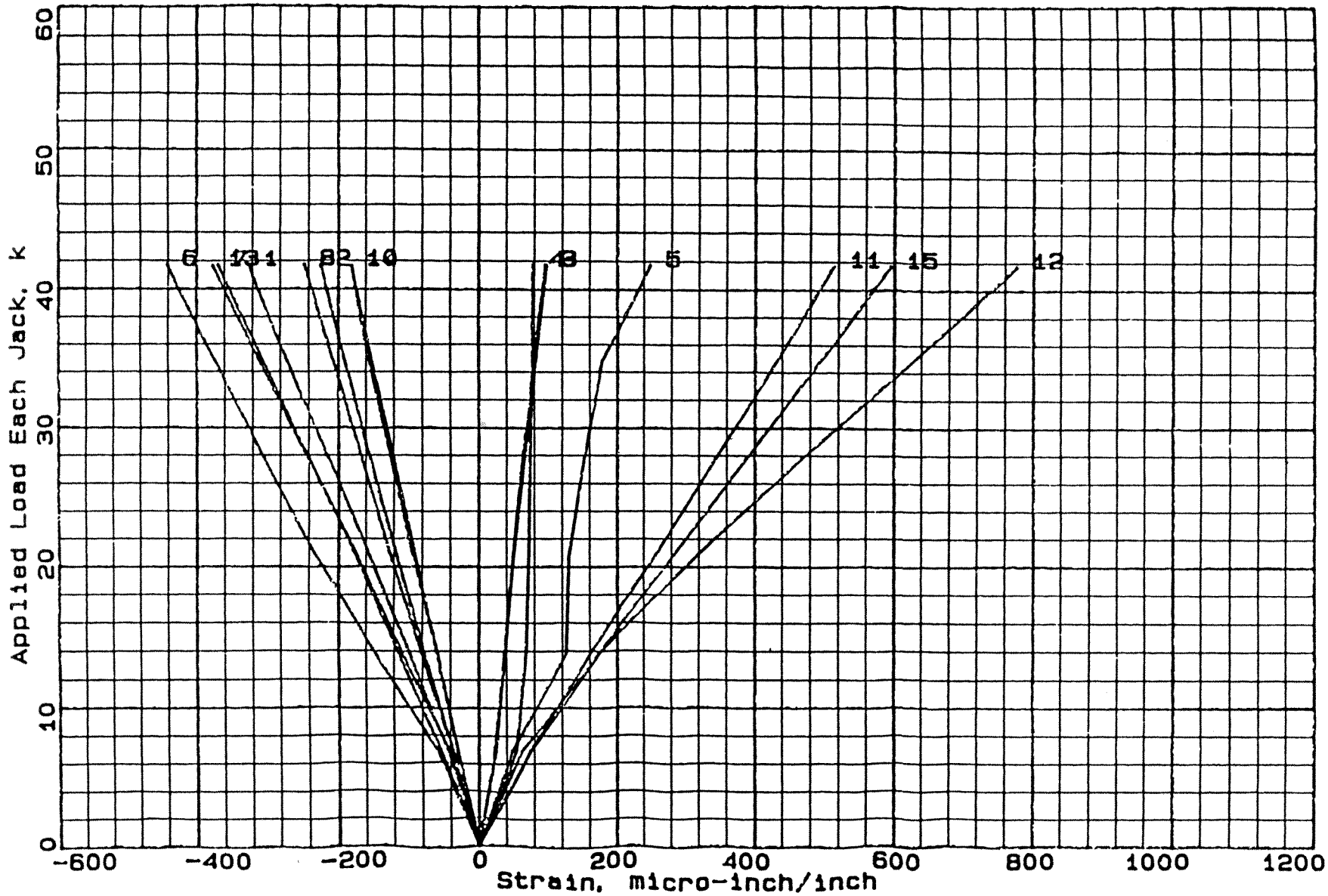

Fig. A-5 - Strain vs Load For All Gages At 0 Fatigue Cycles
(Test #1, Run 5)

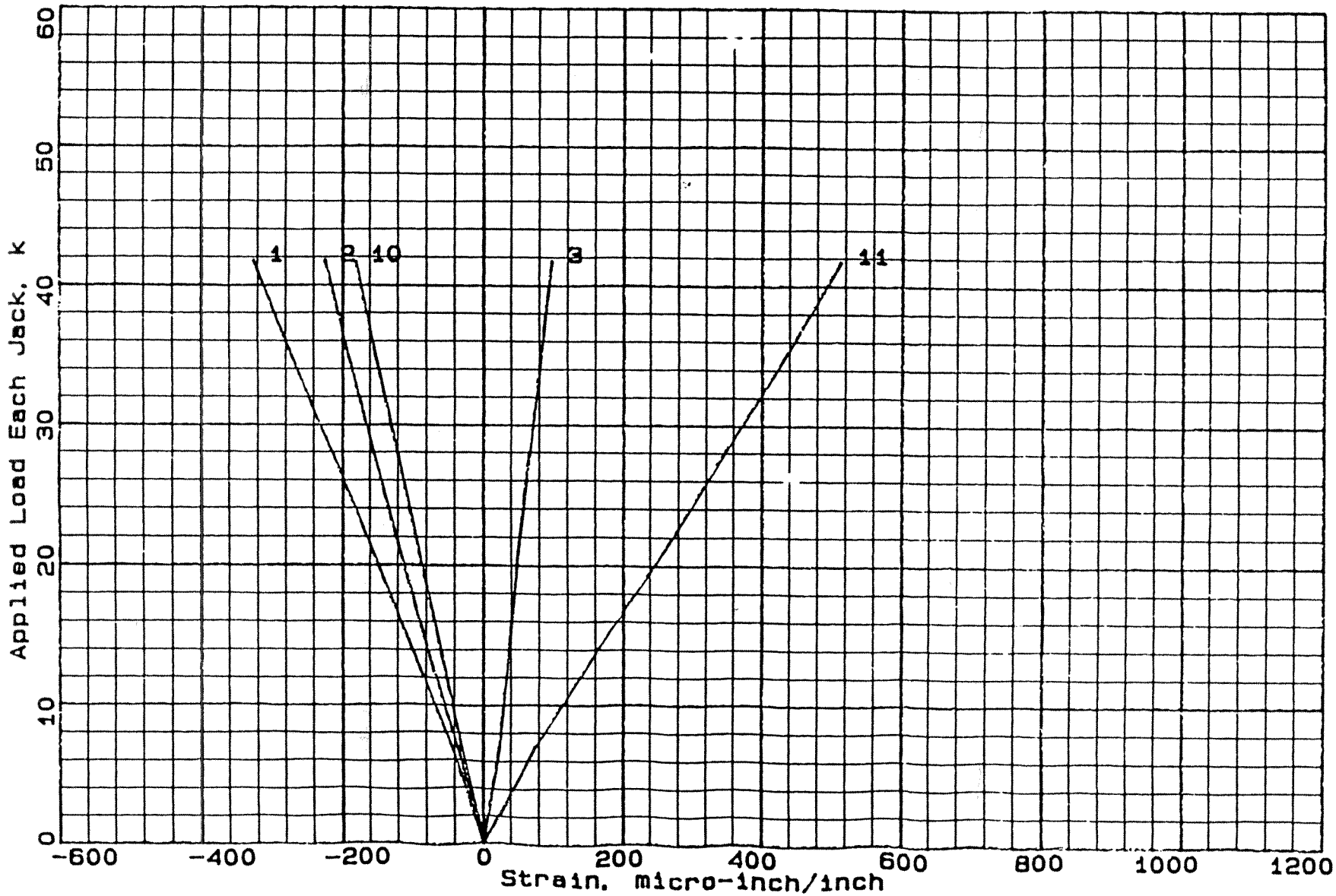

Fig. A-6 - Strain vs Load For West Span Gages 1, 2, 3, 10, And 11 At 0 Fatigue Cycles (Test #1, Run 5)

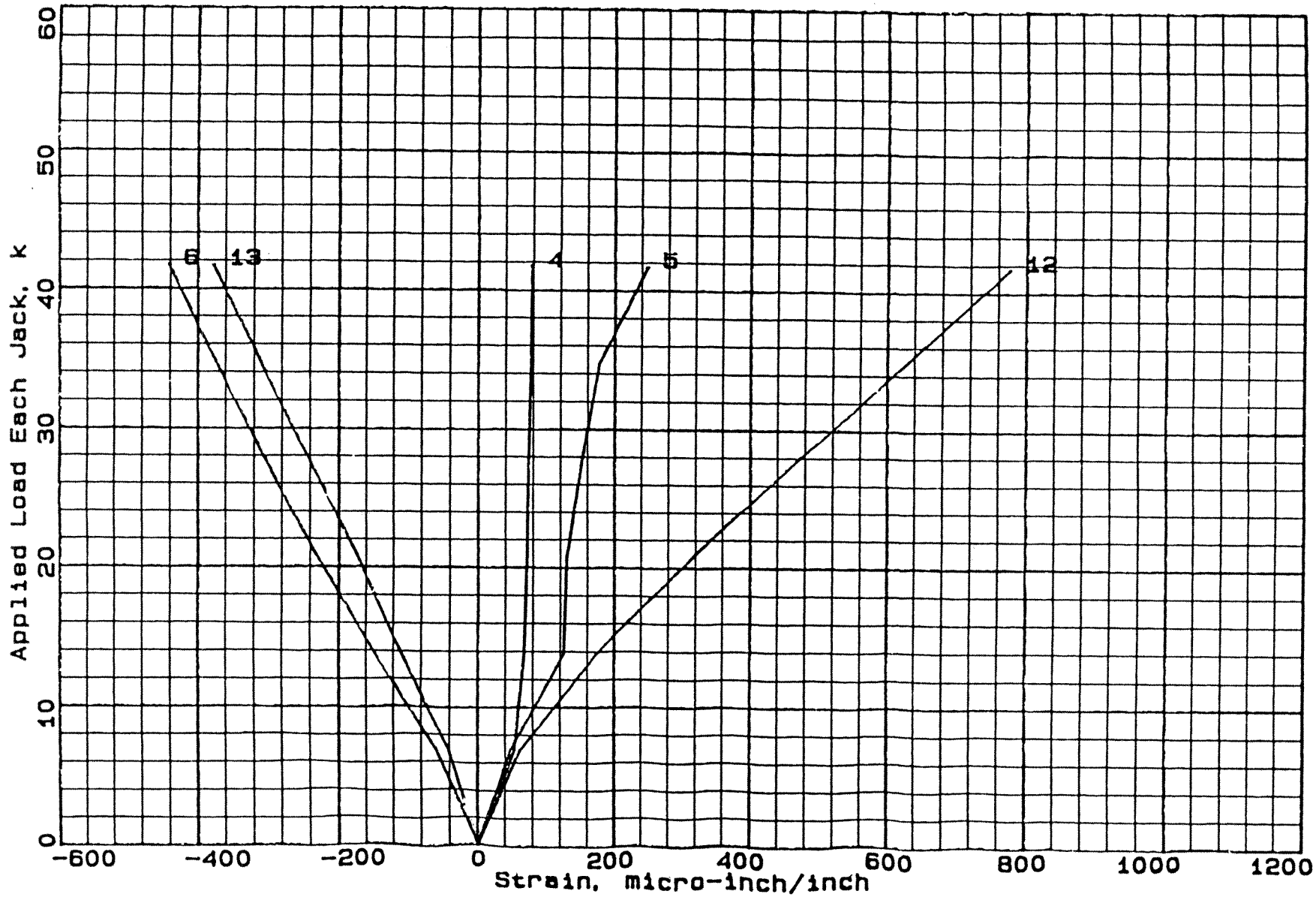

Fig. A-7 - Strain vs Load For Center Support Gages 4, 5, 6, 12, And 13 At 0 Fatigue Cycles (Test #1, Run 5)

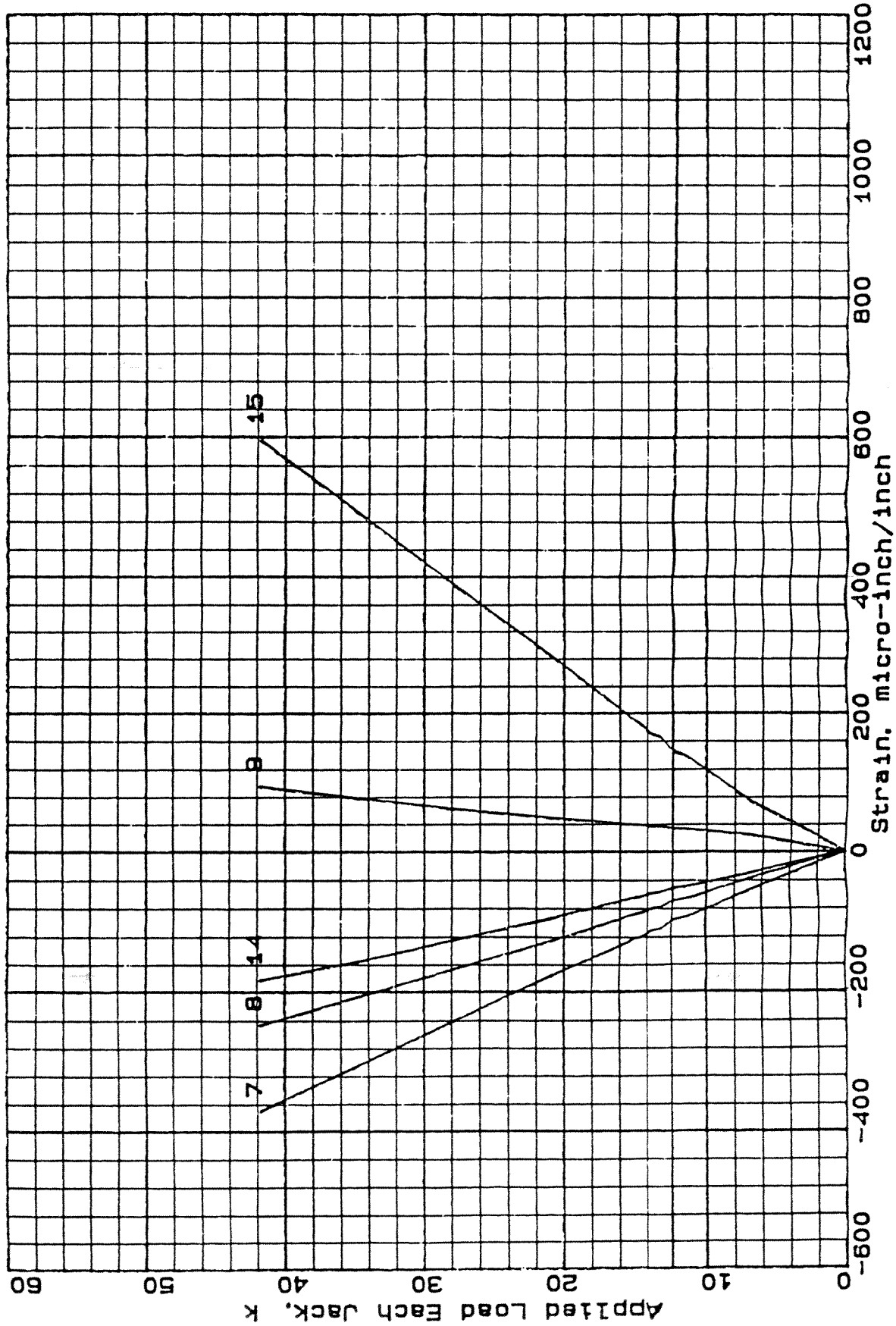

Fig. A-8 - Strain vs Load For East Span Gages 7, 8, 9, 14, And 15
At 0 Fatigue Cycles (Test #1, Run 5)

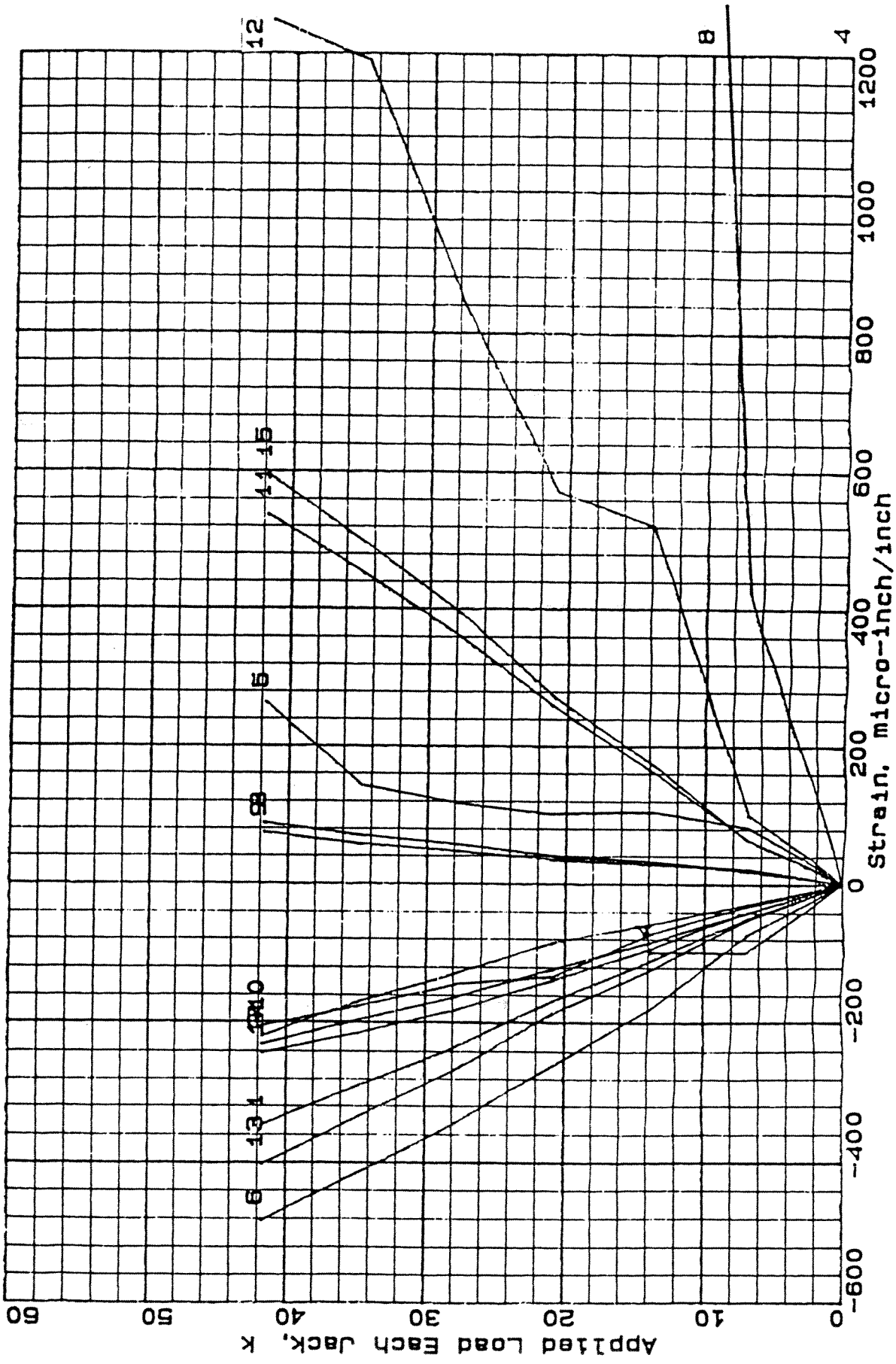

Fig. A-9 - Strain vs Load For All Gages At 541,080 Fatigue Cycles (Test #1)

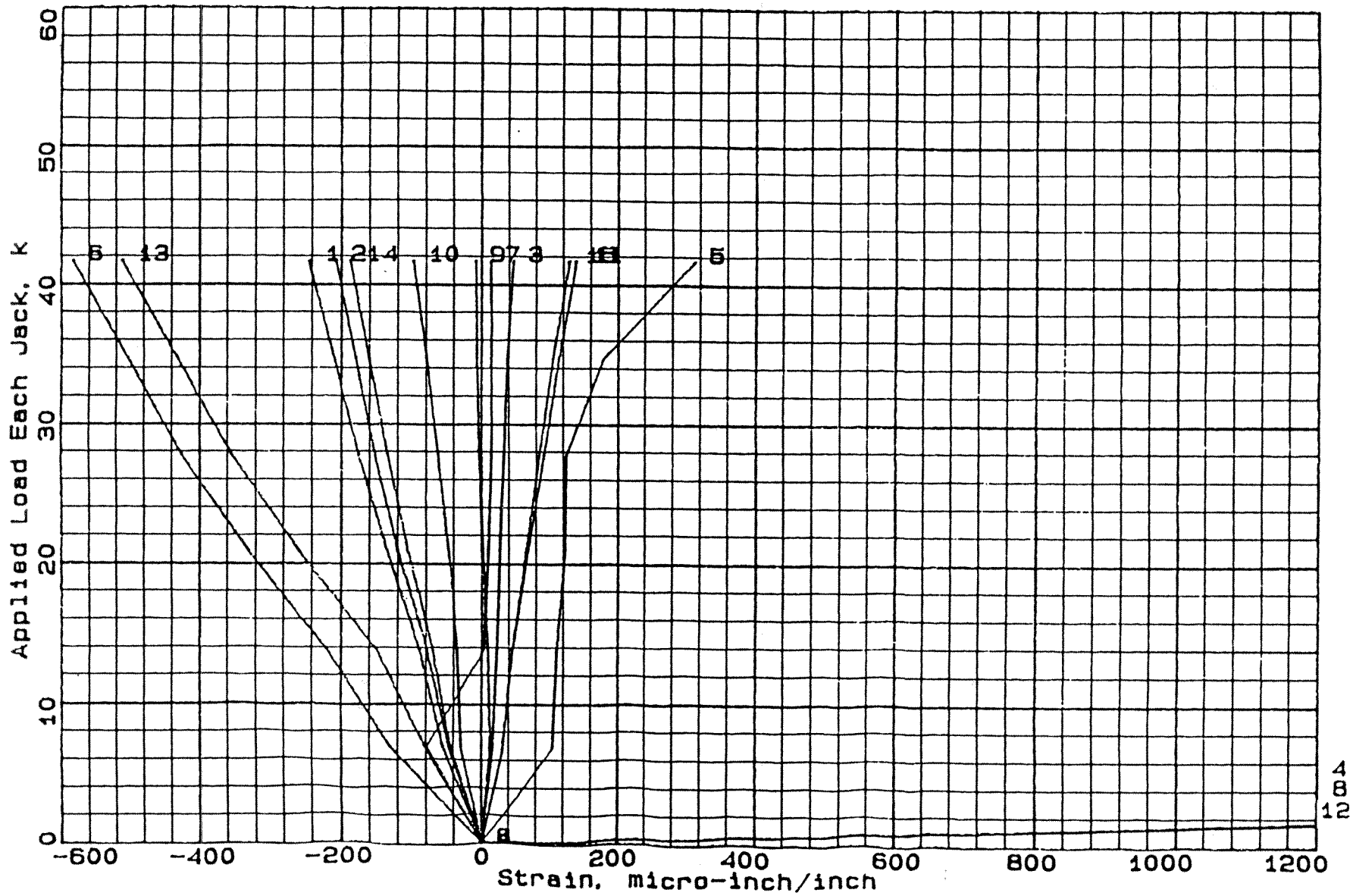

Fig. A-10 - Strain vs Load For All Gages At 900,080 Fatigue Cycles (Test #1)

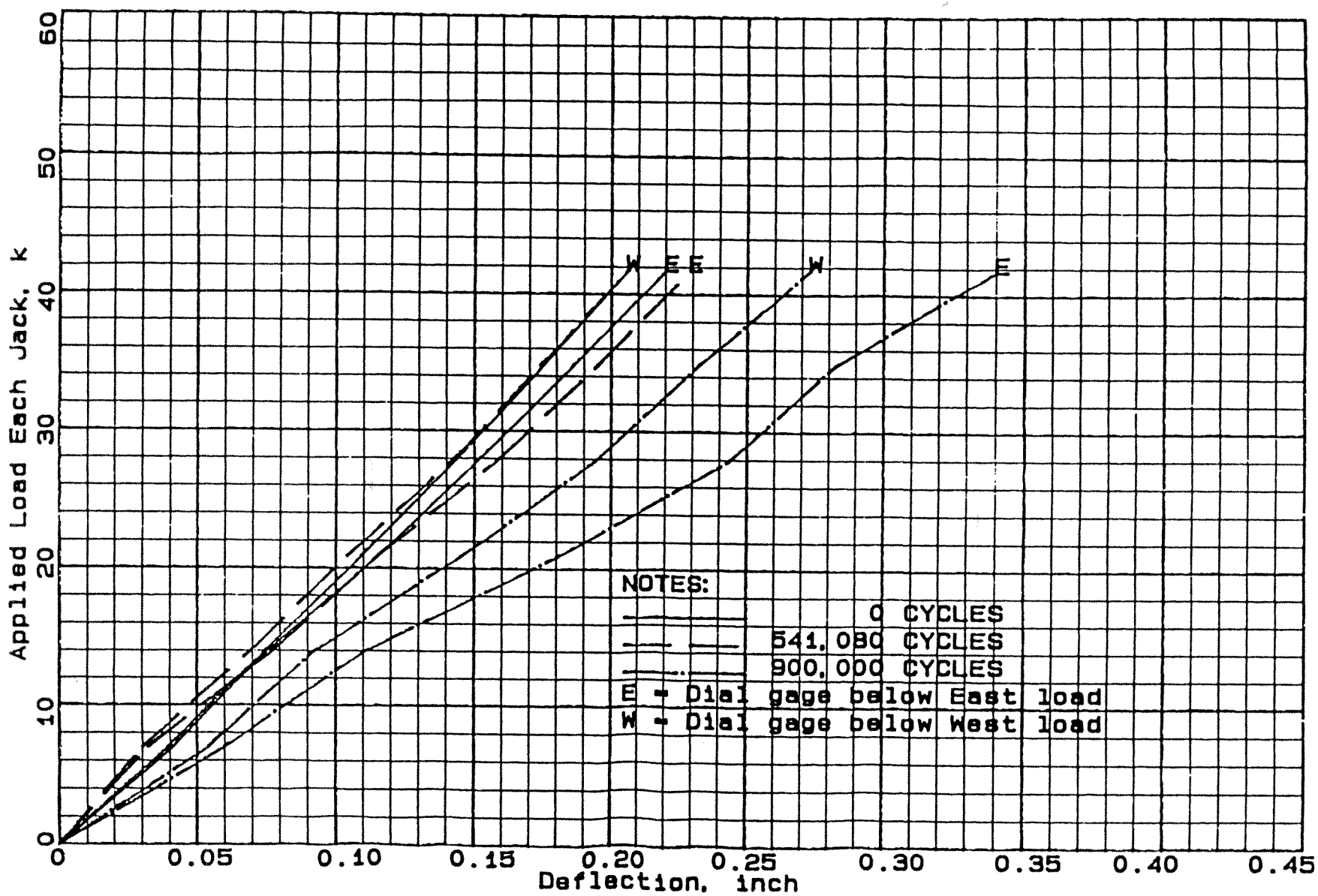

Fig. A-11 - Deflection vs Load In Both Spans At 0, 541,000, And 900,080 Fatigue Cycles (Test #1)

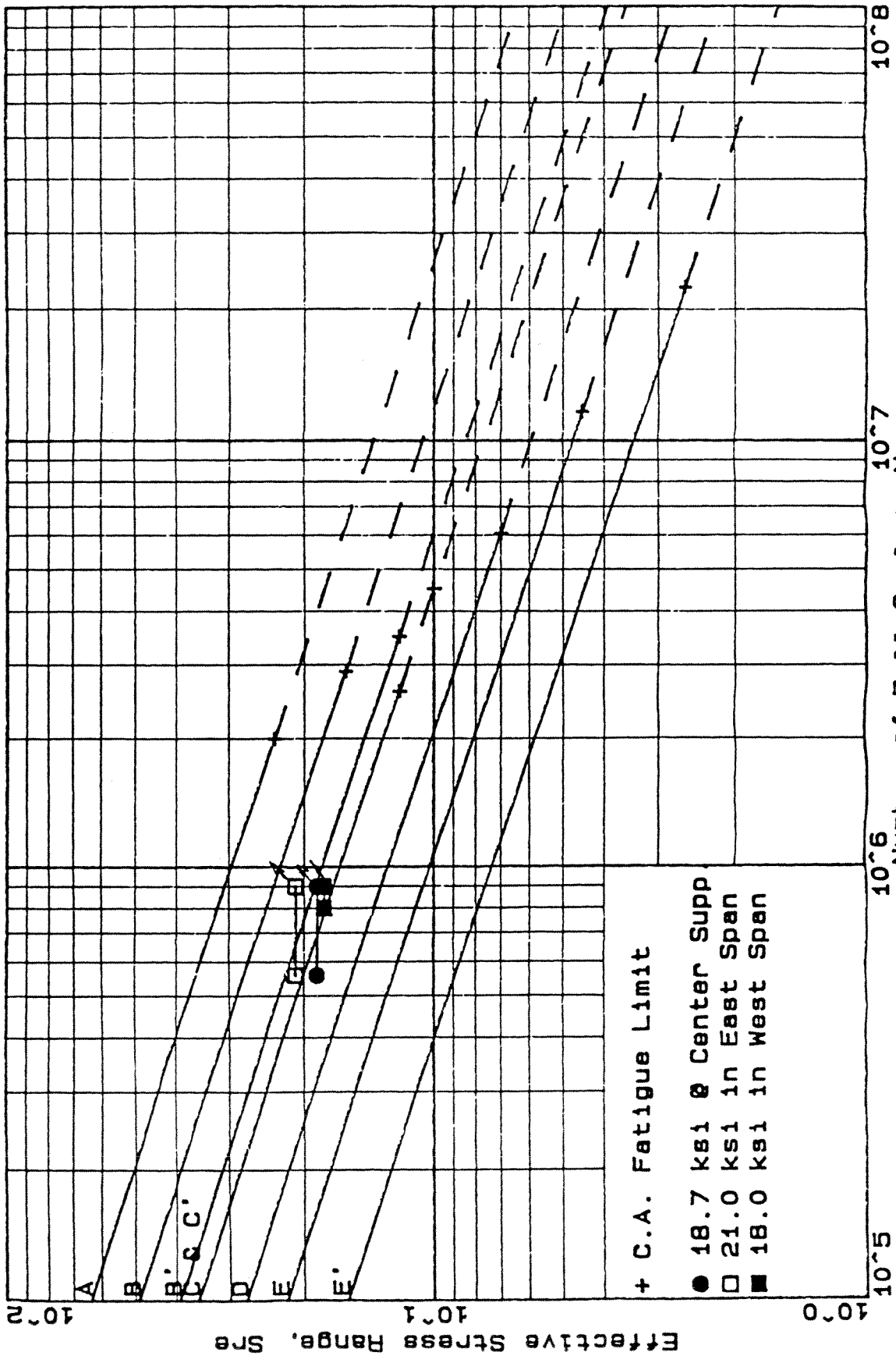

Fig. A-12 - Fatigue Failures Of Main Steel Bars In Test #1 Compared With 1991 AASHTO Fatigue Categories

APPENDIX B - FATIGUE TEST #2

B-1 OBJECTIVES

While Test #1 was very useful in getting the system set up, debugged, and working under expected operating conditions, concern was raised concern was raised by IKG about using 12x12x2-inch steel plates to introduce the loads into the test specimen and using a line support at the center. Thus, the first objective was to make the test setup and loads more representative of actual field conditions where tires introduce the loads and girders or I-beams serve as supports.

To pursue this objective, the center support was changed to a 6-inch wide bearing to simulate a 6-inch-wide girder flange and a 96-inch truck/trailer axle with four rubber-tired wheels was obtained and installed. This necessitated other significant changes in the test setup as discussed later.

In addition, the applied hydraulic actuator loads were chosen such that resulting axle loads would be within legal limits. For Test #1 loads up to 44 kips per actuator were used and the actuators were spaced 138 inch apart (center to center), which was a clearly arbitrary choice.

The second objective for Test #2 was to show how well a fatigue life prediction could be made, based on the information derived from Test #1. For the final test setup chosen, it was anticipated that approximately two million fatigue cycles could be sustained without any cracks in the steel bars, but that cracking according to AASHTO Category C might not occur until 6 million cycles had been reached.

It was also considered important to record more closely the effect of the first cracked bar on the remaining fatigue life of the adjacent or remaining bars. This was considered achievable by a more frequent observation of the strains, deflections, and cracks.

In view of these anticipations the chosen test setup and loads, and the resulting strains, stresses, and deflections were as described below.

B-2 TEST SETUP

As seen from Figures B-1 and B-2, a truck axle (rated capacity 22,000 pounds) was used to introduce a single actuator load through one of the spring-leaf brackets into the wheels, and through the wheels into the deck. Since this deck was not as strong as the one used in Test #1 the span was reduced from 117 to 90 inches and a lower actuator load was chosen. This resulted in a stress range of 11.0 ksi in the top steel fiber above the center support, and 13.1 ksi at the strain gage in the bottom steel fiber below the right (West) set of wheels (Figure B-3).

For this test the O. I. Rhiele console and pulsator (pump) were first connected to one 80-kip hydraulic actuator. The minimum and maximum actuator loads were 2.0 and 20.3 kips respectively. This theoretically caused minimum and maximum stresses of 1.43 and 14.53 ksi, respectively, or a stress range of 13.1 ksi in the positive moment region of the west span.

The load transfer from the actuator to the specimen was accommodated through a truck axle as shown in Figure B-1. However, the axle soon developed a crack (at an approximate cycle count of 500,000) at the differential housing. Therefore, a trailer axle (without differential housing) was procured and installed. At the same time a 40 kip actuator was installed to replace the 80 kip actuator. This smaller actuator had a smaller diameter and did not interfere with the side of the tires. Also, because of its smaller diameter, it required less oil displacement per inch of deflection. Thus, the test speed of 2 cps could be maintained even though the total deflection was much greater than for Test #1.

Dial gages were used below the deck at both mid-spans. The type and location of the strain and dial gages employed are summarized in Table B-1. The strain gage locations are also shown in Figure B-3.

B-3 ADDITIONAL SPECIMEN DETAILS

General physical details of all specimens are described in the main body of this report. Additional geometric details of the Test #2 specimen are shown in Figures B-3 and B-4.

The concrete mix for this specimen contained river bed gravel of 3/8-inch maximum size. While pouring the concrete, a slump of approximately 1-1/2 inch was measured. The average concrete strength after 42 days of curing, based on two 3-inch-diameter samples, was 4,591 psi, which meets the minimum strength requirements of 4,500 psi specified.

B-4 TEST PROCEDURE AND DATA ACQUISITION

At the beginning of the test, and numerous times after the fatigue loading process had been initiated, a static-load test was made. During the static tests, recordings were made of all strain gages and dial gages. The actuator load was incremented from zero to a maximum of about 25 kips in four steps.

The results of the first static-load test provided the minimum and maximum load settings for the fatigue tests such that the desired stress range (13.1 ksi) was obtained. These settings were maintained during the rest of the test even though intermittent static tests showed that the stresses were changing or some strain gages had been destroyed.

B-5 RESULTS

The results of the static-load tests made at the beginning and during the testing process are displayed in strain-versus-load and deflection-versus-load graphs, Figures B-5 through B-12, and Figure B-13, respectively. The fatigue life (number of cycles versus stress range) was summarized in a fatigue graph, Figure B-14. The strain-gage types and locations, and the dial gage locations, are described in detail in Table B-1. In addition, highlights of the inspection recordings are given in Table B-2. The speed of testing achieved was approximately 2 cycles per second. The testing speed eventually slowed down to approximately 1.67 cycles per second when the number of cracked main bars, and thus the actuator-head displacement, increased. More details are discussed below.

B-5.1 Strain-Gage Data

Before the first fatigue loads were applied, a static calibration test was made and the strains at different load levels were recorded. These strains are plotted in

Figures B-5 through B-8. Run 12 indicates that eleven full or partial load cycles (runs) had previously been applied. The plotted strains are almost linear. The strains in the east span shown in Figure B-8 are nearly zero. This is as expected because the moment is nearly zero.

Another record of the strain gages was made after 2,528,680 fatigue cycles had been applied. The results are shown in Figures B-9 through B-12. Since Figures B-5 and B-9 show a plot of all gages, it is difficult to make a comparison of gages. A comparison of Figures B-10 through B-12 with Figures B-6 through B-8, respectively, shows more clearly what has happened to the functioning of the gages and what has happened at or near the strain gage locations.

Figures B-6 and B-10 allow a comparison of concrete Gages 1 and 2 and steel Gages 7 and 8 after about 2.5 million cycles had been applied. These gages are located at or adjacent to the centerline and approximately at the mid-length of the West Span, 46 inch from the center support. It is seen from Figure B-10 that Gages 1, 2, and 7 are not functioning any more. Concrete Gages 1 and 2 were situated close to the location of the west-end pair of wheels (see Table B-1). It is possible that the gage on top of the deck (Gage 1, in compression), was damaged during the replacement of the first axle. Gage 2 was located at the bottom of the deck and initially was in tension. Concrete gages in tension usually fail quickly when exposed to high tensile stresses. Steel Gage 7 was located at the top fiber of Bar 6 and may also have been damaged during the axle exchange or during inspection.

A similar comparison can be made by using Figures B-7 and B-11 which show the stress-strain plots for concrete Gages 3 and 4 and steel Gages 9 and 10, all located along the centerline of the deck, above the center support. At 2,528,600 cycles Gages 3, 4, and 10 had failed while Gage 9, located on top of steel Bar 6 (deck centerline), was still working properly. This confirms the visual inspection results that there were no cracks in the top fiber of the steel bars at that time.

Figures B-8 and B-12 allow a comparison of concrete Gages 5 and 6 and steel Gages 11 and 12 at zero versus 2,528,680 load cycles. All gages are located in the east span, 45 inches from the center support, at or near the centerline of the slab.

Gages 5 and 11 are located at the top, and Gages 6 and 12 at the bottom, of the deck. Figure B-8 confirms that all strains at these locations were low, as expected from the load conditions given. Figure B-12 shows how erratic the concrete gages had become after 2,528,680 load cycles.

B-5.2 Deflection Data

The deflections (change of distance between the bottom of the deck and the floor) were recorded throughout the test. The results from the initial and subsequent static tests are shown in Figure B-13.

At the maximum calibration load of 20.3 kips, the measured west span deflections changed from 0.343 inch at the beginning of the test to 0.485 inch when the test was terminated at 6,025,010 cycles. This represents an increase of 41 percent even though no cracks were observed in the main steel bars when the test was terminated.

Likewise, the measured east span deflections increased from -0.10 inch at the beginning of the test to -0.19 inch at the end of the test. This represents an increase of 90 percent. However, this increase should be viewed with caution because the deflections were very small, and small reading inaccuracies could result in large differences of the percent of increase calculated.

The displacement of the hydraulic actuator was approximately 1-1/2 inch. This also reflects the deflection of the slab, tires, and test frame.

B-5.3 Concrete Cracks

Up to 4,750,000 cycles, all observers looked for concrete cracks but no log-book entries were made. At 4,750,000 cycles, and from then on to the end of the test, the only test-log entries found, as related to concrete cracks, say essentially that "bond breaking" was observed. This refers to the bond between the concrete and the steel bars, and depicts the bond breaking noticed at the top of the deck within in the negative bending moment region around the center support.

Bond breaking may be explained by making a comparison with ice cubes in an ice tray. When the ice tray is bent and twisted, the bond between ice cubes breaks and

the ice cubes may be removed. Similarly, the bond between concrete and steel grid components is broken after a sufficient amount twisting and bending of the deck has occurs. However the concrete cubicles in the bridge deck can not be removed because of several reasons: (a) the sides of the main bars may not be plane, (b) the concrete may have penetrated holes in the main bars, (c) adjacent concrete cubicles are connected to each other below the cross bars, (d) the concrete cubicles may be connected by transverse reinforcing bars, or (e) rust on the steel surfaces in contact with the concrete cubicles may re-freeze the cubicles into its original position. Also, thermal and chemical expansion of the concrete may increase the friction between concrete and steel bars, and not only prevent the concrete cubicles from popping out of their containment but also contribute to composite behavior which makes it so difficult to predict stresses in concrete-filled steel-grid bridge deck.

B-5.4 Steel Bar Cracks

As seen from Table B-2 - Highlights Of Inspection Recordings, the first cracks across the bottom flange in the west span main steel Bars 6 and 7 were observed after 4,562,300 fatigue cycles. Earlier attempts to disclose minute cracks by dye penetration tests did not reveal any cracks.

When an inspection was made at 4,750,000 cycles, an additional crack was found in the west span across the bottom flange of Bar 8. Subsequently, a crack across the bottom flange of Bar 9 was found in the west span at 5,810,000 cycles.

No additional cracks were found at the termination of the test (6,000,000 cycles). This includes the closely inspected bars at the top of the main bars above the center support. All cracks identified are shown in the Plan View of Figure B-3.

Future work has been proposed to remove a 6-inch-wide deck strip below the loads, remove the concrete, and open up the main steel bar cracks to determine the crack initiation sites in the bars. This may allow to change fabrication details and improve the fatigue life.

B-5.5 S-N Fatigue Comparison

Results of the fatigue-crack observations contained in Table B-2 were used to compare the crack occurrences in the floor slab tested with the present (1991)

AASHTO fatigue design provisions. Both, the AASHTO fatigue design lines and the fatigue-crack observations are shown in Figure B-14. Details of the AASHTO fatigue design curves were discussed previously.

The cycle ranges of the fatigue crack data obtained for the positive moment in the west span are plotted as a horizontal line at the stress range level of 13.1 ksi. This stress was measured at steel Gage 8 when fatigue testing began. The gage was located at the bottom fiber of Bar 6, 46 inch away from the center support. The left symbol of the cycle range denotes the number of fatigue cycles at which a crack was first observed (4,562,300 cycles), and the right symbol denotes the number of fatigue cycles at which the fatigue test was terminated (6,024,010 cycles). As seen from Figure B-14, the bar straddles fatigue Category B but is definitely to the right of Category B'.

No cracks were observed in the top fibers of the steel bars at the center supports where a negative bending moment occurs. Therefore, a run-out symbol was used at the stress range level of 11.0 ksi and 6,024,010 cycles. The stress range of 11.0 ksi was established at the start of the fatigue test and measured at the top fiber of Bar 6. As seen from Figure B-14, the test termination symbol falls to the right of fatigue Category B'. However, had the test been continued, the first fatigue crack may have occurred to the right of fatigue Category B.

B-6 CONCLUSIONS

Fatigue testing was discontinued after 6,024,010 cycles had been applied. During the life of the specimen, the fatigue test was frequently halted to record strain and deflection data under static load conditions. Some of the records considered typical were presented in the figures and tables.

The strain gage data collected and presented indicate that there was a shift in strains and stresses while the fatigue test proceeded. However, the magnitude of the change can not accurately be determined because many gages failed in the testing process and because the moment distribution within the specimen shifted. It is concluded that the shift of the moments occurred because of bond breaking, a pheno-

menon briefly described before. Since the moment distribution changed, the strain and stress distribution within the specimen also changed.

Test data obtained for the combined specimen and test frame displacements indicate that the deflections of the test specimen alone increase while the fatigue test proceeds. Since no steel cracks were found over the center support when the test was terminated, it is concluded that the initial increase was caused by bond breaking, and later on by the breaking of the main longitudinal steel bars, as confirmed by the strain gage observations.

When the test was terminated, no distinct concrete cracks were found on the top surface of the specimen. However, at 4,750,000 cycles, and from then on to the end of the test, "bond breaking" was observed in the negative bending moment region. This may just be a laboratory occurrence because no bond breaking was observed in samples recently removed from a demolished bridge deck that had been in service for more than 50 years.

The fatigue results obtained indicate that the applicable fatigue category for the 3-Inch T panel is Category B'. This category is applicable for the positive as well as the negative bending moment region of a deck without overfill.

An upgrading to Category B may be possible for the negative bending moment region of the deck. Further tests on small specimens are recommended to confirm this.

Table B-1 - Strain Gage Types And Locations For Test #2

Gage Number	Type	Location
1	Concrete	Top of concrete (flush), west span, 46 inch from center support, near centerline of slab.
2	Concrete	Bottom of concrete (steel pan locally removed), west span, 46 inch from center support, near centerline of slab.
3	Concrete	Top of concrete, at center support, near centerline of slab.
4	Concrete	Bottom of concrete (steel pan locally removed), at center support (shimmed), near centerline of slab.
5	Concrete	Top of concrete, east span, 45 inch from center support, near centerline of slab.
6	Concrete	Bottom of concrete (steel pan locally removed), east span, 45 inch from center support, near centerline of slab.
7	Steel	Top of steel grid, west span, 46 inch from center support, on Bar 6.
8	Steel	Bottom of steel grid, west span, 46 inch from center support, on Bar 6.
9	Steel	Top of steel grid, at center support, on Bar 6.
10	Steel	Bottom of steel grid, at center support, on Bar 6 (shimmed).
11	Steel	Top of steel grid, east span, 45 inch from center support, on Bar 6.
12	Steel	Bottom of steel grid, east span, 45 inch from center support, on Bar 6.

Table B-2 - Highlights Of Inspection Recordings For Test #2

Number of Cycles	Notes
83,740	Spring on one actuator broke and was replaced. No visible cracks (NVC).
249,130	Truck rear axle with differential housing broke (fatigue) and was replaced by a trailer axle. During exchange of axles Gage 9, located on top of steel Bar 6 (at mid-width of slab) and above center support, was ruined. Also, concrete Gage 1 did not function any more. NVC in test specimen.
446,000	Pulsator needed repair. NVC in specimen.
567,300	Oil leak at actuator needed fixing. NVC in specimen.
950,000	Coupling in hydraulics line started to leak and needed to be replaced. NVC in specimen.
1,007,000	T-joint on pulsator had severe oil leaks. A new part was machined and installed. NVC in specimen.
1,266,660	AutoData down for repairs. NVC.
1,501,000	Small auxiliary oil pump broke. Ordered and installed new one. NVC.
2,714,950	Performed dye-penetrant inspection on main grid bars (bottom flange, both spans). NVC in steel specimens.
3,247,340	Performed dye-penetrant inspection on main grid bars (top of T, at center support. NVC.
4,562,300	Cracks across bottom flange of Bars 6 and 7, in west span, visible by eye.
4,750,000	Additional crack across bottom flange in Bar 8, west span.
5,810,000	Additional crack across bottom flange in Bar 9, west span.
6,024,010	New crack across bottom flange in Bar 10, west span. Stopped test.

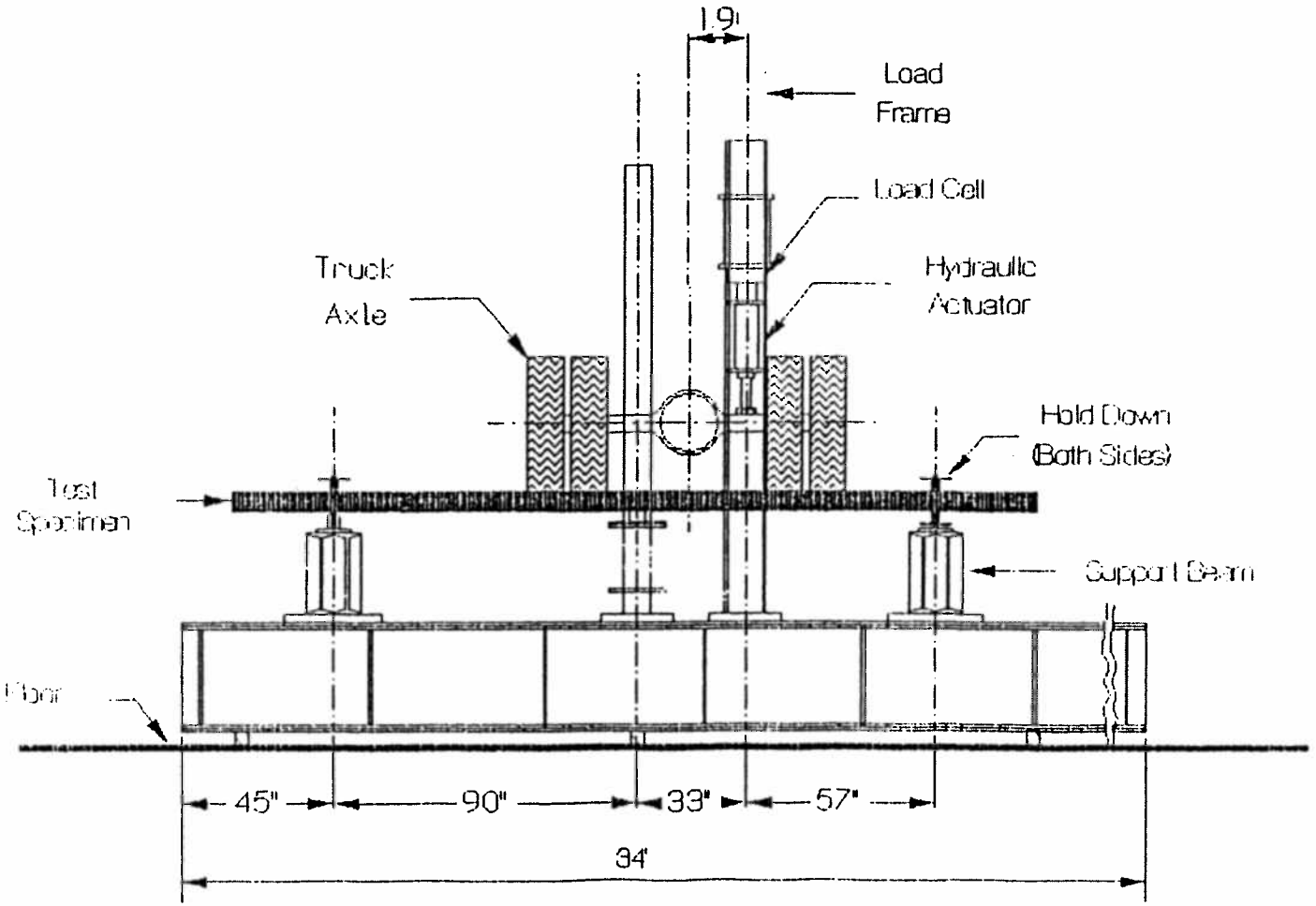

Fig. B-1 - Test Frame Setup For Test #2 - Section Along Centerline, Viewing South

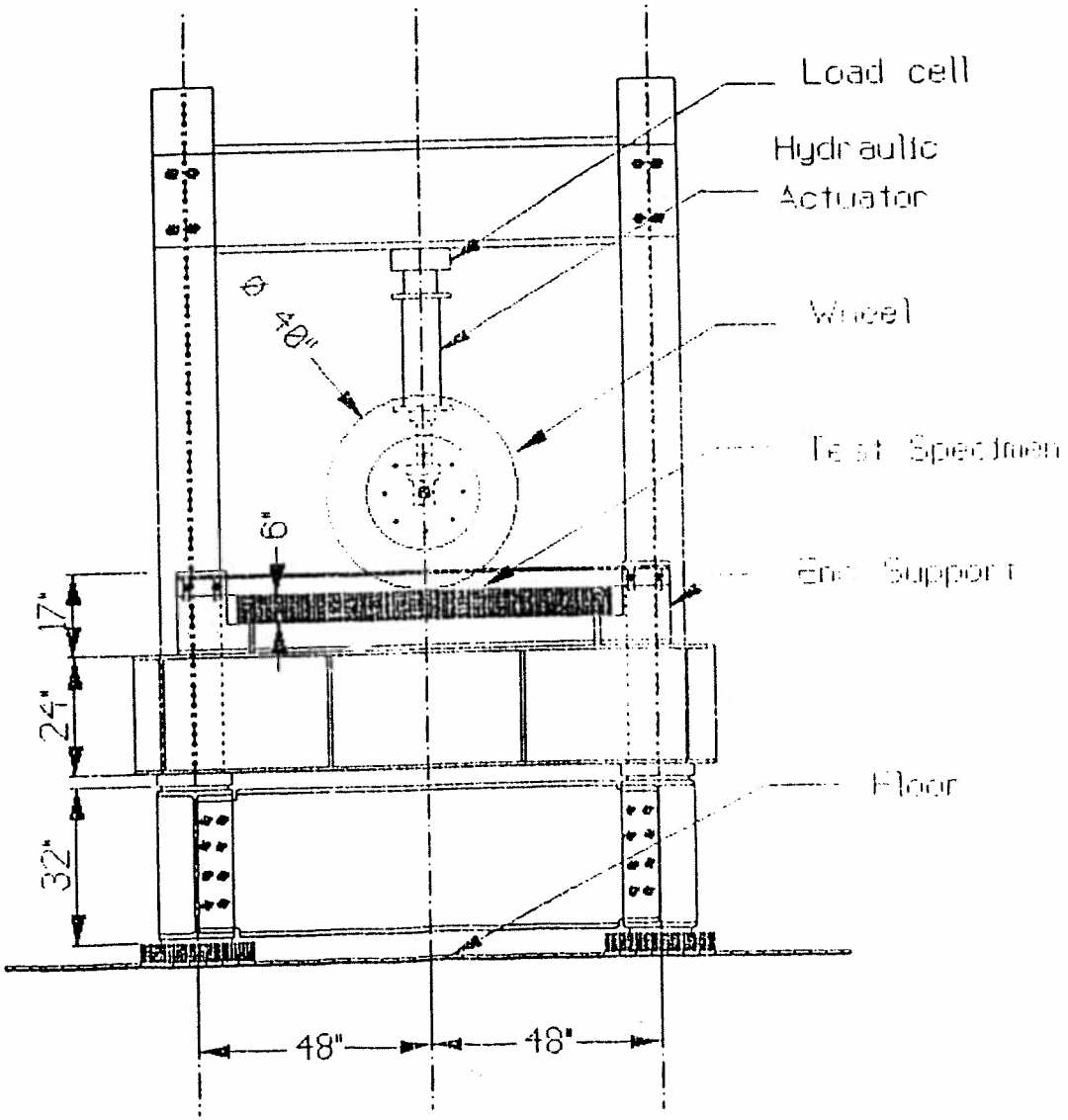

Fig. B-2 - Test Frame Setup For Test #2 - End View

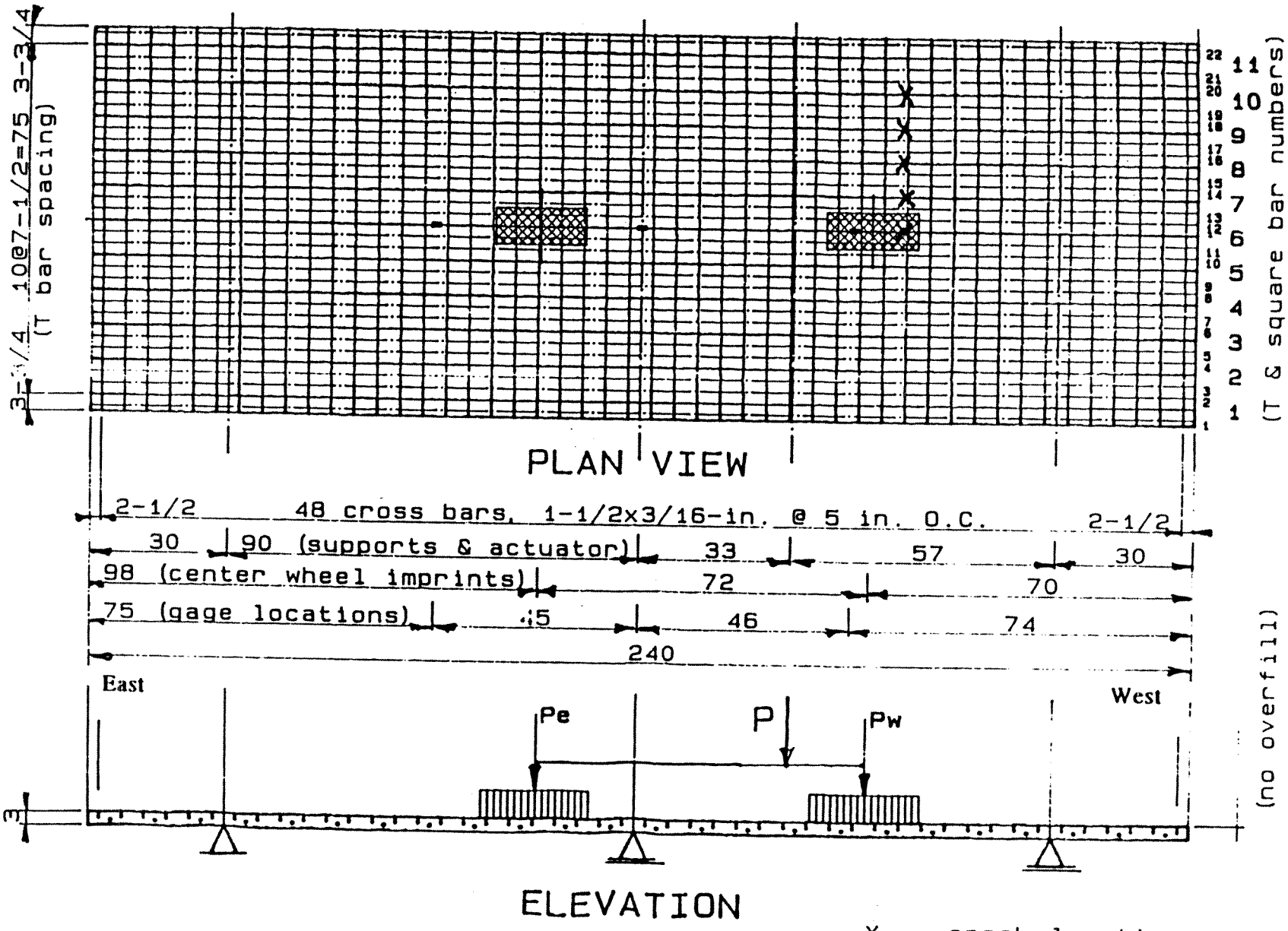

Fig. B-3 - Fatigue Test #2 Specimen - General Arrangement, Including Gage And Crack Locations

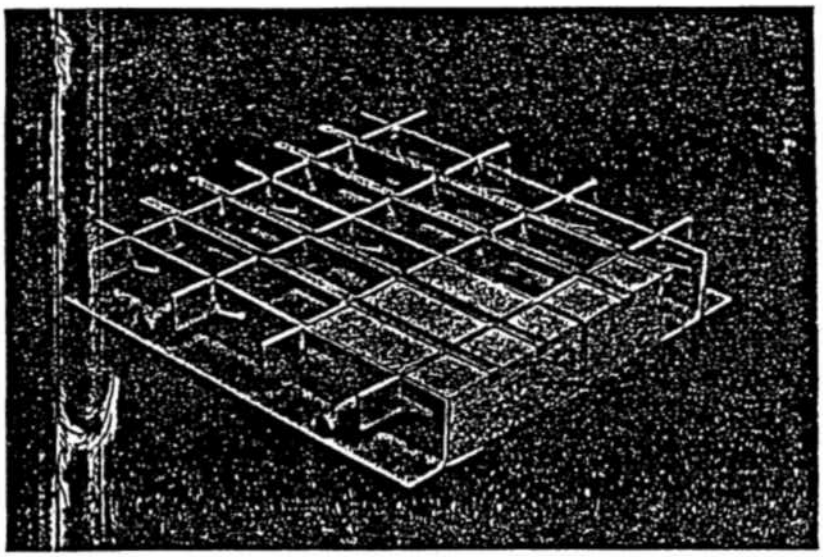

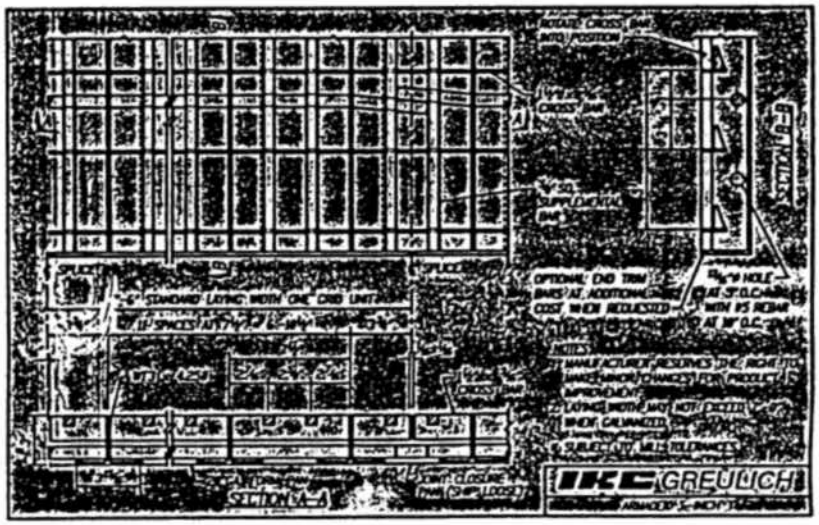

Fig. B-4 - 3-Inch T Panel Details For Test #2, Without Overfill

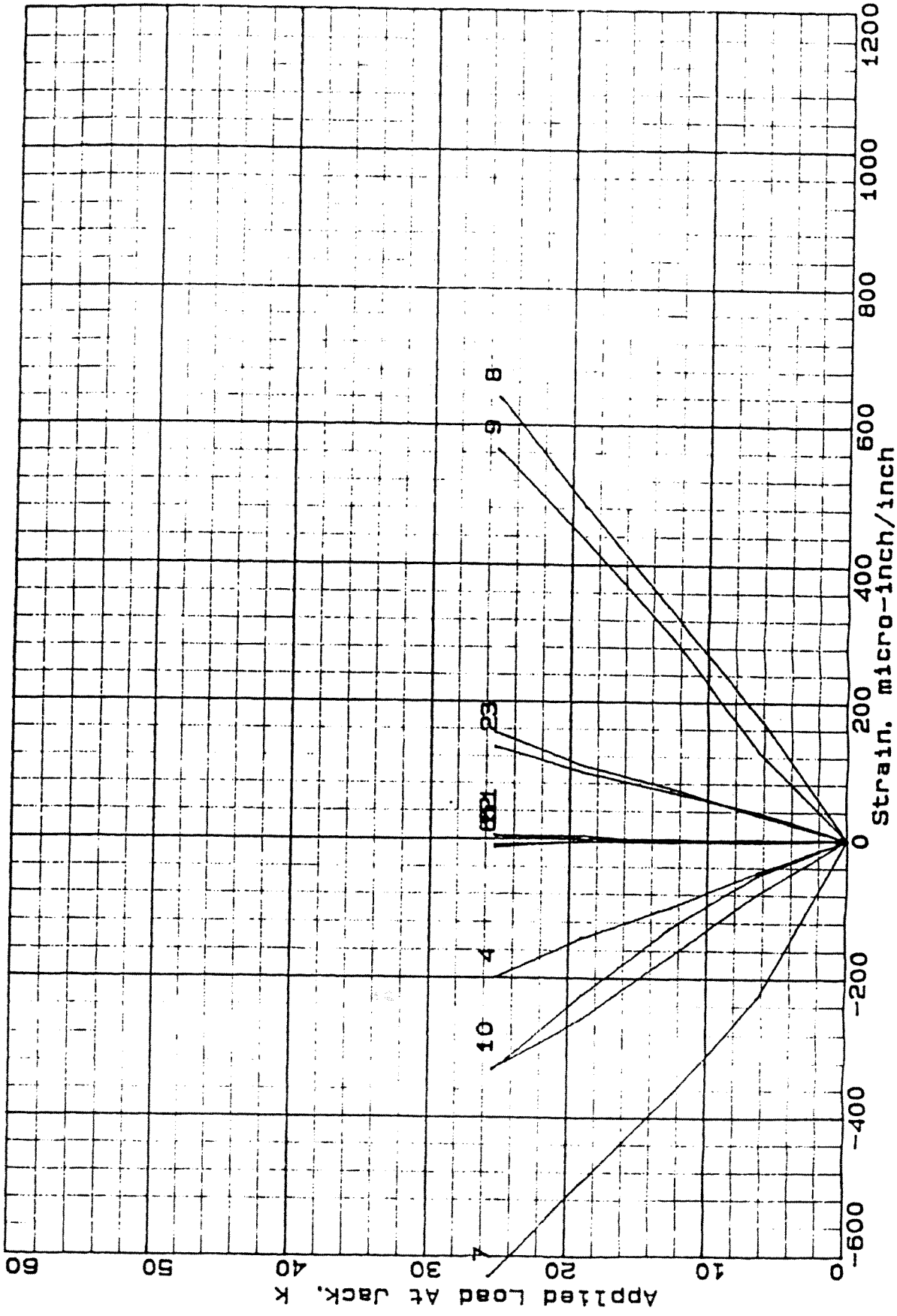

Fig. B-5 - Strain vs Load For All Gages At 0 Fatigue Cycles (Test #2, Run 12)

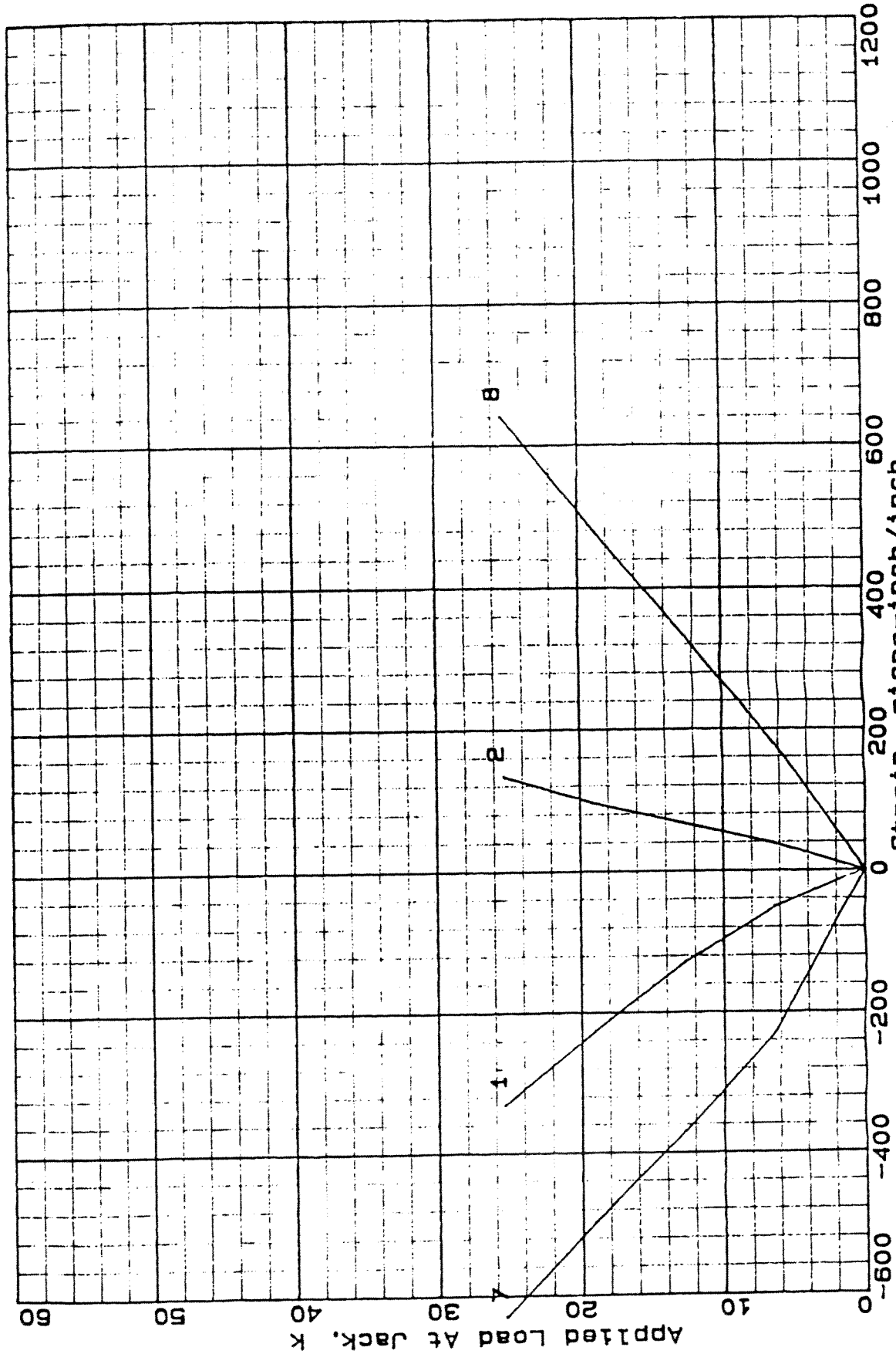

Fig. B-6 - Strain vs Load For West Span Gages 1, 2, 7, And 8 At 0 Fatigue Cycles (Test #2, Run 12)

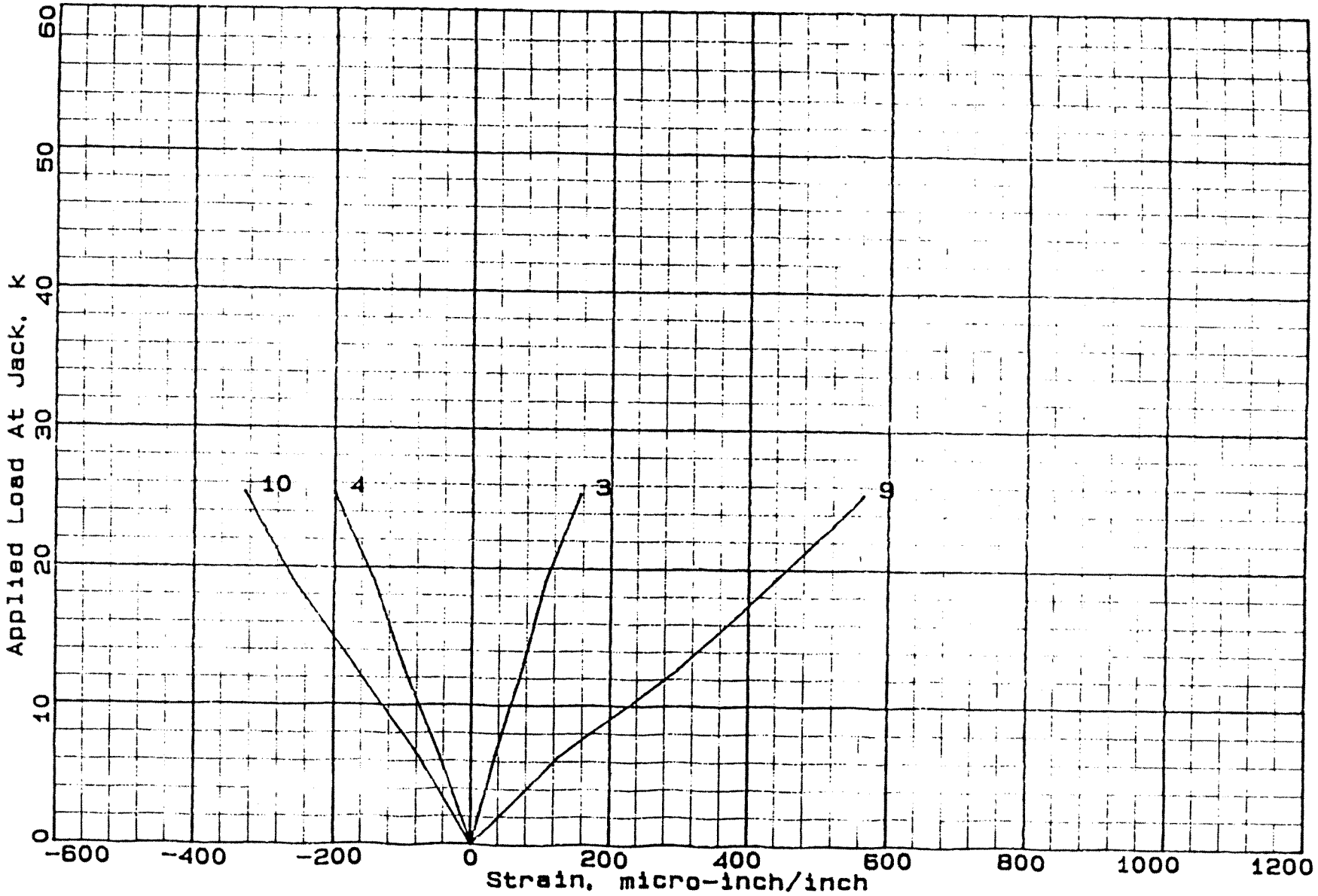

Fig. B-7 - Strain vs Load For Center Support Gages 3, 4, 9, And 10 At 0 Fatigue Cycles (Test #2, Run 12)

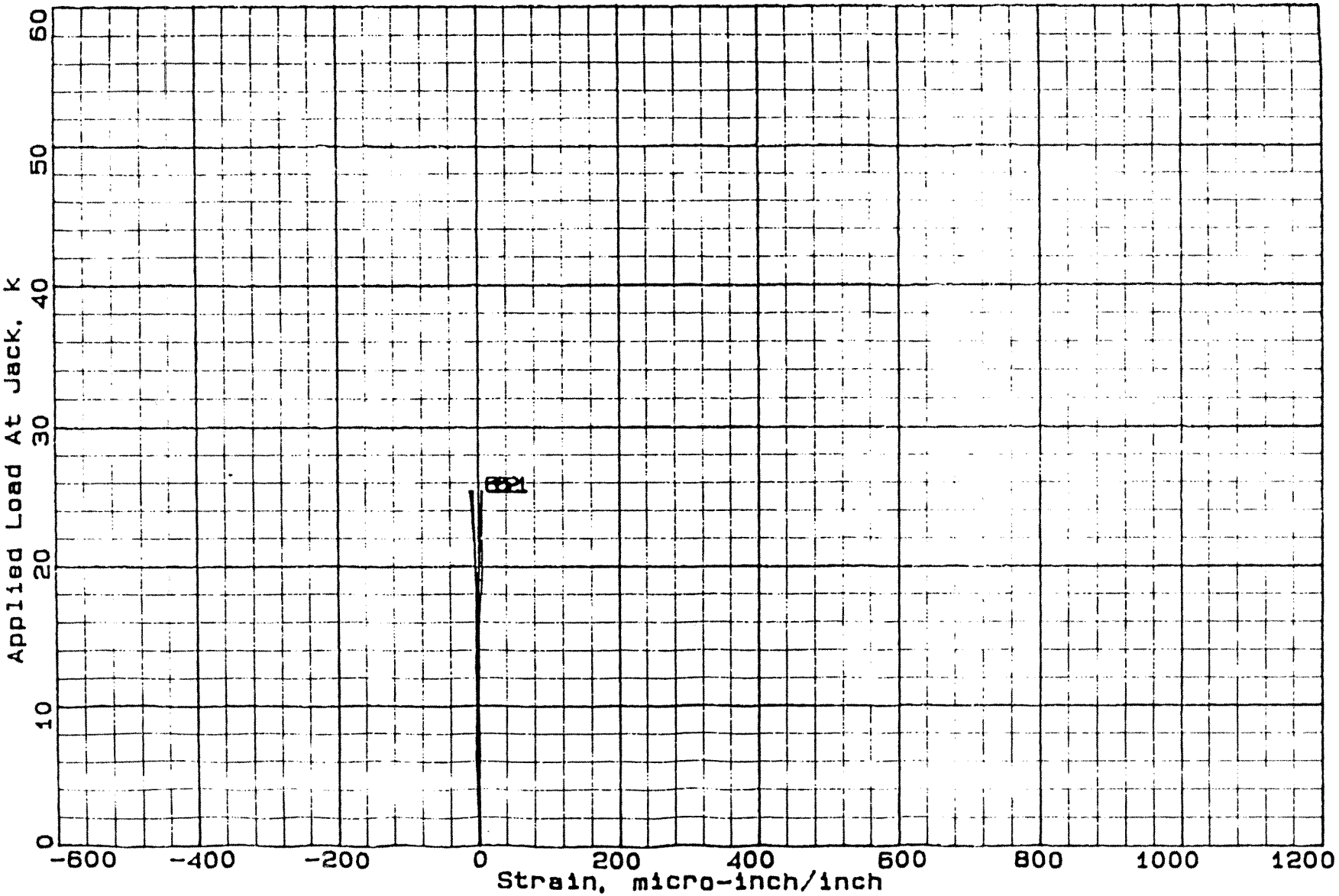

Fig. B-8 - Strain vs Load For East Span Gages 5, 6, 11, And 12 At 0 Fatigue Cycles (Test #2, Run 12)

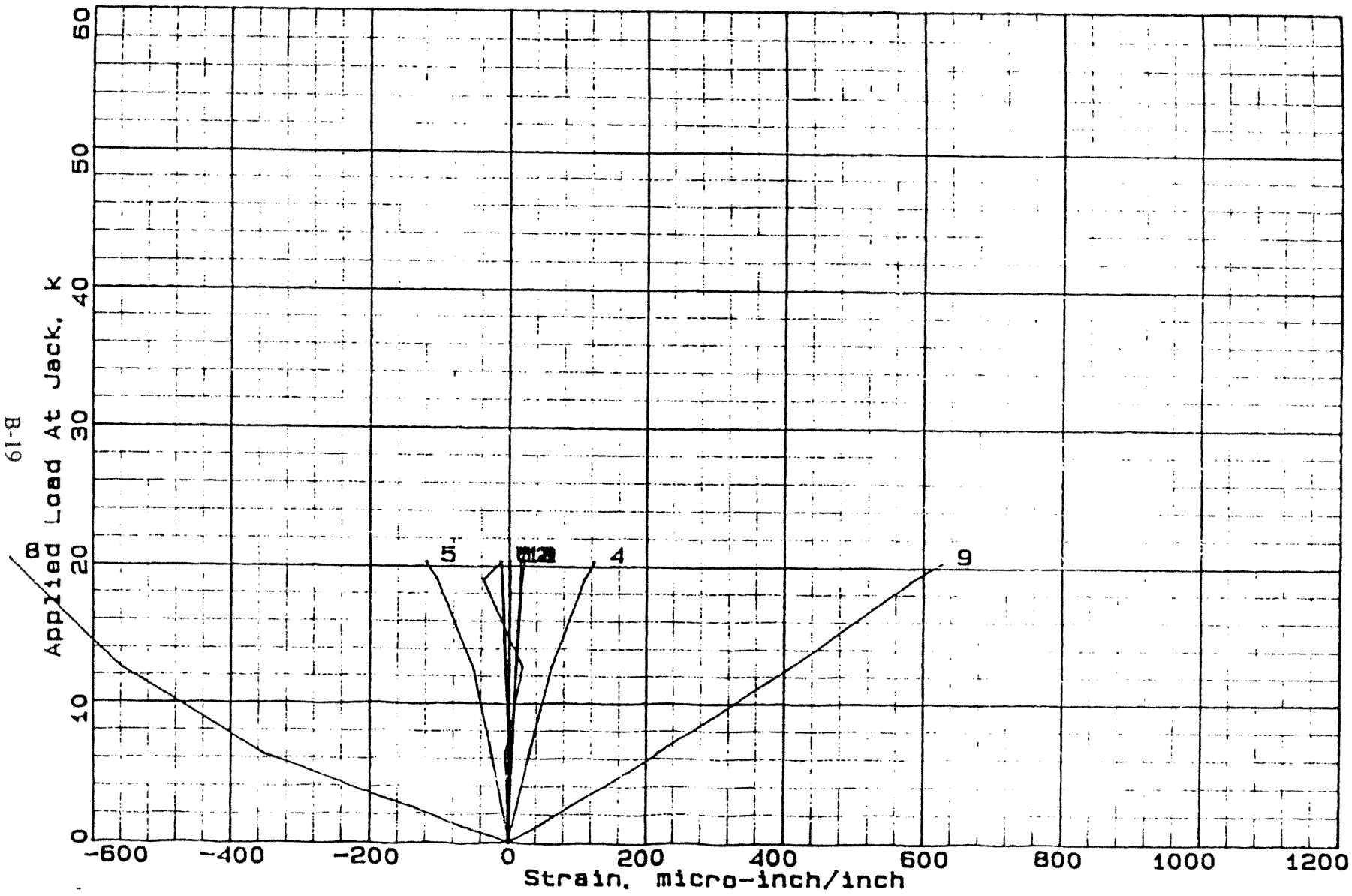

Fig. B-9 - Strain vs Load For All Gages At 2,528,600 Fatigue Cycles (Test #2)

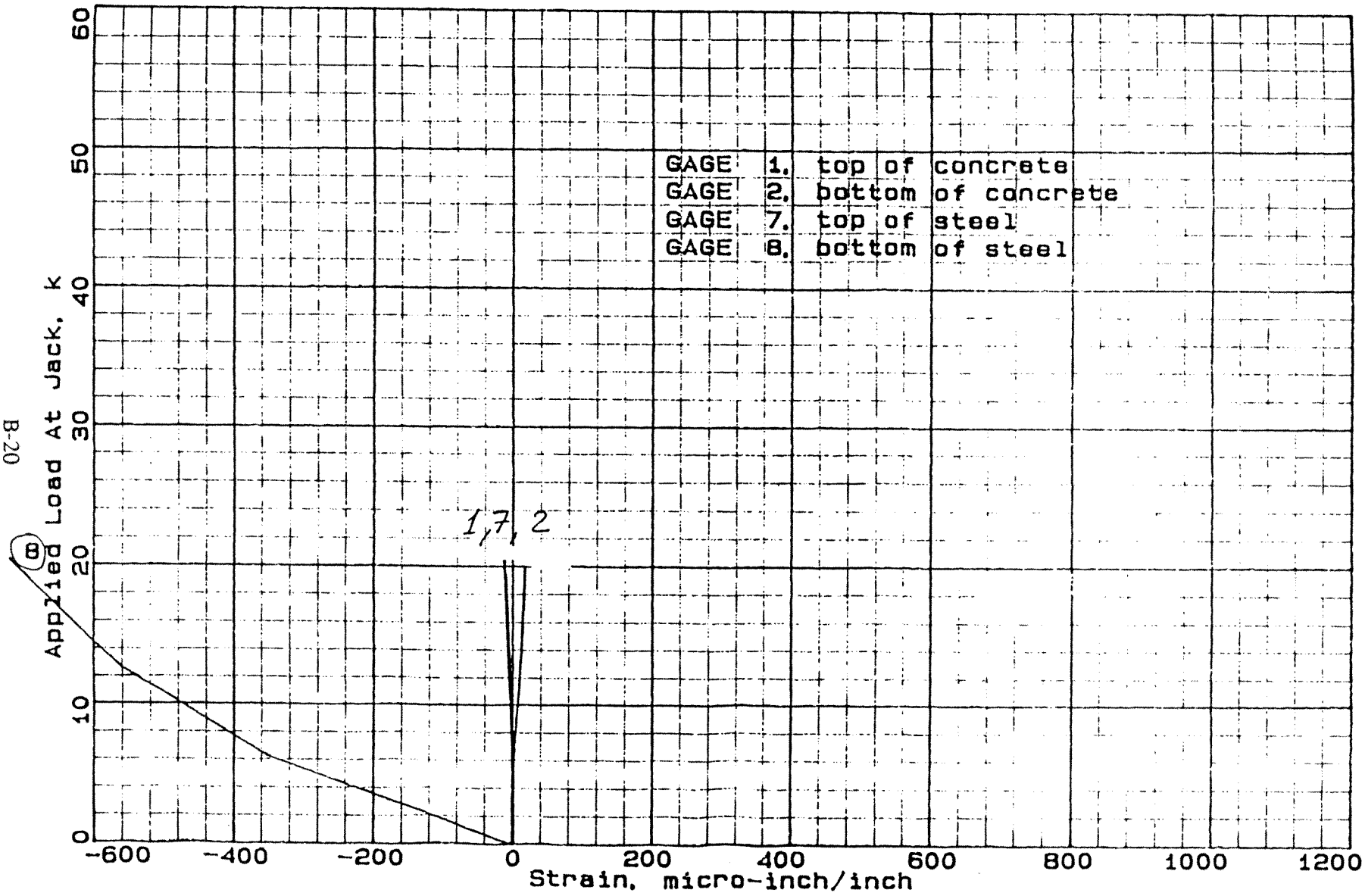

Fig. B-10 - Strain vs Load For West Span Gages 1, 2, 7, And 8 At 2,528,680 Fatigue Cycles (Test #2)

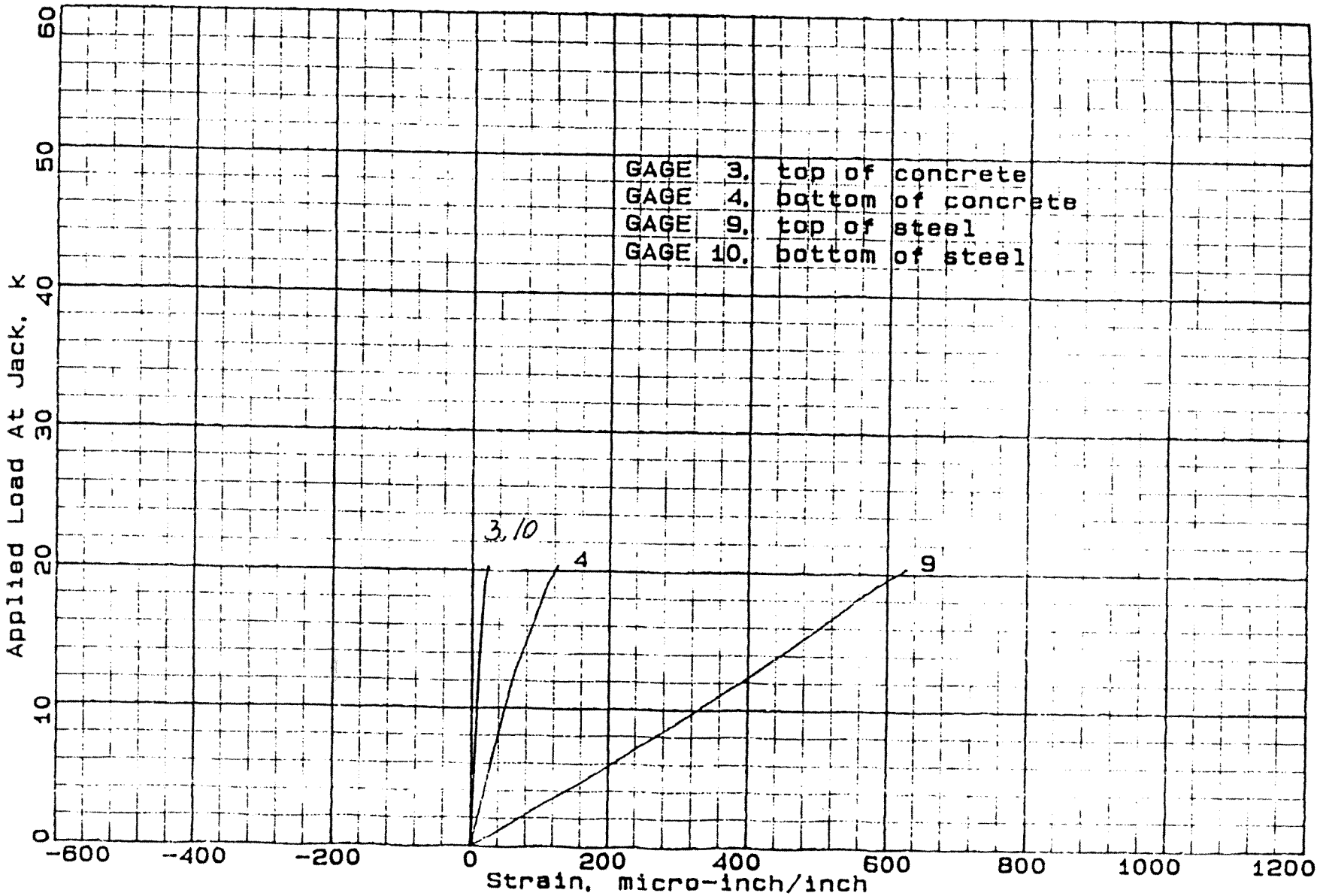

Fig. B-11 - Strain vs Load For Center Support Gages 3, 4, 9, And 10 At 2,528,680 Fatigue Cycles (Test #2)

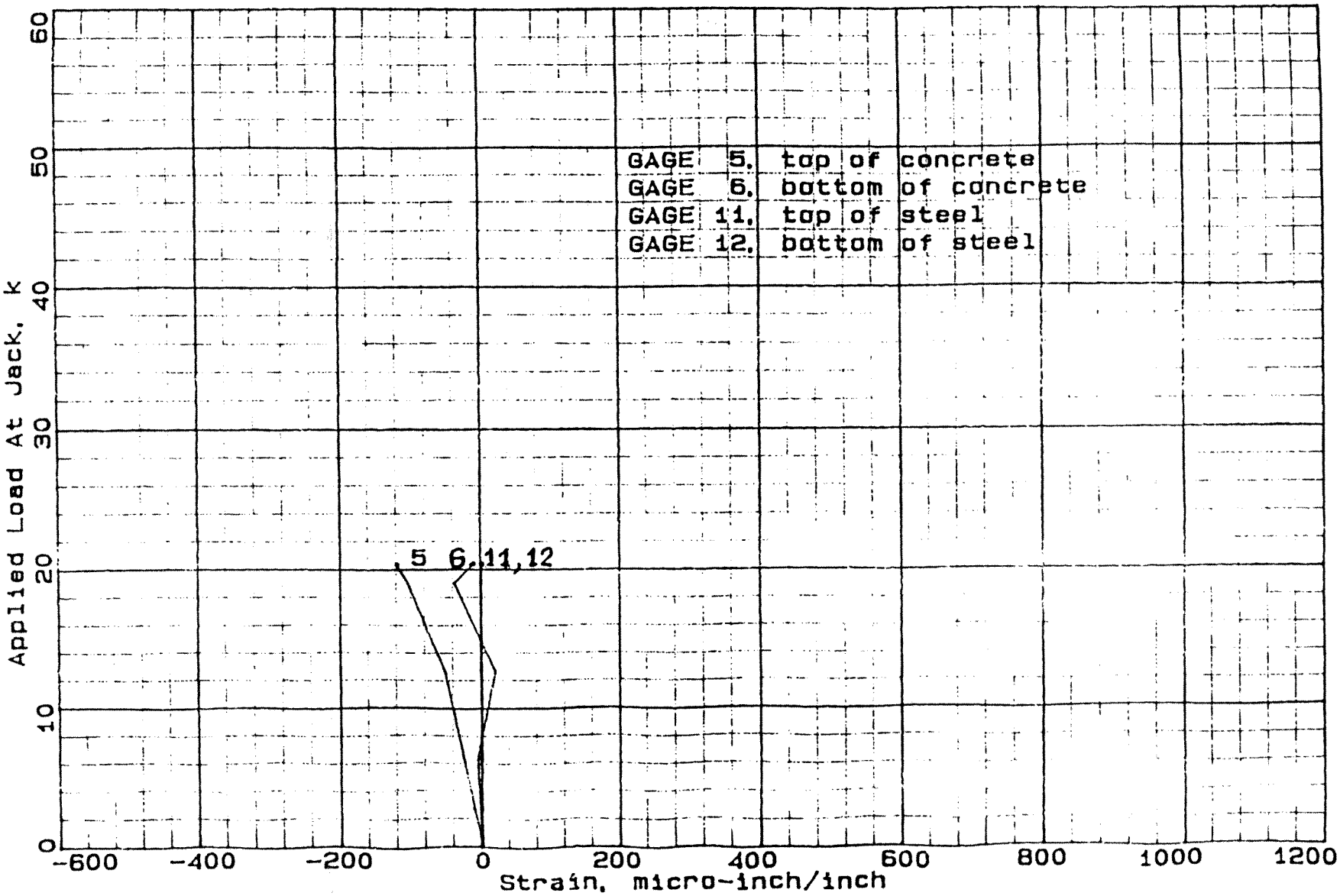

Fig. B-12 - Strain vs Load For East Span Gages 5, 6, 11, And 12 At 2,528,680 Fatigue Cycles (Test #2)

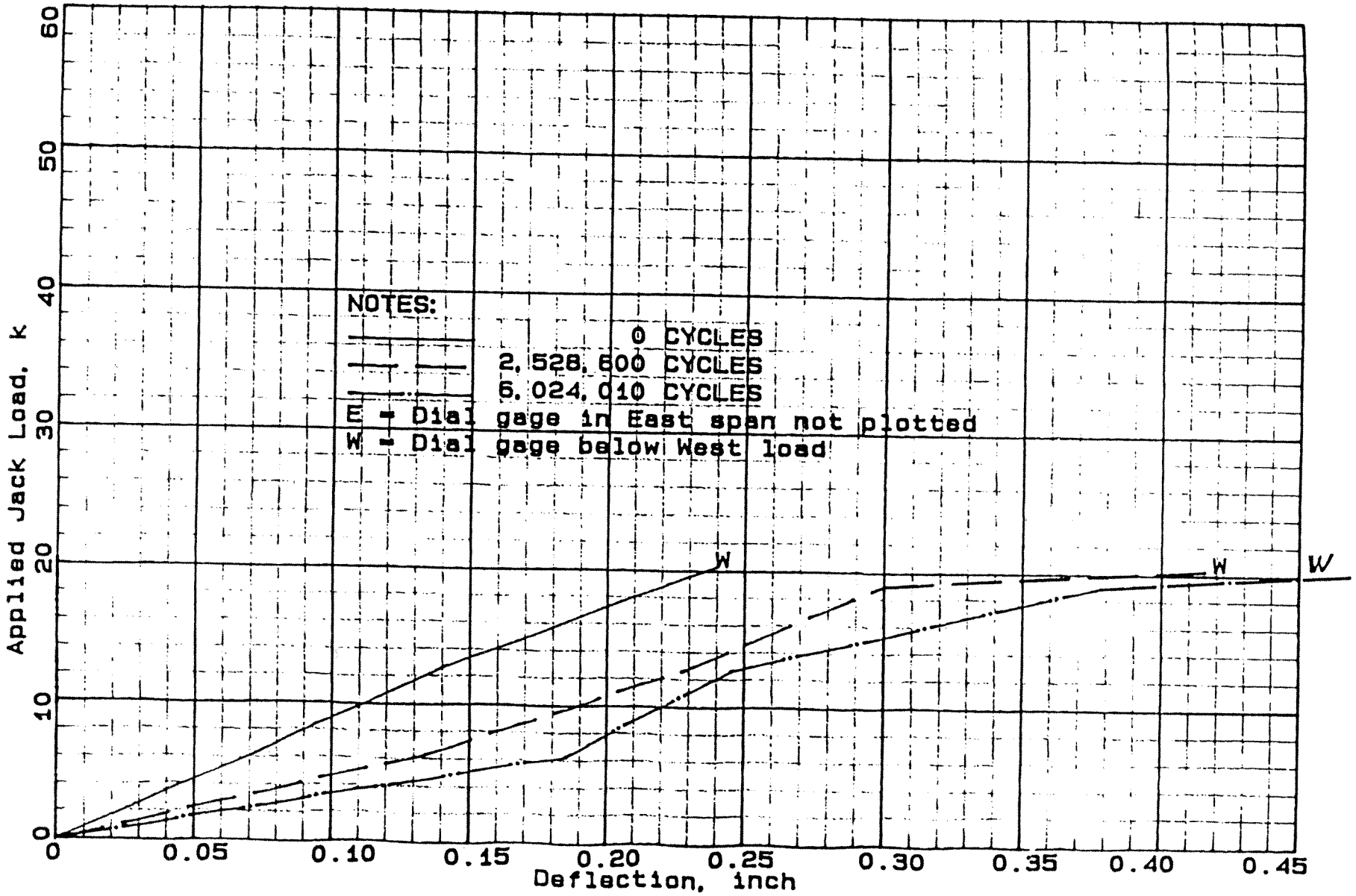

Fig. B-13 - Deflection vs Load In Both Spans At 0, 2,528,680, And 6,024,010 Cycles (Test #2)

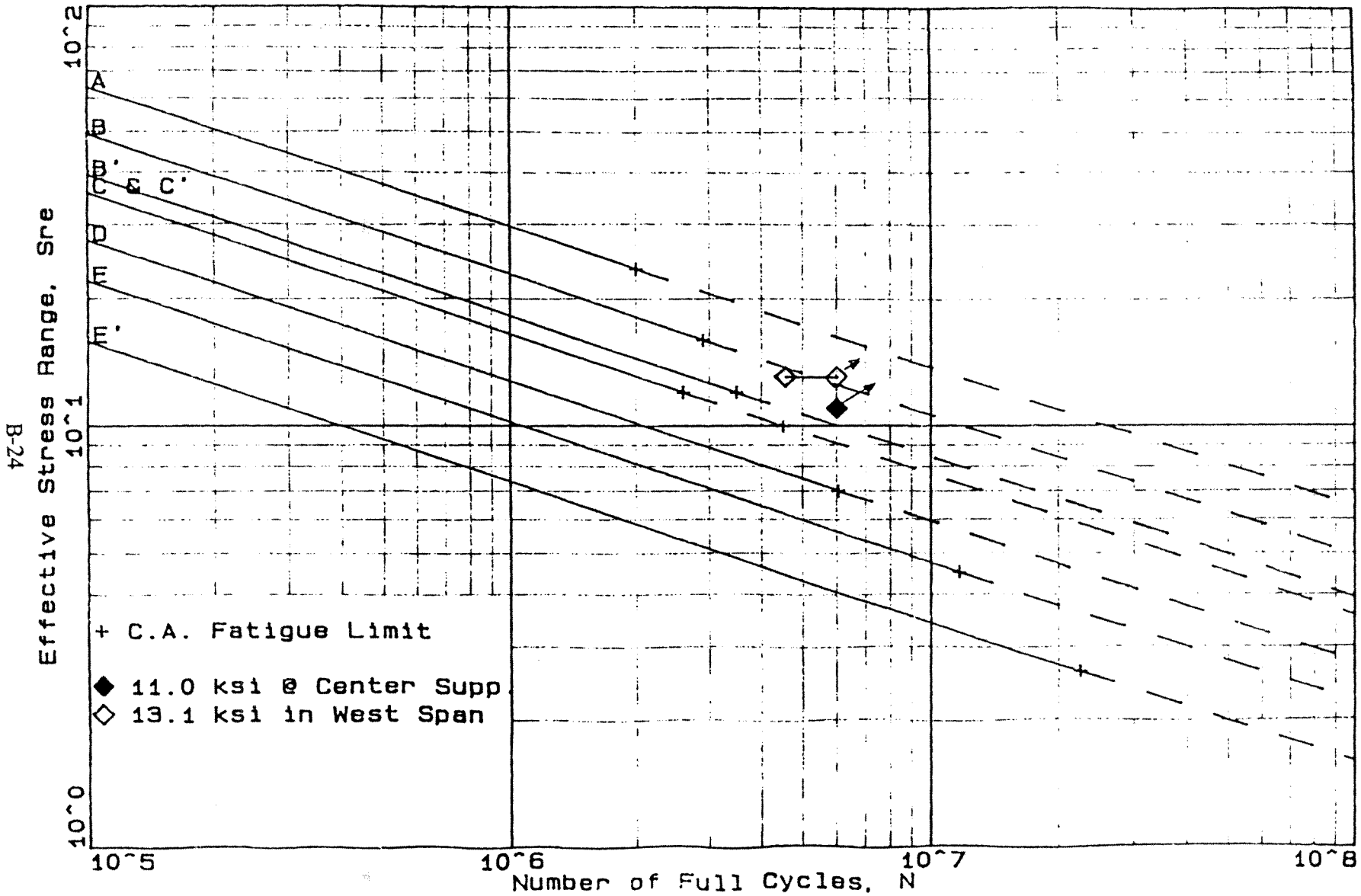

Fig. B-14 - Fatigue Failures Of Main Steel Bars In Test #2 Compared With 1991 AASHTO Fatigue Categories

APPENDIX C - FATIGUE TEST #3

C-1 OBJECTIVES

Based on what had been learned from Test #1 and Test #2 it was decided to essentially use the same approach for Test #3 as was used for Test #2, but utilize the same type of steel grid as in Test #1 because the 4-1/4 INCH INTERLOCK filled with concrete and overfill is the most popular type of steel grid for which more information was highly desirable. However, steel deck used for Test #3 had a main bar spacing of 8 inch whereas the steel deck in Test #1 had a main bar spacing of 6 inch. Otherwise, the steel decks in Test #3 and Test #1 were the same.

Another objective for Test #3 was to obtain static strain/deflection and fatigue data more frequently. This objective was implemented because it was felt to be important to find out if and when strains and deflections are shifting and to have a better assurance of the number of cycles at which the first fatigue cracks occur, similar to the approach used for Test #2.

As for Test #2, another objective was to utilize the 6-inch-wide center support and the trailer axle with a 40 kip actuator. Also it was decided to utilize the same span as for Test #1 and a load range such that failure would not occur before 2 million cycles.

C-2 TEST SETUP

As seen from Figures 1 and 2, the trailer axle used during Test #2 with a rated capacity 22,000 pounds was used to introduce a single actuator load through one of the spring-leaf brackets into the wheels, and through the wheels into the deck. Since the deck was stronger than the one used in Test #2 but nearly as strong as the one used in Test #1, the span increased to 117 inches, which exceeds the maximum clear span recommended in IKG's product catalog.

The load transfer from the actuator through the trailer axle causes tire imprints as shown in Figure 3. As in Test #2, a 40-kip actuator was used which provided enough load capacity to provide the desired loads.

Dial gages were used below the deck at both mid-spans. The type and location of the strain and dial gages employed are summarized in Table C-1. The strain gage locations are also shown in Figure C-3.

C-3 ADDITIONAL SPECIMEN DETAILS

Geometric details of the Test #3 specimen are shown in Figures C-3 and C-4. Physical and other geometrical data are described in the main body of this report. The main bar spacing of the steel grid was 8 inches.

The concrete mix contained river gravel with a maximum size of 3/4 inch. While pouring the concrete, a slump of approximately 1 inch was measured. The average concrete strength after 42 days of curing, based on the average of two 3-inch-diameter samples, was 4,385 psi, which almost met the minimum specified strength requirement of 4,500 psi.

C-4 TEST PROCEDURE AND DATA ACQUISITION

At the beginning of the test a static-load calibration test was made such that the stress range at the bottom fiber of main Bar 6 at the middle of the west span would be 13.1 ksi. This was done with the intent to establish that the fatigue details at the bottom of the deck would fall into AASHTO fatigue Category C if no cracks were observed before 2 million cycles were reached. If under such stress ranges a minimum of 6 million cycles would be reached without any fatigue failure in any of the main bars, the details could be classified as Category B.

After calibration, when it was attempted to initiate the fatigue test, it soon was to be realized that the desired stress range along with a minimum stress of 1.31 ksi could not be realized with the hydraulic equipment at hand. The reason for this disappointing finding was twofold: (1) the use of a trailer axle with tires had increased the required jack/oil displacement significantly by comparison with that required during Test #1 during which steel plates were used to imprint the loads, and (2) the mechanical setting of the test speed could not be lowered any further. Thus, the oil

supply was not sufficient to meet the demand, and the maximum load reached during fatigue testing fell to about 65 percent (26 kip) of the 40-kip jack capacity. This was especially disappointing in view of the fact that loads up to 35 kip for two very large diameter actuators (80 kip capacity) were successfully operating at 2 cps during Test #1.

Consequently, it was decided to continue the use of the trailer axle and the 40 kip actuator. The upper and lower loads during the fatigue test were set at 24.6 and 2.2 kip (61.5 and 5.5 percent), respectively. This provided maximum and minimum stresses of 11.5 and 1.0 ksi, respectively, or a stress range of 10.5 ksi at Bar 6. To qualify the positive bending moment region as Category C, a minimum of 3.9 million cycles without cracks had to be applied. To qualify this region as Category B, this region of the deck had to endure a minimum of 10.3 million cycles without any cracks.

With the above settings the maximum and minimum stresses in the negative bending moment region, at the top fiber of the steel grid above the interior support, were 10.3 and 1.0 ksi, respectively, resulting in a stress range of 9.3 ksi at Bar 6. To qualify the negative bending moment region as Category C, the deck had to survive a minimum of 5.6 million cycles without cracks. To qualify this region as Category B, this region of the deck had to sustain a minimum of 14.8 million cycles without any cracks.

In addition to the initial static calibration test made at the beginning of the fatigue test, several other static calibration tests were made during the testing process. The fatigue test was stopped and the static strain/deflection/load data were taken at three load levels. The load levels used (0, 6.34, 12.68, 19.02, 25.36, and 0 kip) were equivalent to voltmeter settings of 0, 1, 2, 3, 4, and 0 Volt.

C-5 RESULTS

The results of the static-load tests made at the beginning and during the testing process are displayed in strain-versus-load and deflection-versus-load graphs identified below. For easier reference, the strain-gage types and locations are described in detail

in Table C-1. In addition, highlights of the inspection recordings are given in Table C-2. As seen from this table, numerous inspections were made. Only the most pertinent inspection records are given in Table C-2 and will be discussed below.

The speed of testing achieved was slightly less than 2 cycles per second. Minor variations unintentionally occurred during the testing process.

C-5.1 Strain-Gage Data

Static strain gage calibration checks were made at several stages of the fatigue test. The results are described below.

C-5.1.1 Strain Gage Data At Zero Fatigue Cycles

Prior to applying the first fatigue loads, static calibration checks were made, and the recorded strains at chosen load levels were plotted. The recorded strains for Run 4 are plotted in Figures C-5 through C-13. Only three static incremental cycles had been applied prior to the results shown in the figures.

For most of the gages the plotted strains are almost linear. As seen from Figure C-5, the least linear behavior is found in concrete Gage 1 which was located on the top surface of the test slab at the mid-length of the west span, along the longitudinal centerline. This is confirmed by Figure C-6, which is an assembly of all concrete strain gage readings at zero fatigue cycles, and by Figure C-7, which represents an assembly of all readings of concrete strain gages below the west span load.

Figure C-8 is an assembly of the concrete strain gage readings (Gages 5 through 7) for the west span. All strain gages appear to show a fairly linear behavior. This is most likely true because the stress/strain levels are not as intense as at the longitudinal centerline of the specimen.

Figure C-9 represents the concrete strain gage readings (Gages 8 through 10) recorded at the center support near the longitudinal centerline. The plot indicates an almost perfect linear behavior of all gages, which also is attributed to the low stress/strain intensity experienced at this location. The behavior of the strain gages at this location is even more linear because of the lower strain intensity.

The readings for all steel gages (Gages 11 through 16) are accumulated in Figure C-10. The tendency of their behavior is predominantly linear. This is

confirmed by the isolated steel strain gage plots provided in Figure C-11 through Figure C-13.

C-5.1.2 Strain Gage Data At 1,489,930 Fatigue Cycles

After 1,489,930 fatigue load cycles had been applied, the resulting static strain gage readings accumulated in Figure C-14 seem to be more widely dispersed than the readings recorded prior to the commencement of the fatigue tests previously presented in Figure C-5. This is confirmed by the plot shown for all concrete gages in Figure C-15, and in isolated plots for concrete strain gage locations shown in Figures C-16 through C-18.

Also, some of the steel gages seem to have become slightly non-linear as shown in the accumulation of all steel strain gage data presented in Figure C-19. Figures C-20, C-21, and C-22 isolate the strain vs load behavior for specific locations such as the west span below the tire load, west span away from the tire load, and the center support, respectively. As indicated in Table C-2, no cracks had yet been detected in the main steel bars. Thus, the non-linearity observed is mainly contributed to the possibility that de-bonding between concrete cubicles and the steel grid had progressed, and mainly so in the region of the west span below the tire load.

C-5.1.3 Strain Gage Data At 4,278,610 Fatigue Cycles

Results of another static load record of the strain gages, logged after 4,278,610 fatigue cycles had been applied, are shown in Figures C-23 through C-30. As seen from Table C-2, at this point in time, cracks had already been observed in the bottom flanges of Bars 5, 6, and 7, and at multiple locations in the top surface of the concrete below and around the wheel load in the west span.

As seen from Figures C-24 and C-25, the concrete strain gages in the west span below the wheel load (Gage 1 and 4, see Table C-1) behaved non-linearly or did not function any more (Gage 2, at mid span, close to top of steel bars). Figure C-25 shows non-linear behavior of concrete Gages 5 and 7. Concrete Gages 8 through 10, located at the center support along the longitudinal centerline still showed a linear response to the applied loads, as seen from Figure C-27.

The response of all steel gages (Gages 11 through 16) is shown in Figure C-28. For distinct locations such as West Span Below Load, West Span Off Load, and Center Support, the response is shown in Figures C-29, C-30, and C-31, respectively. A s seen from Figure C-29, Gage 11 (located at the top of center steel Bar 6, on compression side) still shows a linear response to the applied static loads while Gage 12 (located at the bottom of center steel Bar 6) hardly shows any response at all because of adjacent cracks (see Table C-2). A comparison of Figure C-29 with Figure C-11 shows that the strain in Gage 11, after application of 4,278,610 load cycles, was about two times the magnitude of the strain recorded at zero load cycles. This confirms the expected major shift in strains and stresses after cracks have occurred in the main steel bars.

As shown in Figure C-30, steel Gages 13 and 14, which are located in the west span away from the wheel load, are still responding correctly in the negative (compressive) and positive (tensile) direction. By comparison with Figure C-12 at zero fatigue cycles, the strains have also about doubled. This is also the case for steel strain Gages 15 and 16, which are located at the center support, as seen from a comparison of Figure C-31 with Figure C-13.

C-5.1.4 Strain Gage Data At 5,350,580 Fatigue Cycles

No strain gage records were made after the test was terminated. The researchers felt that no further documentation was needed to show the shift of strain/stress from the center bars to the adjacent bars after cracking of the bars below the applied wheel load had occurred.

C-5.2 Deflection Data

Deflections (the change of distance between the bottom of the deck and the floor) were recorded throughout the test. The results of the initial and subsequent static test measurements are shown in Figure C-32. This figure assembles and allows a comparison of the deflections in the west span after 0, 1,489,930, and 4,278,610 had been applied.

At the maximum calibration load of 25.36 kips, the measured west span deflections changed from about 0.175 inch at the beginning of the fatigue test to

0.275 inch after 4,278,610 load cycles had been applied. This represents an increase of 57 percent while the test was still going on. Eventually, the test was discontinued after 5,350,580 cycles. No load-deflection records were made at that time.

C-5.3 Concrete Cracks

As indicated in the described highlights of the inspection recordings summarized in Table C-2, concrete cracks were observed at the top of the slab in the center support region immediately after the slab was installed for fatigue testing. This indicates that, in field applications, utilization of pre-poured steel/concrete slabs, may result in concrete cracking before the slab is exposed to regular traffic.

C-5.4 Steel Bar Cracks

Highlights of inspection recordings contained in Table C-2 show that the first visible steel cracks occurred across the bottom flange in the west span main steel Bars 5, 6, and 7 after 3,590,050 fatigue cycles had been applied. Earlier attempts to reveal minute cracks by dye penetration procedures were not successful.

When an inspection was made at 4,275,500 cycles, an additional crack was found in the west span across the bottom flange of main steel Bar 6. As seen from Figures C-28 and C-29, steel strain Gage 12 (located in west span, below load, at bottom of center Bar 6) did not show any load response any more, and other gages showed increased load responses (compare Figure C-28 with C-10), as would be expected when some of the main bars (Bars 5, 6, and 7) had already failed.

At 5,350,580 load cycles, ten of the eleven main bars had cracked, Bars 5 and 6 at two placed, and the system automatically shut off because of the installed limit deflection switch. More details are recorded in Table C-2 which summarizes the highlights of the inspection recordings.

Future work has been proposed to remove a 6-inch-wide deck strip below the loads, remove the concrete, and open up the main steel bar cracks to determine the crack initiation sites in the bars. In the final fatigue evaluation of the steel grids tested, it is important to fatigue-categorize the decks on the basis of where the fatigue crack initiated, and at what nominal stress this occurred. Regarding the lower portion of the

tested steel grid tested, the unanswered question is if the fatigue cracks initiated at the outer fiber of the tension flange, at the tack welds that attach the pan sheets to the main bars, or at the lower fiber of the web punchouts.

C-5.5 S-N Fatigue Comparison

The results of the fatigue-crack observations contained in Table C-2 were used to compare the crack occurrences in the floor slab tested with the present (1991) AASHTO fatigue design provisions. The AASHTO fatigue design lines and the fatigue-crack observations are shown in Figure C-33. Criteria for the AASHTO fatigue design curves were discussed previously.

The cycle ranges of the fatigue crack data obtained for the positive moment in the west span are plotted as a horizontal line at the stress range level of 10.5 ksi. This stress was measured at steel Gage 11 when fatigue testing began. The gage was located below the tire load at the bottom fiber of Bar 6, 58.5 inch from the center support. The left symbol of the cycle range denotes the number of fatigue cycles at which a crack was first observed (3,590,050 cycles), and the right symbol denotes the number of fatigue cycles at which the fatigue test was terminated (5,350,580 cycles). As seen from Figure C-33, the bar straddles the fatigue Category C, C', and B' lines.

Cracks could not be observed in the top fibers of the steel bars at the center supports where a negative bending moment occurs. As seen from Figure C-31 and Table C-2, strain Gage 15, which was located on top of Bar #6 at the longitudinal centerline of the center support, was still working satisfactorily at 4,278,610 cycles. Therefore, a run-out symbol was used in Figure C-33 at the stress range level of 9.3 ksi and 5,350,580 cycles.

As seen from Figure C-33, the results for Test #3 fall slightly to the left of the Category C fatigue line but, in the opinion of the researchers, are still justified to be considered a Category C detail. Since the study did not show where the cracks initiated (possibly at tack welds or at punch outs rather than at the extreme bottom fiber), no further refinements regarding the categorization can be made.

C-6 CONCLUSIONS

Testing of the Test #3 specimen was discontinued after numerous static and fatigue data had been obtained and 5,350,580 load cycles had been applied. Some of the data taken and considered typical and important to explain or back up conclusions drawn were presented in this appendix.

The strain gage data presented indicate that there was a significant shift in strains and stresses while the fatigue test proceeded. However, the magnitude of the change can not accurately be determined because many gages failed in the testing process and because the moment distribution within the specimen shifted.

The fatigue results obtained indicate that the applicable fatigue category for the 4-1/4-Inch Interlock Panel used, with a main bar spacing of 8 inch, filled with concrete and an overfill of 1-5/8 inch, should be classified as Category C. This category is applicable for the positive as well as the negative bending moment region of this type of deck.

It is suspected, that if tack welds could be avoided at the bottom of the steel deck in the positive bending moment region and at the top in the negative bending moment region, an upgrading to Category B may be possible. Further tests on small specimens are recommended to confirm this.

Table C-1 - Strain Gage Types And Locations For Test #3

Gage Number	Gage Type	Gage Location
1	Concrete	Top of concrete, west span, 58.5 inch from center support, along longitudinal centerline of slab, above main steel Bar 6, placed after concrete was poured.
2	Concrete	Embedded in concrete, west span, 58.5 inch from center support, at elevation close to top of steel cross bars, approximately 1-5/8 inch below top of finished concrete, near longitudinal centerline of slab, between main steel Bars 6 and 7, placed before concrete was poured.
3	Concrete	Embedded in concrete, west span, 58.5 inch from center support, at elevation close to bottom of steel cross bars, near longitudinal centerline of slab, between main steel Bars 6 and 7, approximately 3-1/8 inch below top of finished concrete, placed before concrete was poured.
4	Concrete	Bottom of concrete, west span, 58.5 inch from center support, near longitudinal centerline of slab, between Bars 6 and 7, steel pan locally removed, placed after concrete was poured.
5	Concrete	Top of concrete, west span, 58.5 inch from center support, approximately 20 inch south of longitudinal centerline of slab, between main steel Bars 8 and 9, placed after concrete was poured.
6	Concrete	Embedded in concrete, west span, 58.5 inch from center support, at elevation close to top of steel cross bars, approximately 20 inch south of longitudinal centerline of slab, between main steel Bars 8 and 9, approximately 1-5/8 inch below top of finished concrete, placed before concrete was poured.
7	Concrete	Bottom of concrete, west span, 58.5 inch from center support, approximately 20 inch south of longitudinal

(continued)

Table C-1, continued

Gage Number	Gage Type	Gage Location
		centerline of slab between Bars 8 and 9, steel pan locally removed, placed after concrete was poured.
8	Concrete	Top of concrete, above center support, along longitudinal centerline of slab, above main steel Bar 6 placed after concrete was poured.
9	Concrete	Embedded in concrete, above center support, at elevation close to bottom of steel cross bars, approximately 3-1/8 inch below top of finished concrete, near longitudinal centerline of slab, between main steel Bars 6 and 7, placed before concrete was poured.
10	Concrete	Bottom of concrete, above center support, near longitudinal centerline of slab, between main Bars 6 and 7, steel pan locally removed, placed after concrete was poured.
11	Steel	West span below load, top of main steel Bar 6 along longitudinal centerline of slab, 58.5 inch from center support, 1-5/8 inch below concrete surface, placed before concrete was poured.
12	Steel	West span below load, bottom of main steel Bar 6 along longitudinal centerline of slab, 58.5 inch from center support, placed before concrete was poured.
13	Steel	West span off load, 58.5 inch from center support, top of main steel Bar 8, 16 inch south of longitudinal centerline of slab, placed before concrete was poured.
14	Steel	West span off load, 58.5 inch from center support, bottom of main steel Bar 8, 16 inch south of longitudinal centerline of slab, placed before concrete was poured.

(continued)

Table C-1, continued

Gage Number	Gage Type	Gage Location
15	Steel	Above center support, top of main steel Bar 6, along longitudinal centerline of slab, placed before concrete was poured.
16	Steel	Above center support, bottom of main steel Bar 6, along longitudinal centerline of slab, placed before concrete was poured.

Table C-2 - Highlights Of Inspection Recordings For Test #3

Number of Cycles	Notes
0	During static calibration, concrete cracks were observed at top above center support. Although a higher fatigue load was desired to cause expected fatigue failure between 2 and 6 million cycles, only an upper load of 61.3 percent of the maximum jack load of 40 kips could be attained, along with a lower load of 5.1 percent, or 24.5 and 2.0 kips, respectively. Thus, the applied load range was 24.5 - 2.0 = 22.5 kips, with approximately up to 5 percent variation below the programmed values while the test proceeded between inspections.
193,390	System shut down automatically. Hydraulic leak in pulsator caused low oil level. System shut off automatically.
533,180	System was shut down because one elbow joint on the pulsator was spewing oil profusely. Elbow joint was later replaced before fatigue testing commenced. Also, at and parallel to center support, three cracks were recorded on top of the concrete overfill.
3,590,050	Inspections were conducted at intermittent cycles (550,000 cycles; 776,550 cycles; 1,489,930 cycles; 1,492,780 cycles; 1,985,000 cycles; 2,467,510 cycles; 2,468,540 cycles; 2,680,000 cycles; and 3,009,320 cycles) without revealing any cracks in the main longitudinal steel bars. At 3,590,050 cycles, cracks were detected at the bottom of Bars 5, 6, and 7. Also found concrete cracks at top of slab below wheel load in west span.
4,275,500	Additional crack was found on main longitudinal steel bar 6 and multiple cracks in concrete below wheel in west span.

(continued)

Table C-2 - continued

Number of Cycles	Notes
5,350,580	System was automatically shut off by a limit-deflection switch located below the west-span wheel load, underneath the concrete slab. Ten of eleven main longitudinal steel bars had cracked in the west span, as visually observed from below the test specimen. Ten of eleven bars were cracked. Bars 5 and 6 were cracked at two places, although the crack in Bar 5 only extended partially through the width of the bar.

POST MORTEM NOTES:

Dr. C. P. Mangelsdorf (University of Pittsburgh) and Mr. Darko Jurkovic (IKG/Greulich Industries) visited the test site at approximately 5,150,00 cycles without finding the test specimen under any distress to sustain the imposed loads.

Fatigue crack initiation sites need to be investigated in a future study to find out what manufacturing detail is critical.

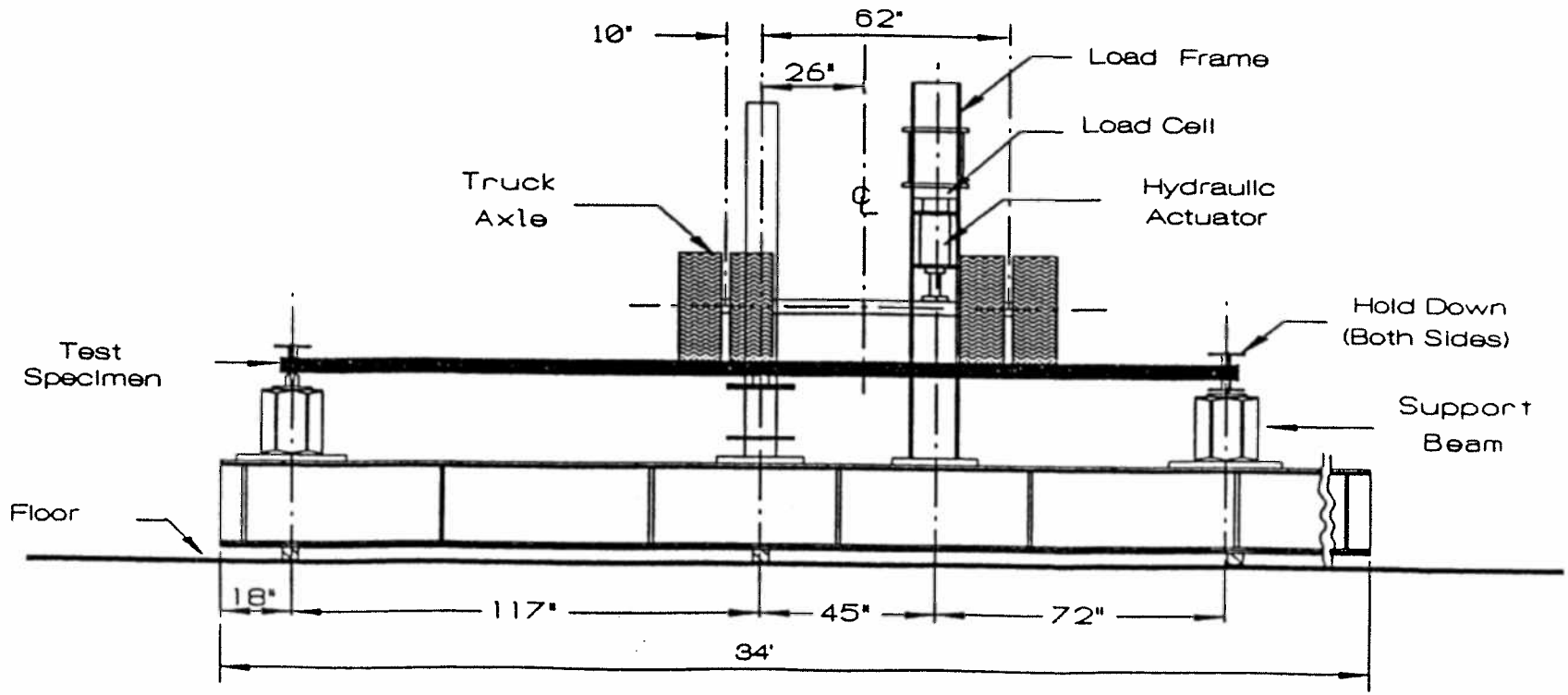

Fig. C-1 - Test Frame Setup For Test #3 -
Section Along Centerline, Viewing South

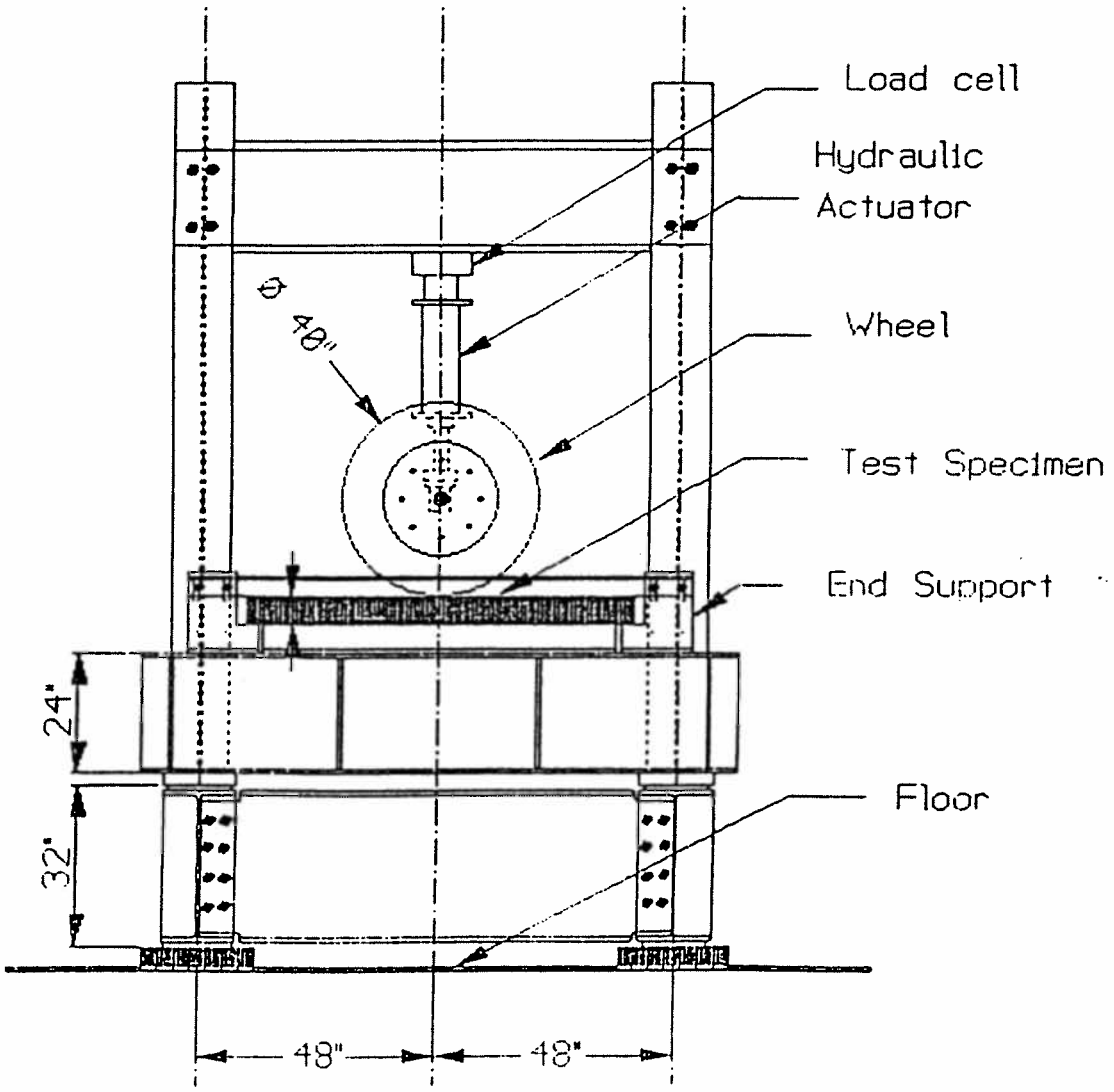

Fig. C-2 - Test Frame Setup For Test #3 - End View

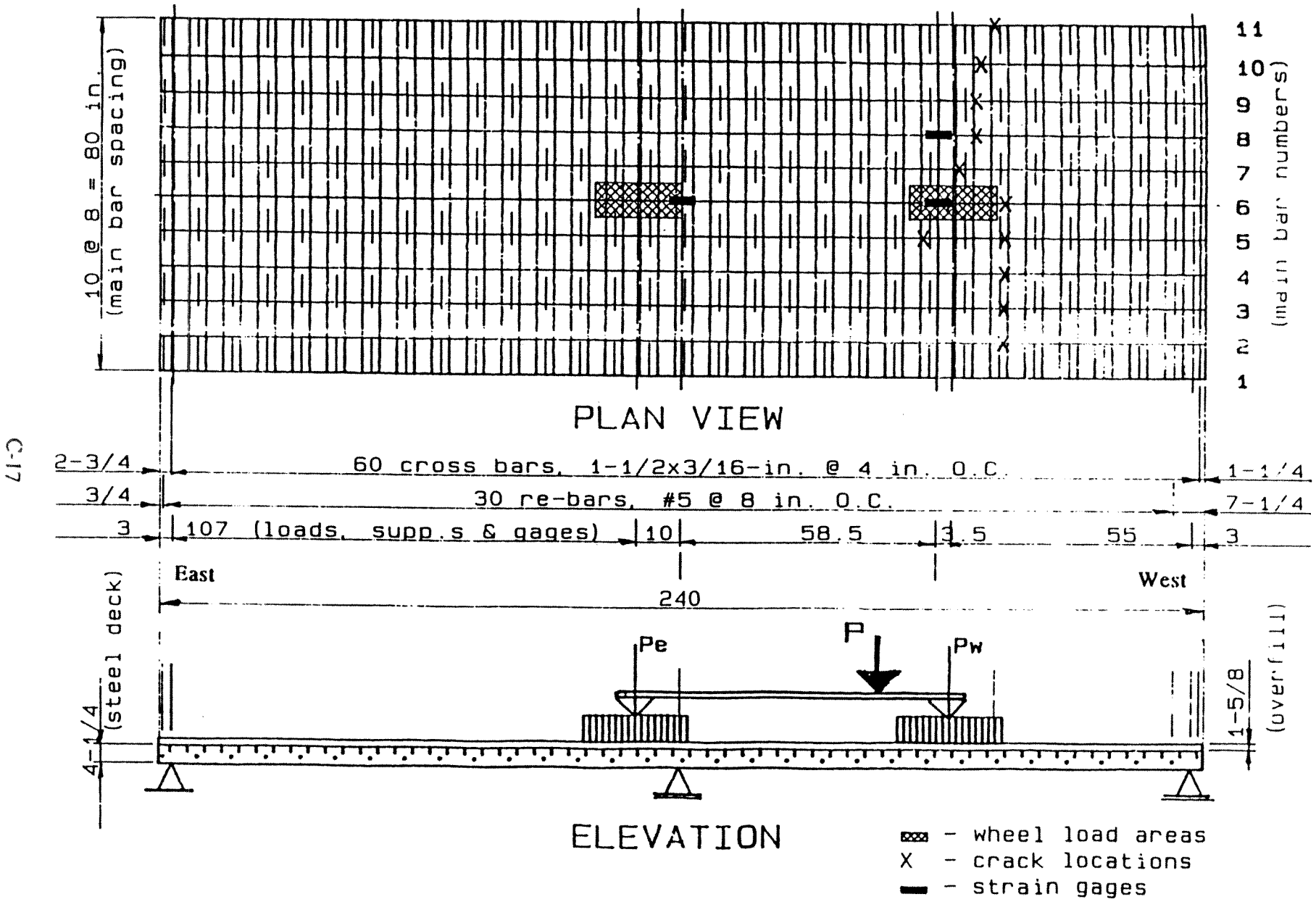

Fig. C-3 - Fatigue Test #3 Specimen - General Arrangement, Including Gage And Crack Locations

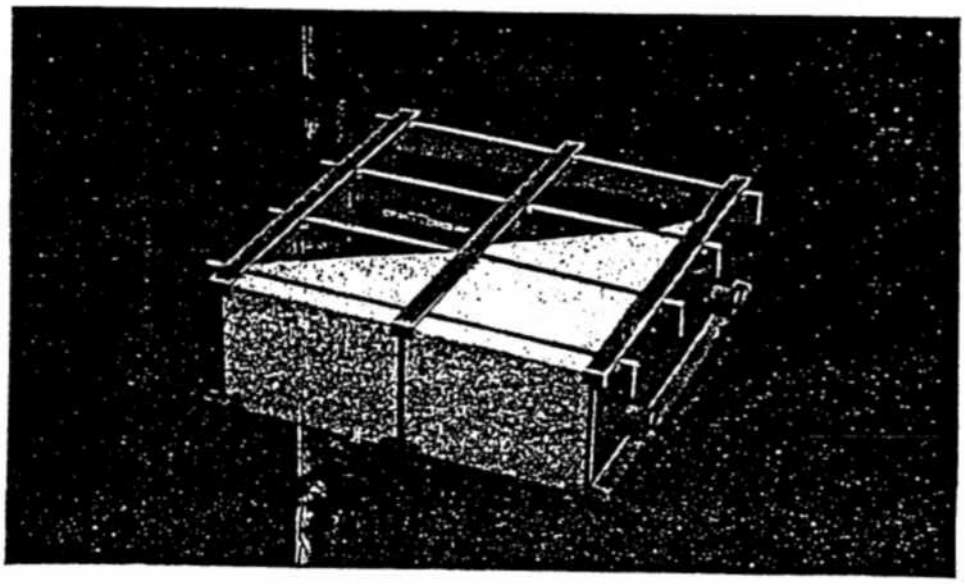

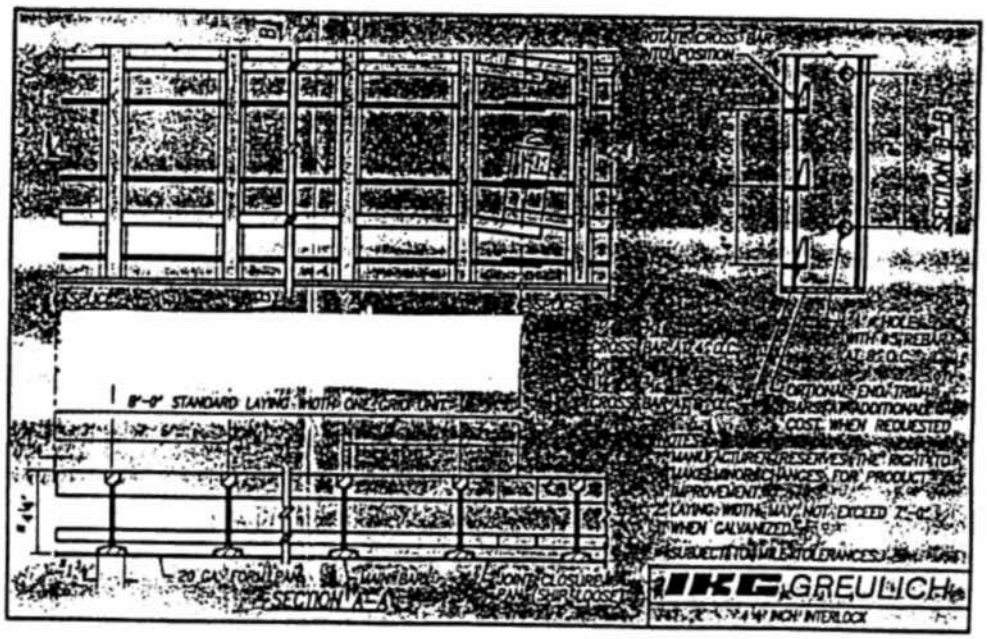

Fig. C-4 - 4-1/4 Inch Interlock Panel Details For Test #3
With 1-5/8-Inch Overfill

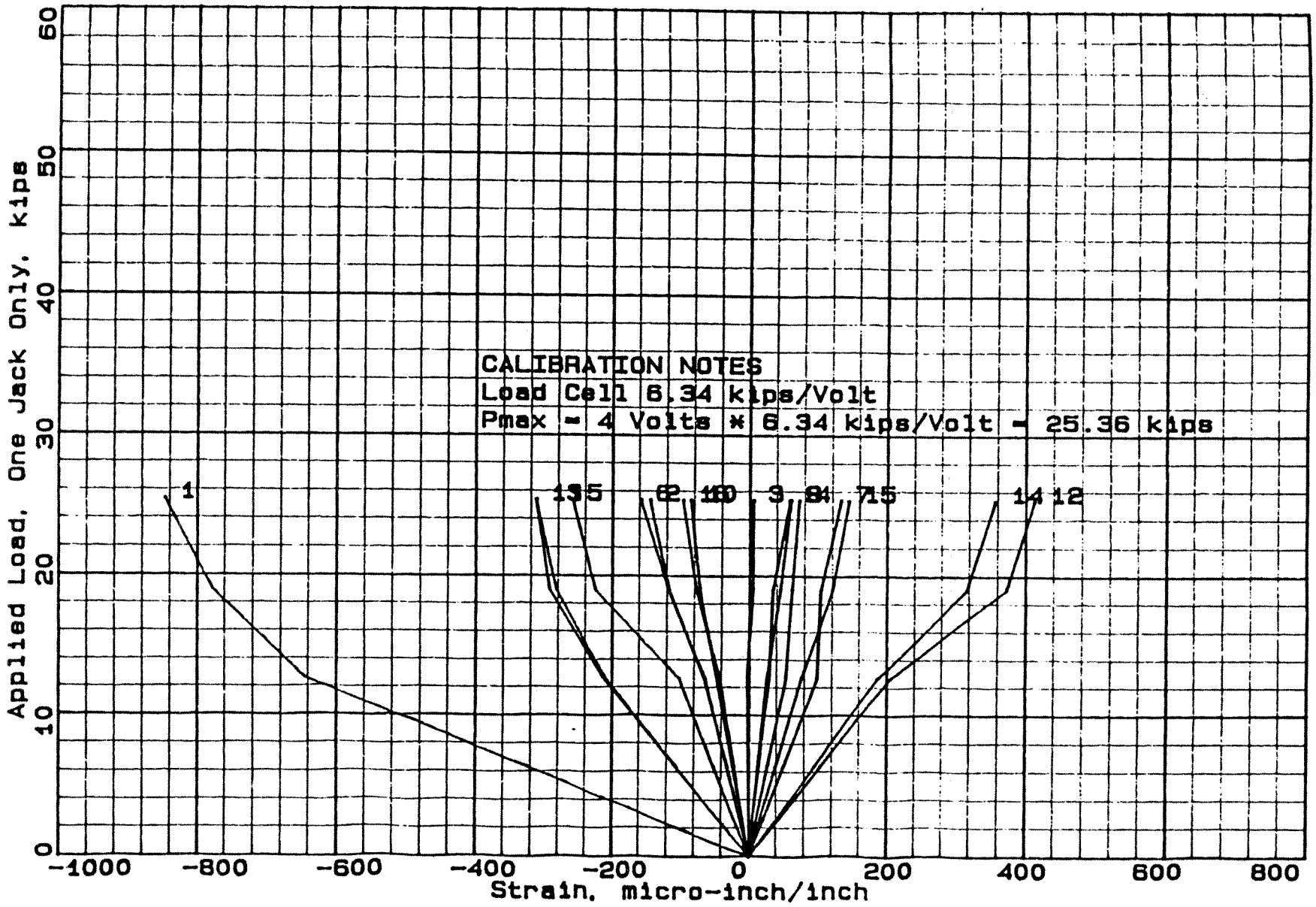

Fig. C-5 - Strain vs Load For All Concrete And Steel Gages At 0 Fatigue Cycles (Test #3, Run 4)

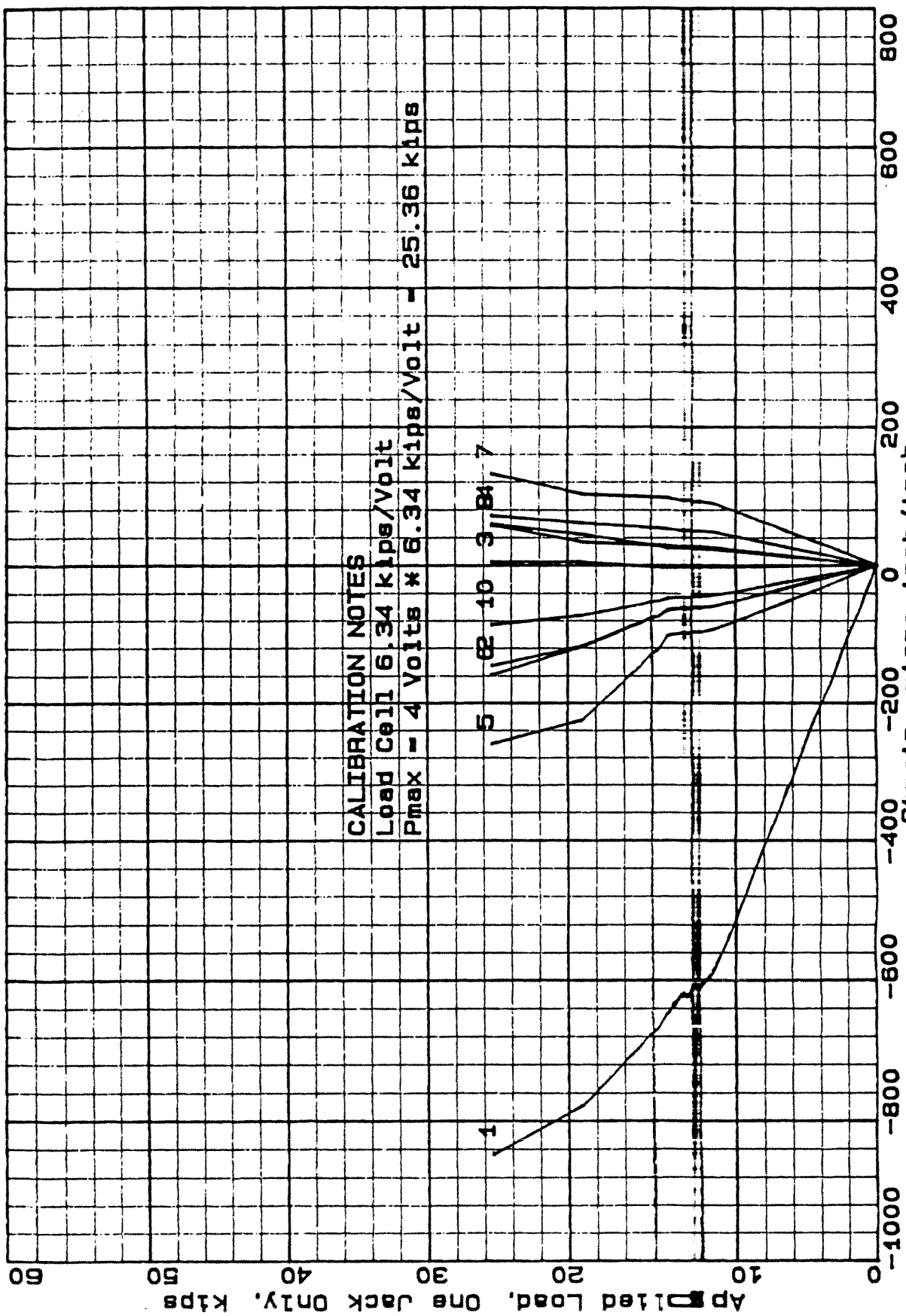

Fig. C-6 - Strain vs Load For All Concrete Gages 1 Through 10
At 0 Fatigue Cycles (Test #3, Run 4)

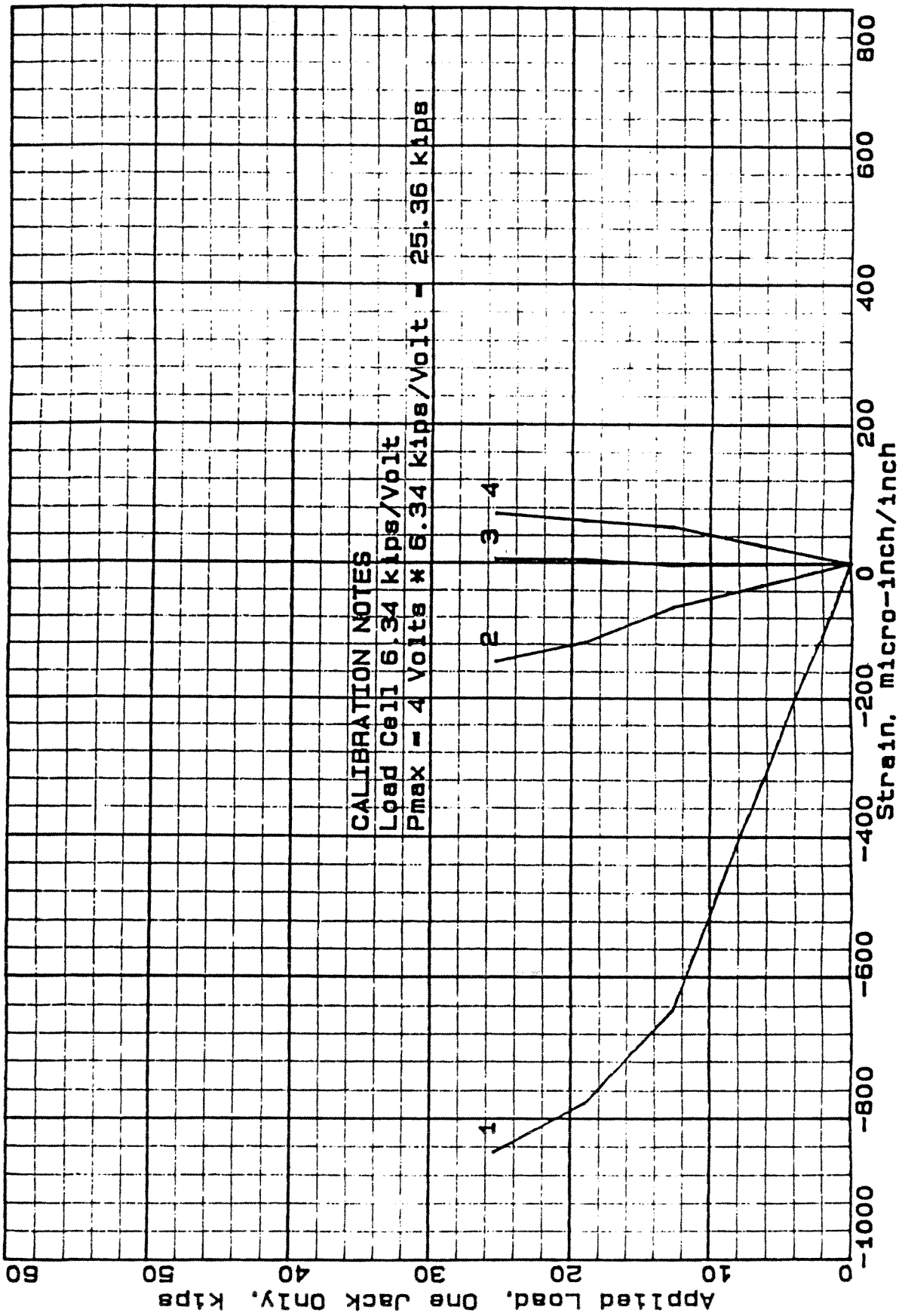

Fig. C-7 - Strain vs Load For West Span Below-Load Concrete Gages 1 Through 4 At 0 Fatigue Cycles (Test #3, Run 4)

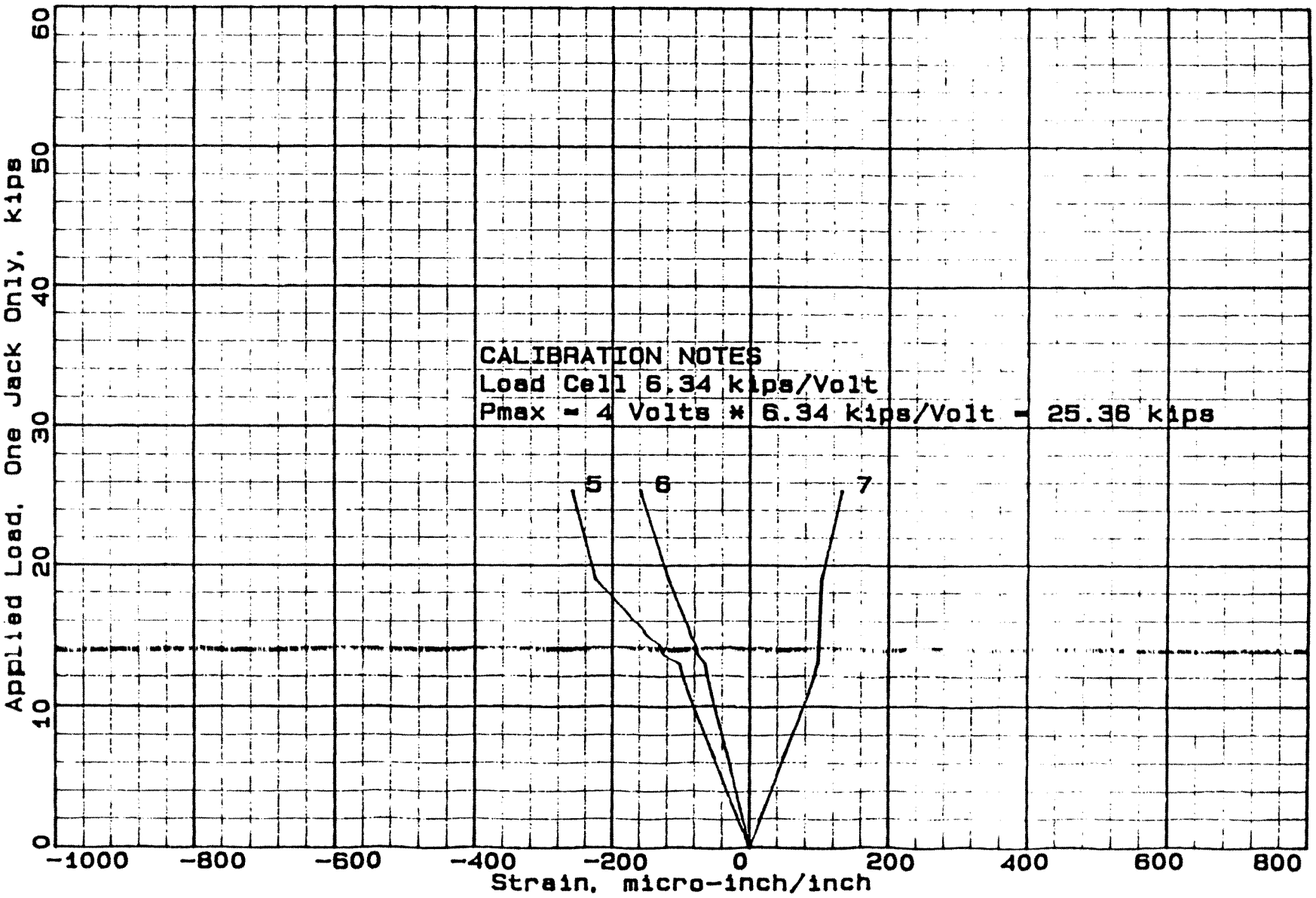

Fig. C-8 - Strain vs Load For West Span Off-Load Concrete Gages 5 Through 7 At 0 Fatigue Cycles (Test #3, Run 4)

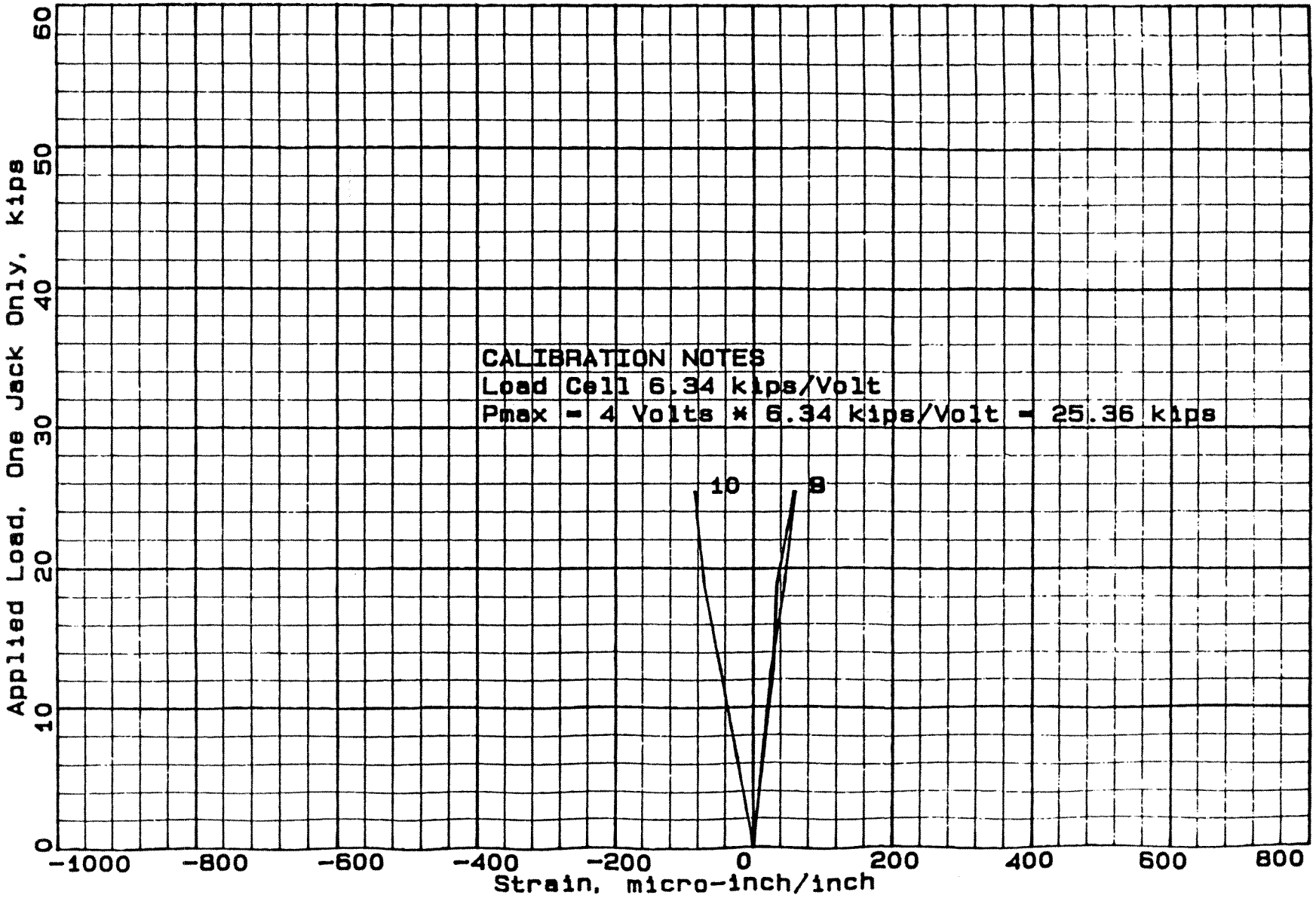

Fig. C-9 - Strain vs Load For Center Support Concrete Gages 8 Through 10 At 0 Fatigue Cycles (Test #3, Run 4)

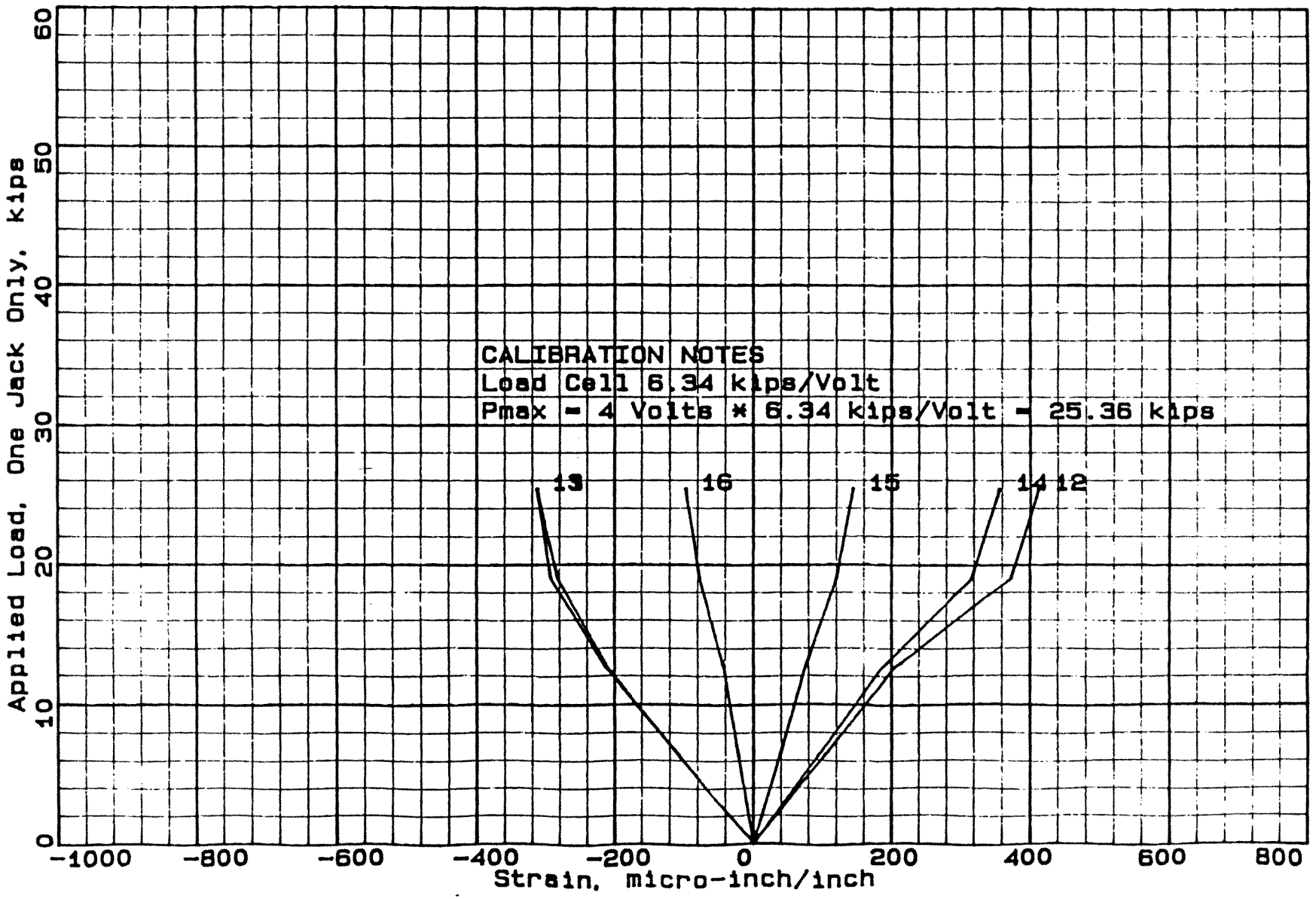

Fig. C-10 - Strain vs Load For All Steel Gages 11 Through 16
At 0 Fatigue Cycles (Test #3, Run 4)

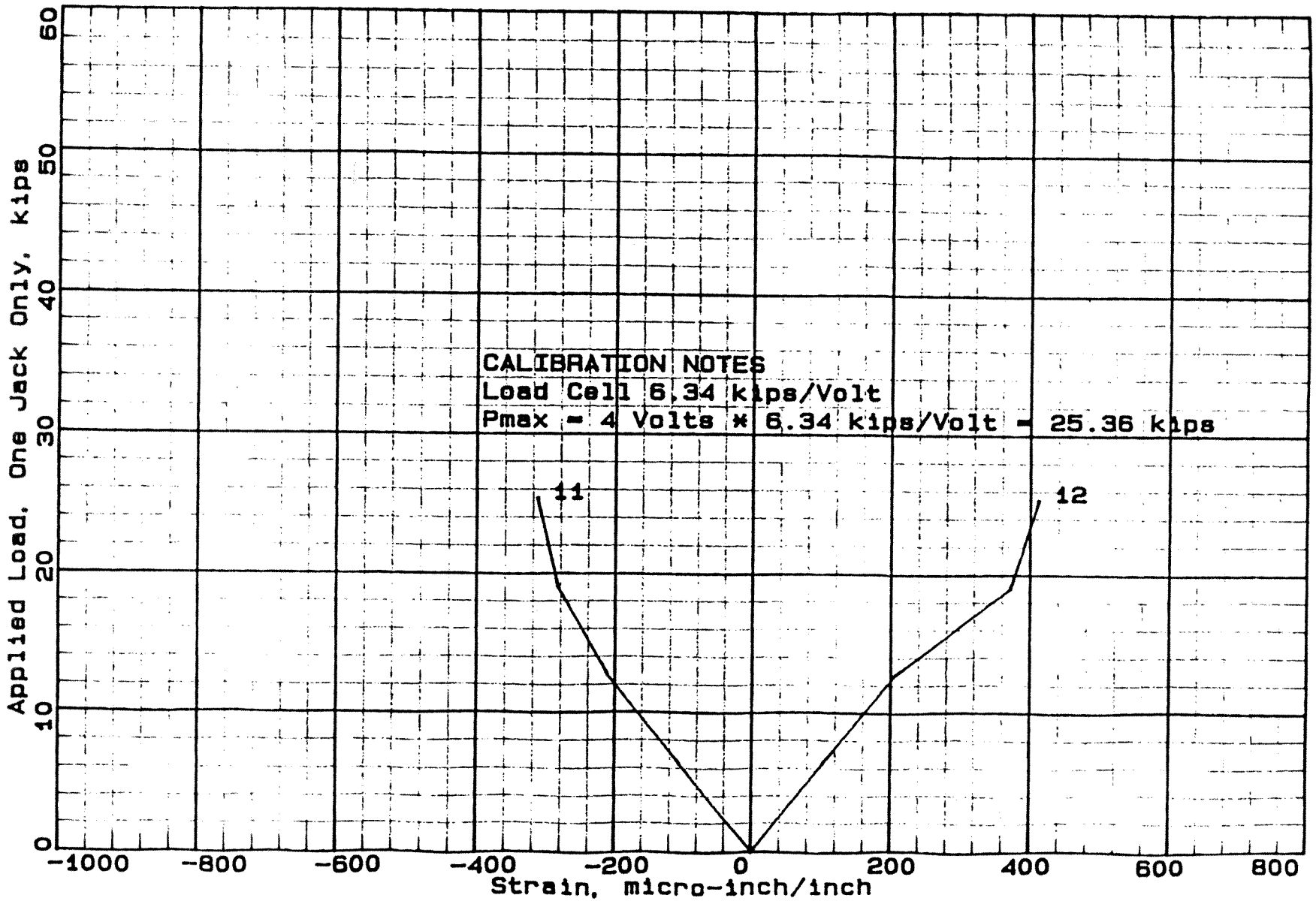

Fig. C-11 - Strain vs Load For West Span Below-Load Steel Gages 11 And 12 At 0 Fatigue Cycles (Test #3, Run 4)

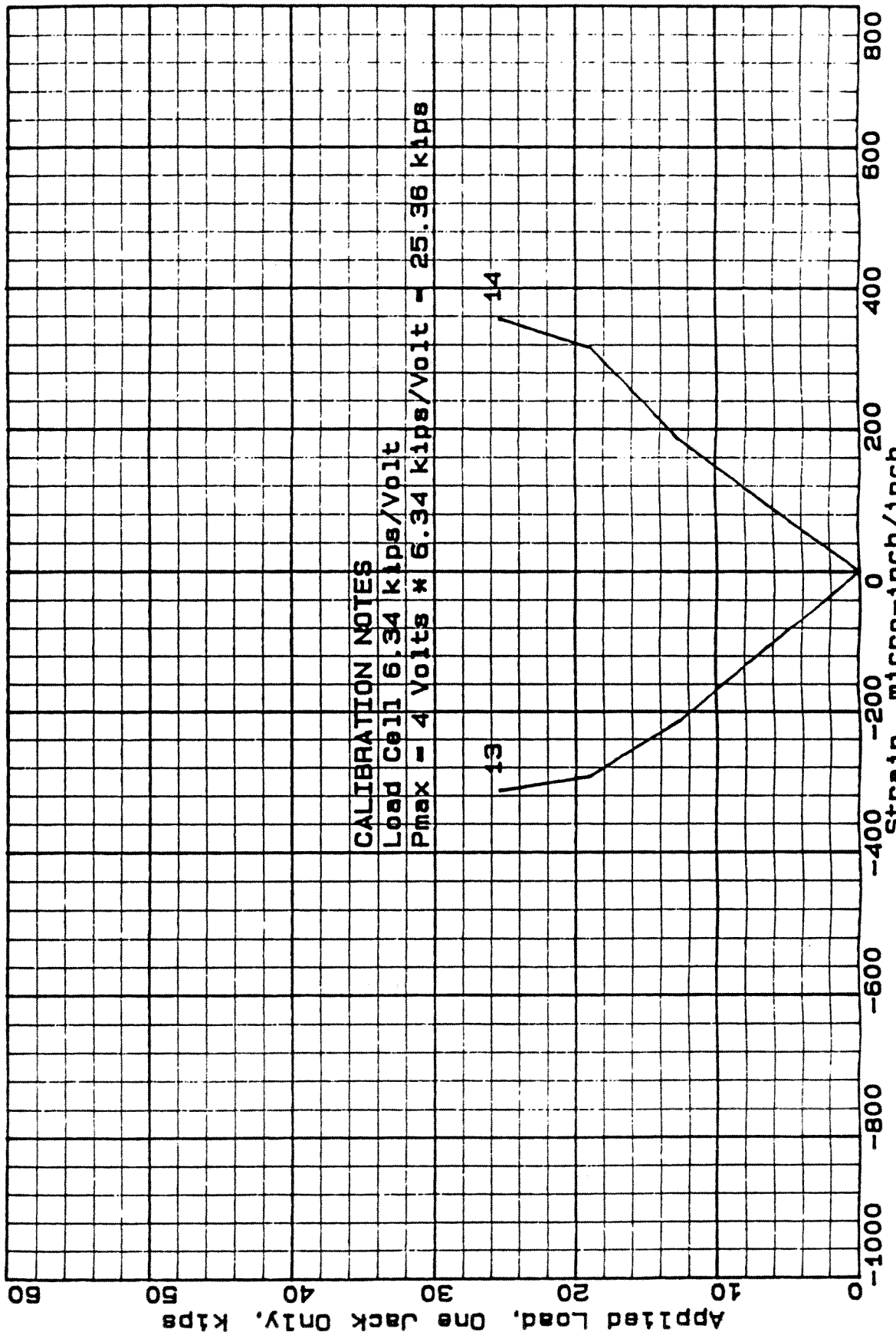

Fig. C-12 - Strain vs Load For West Span Off-Load Steel Gages 13 And 14 At 0 Fatigue Cycles (Test #3, Run 4)

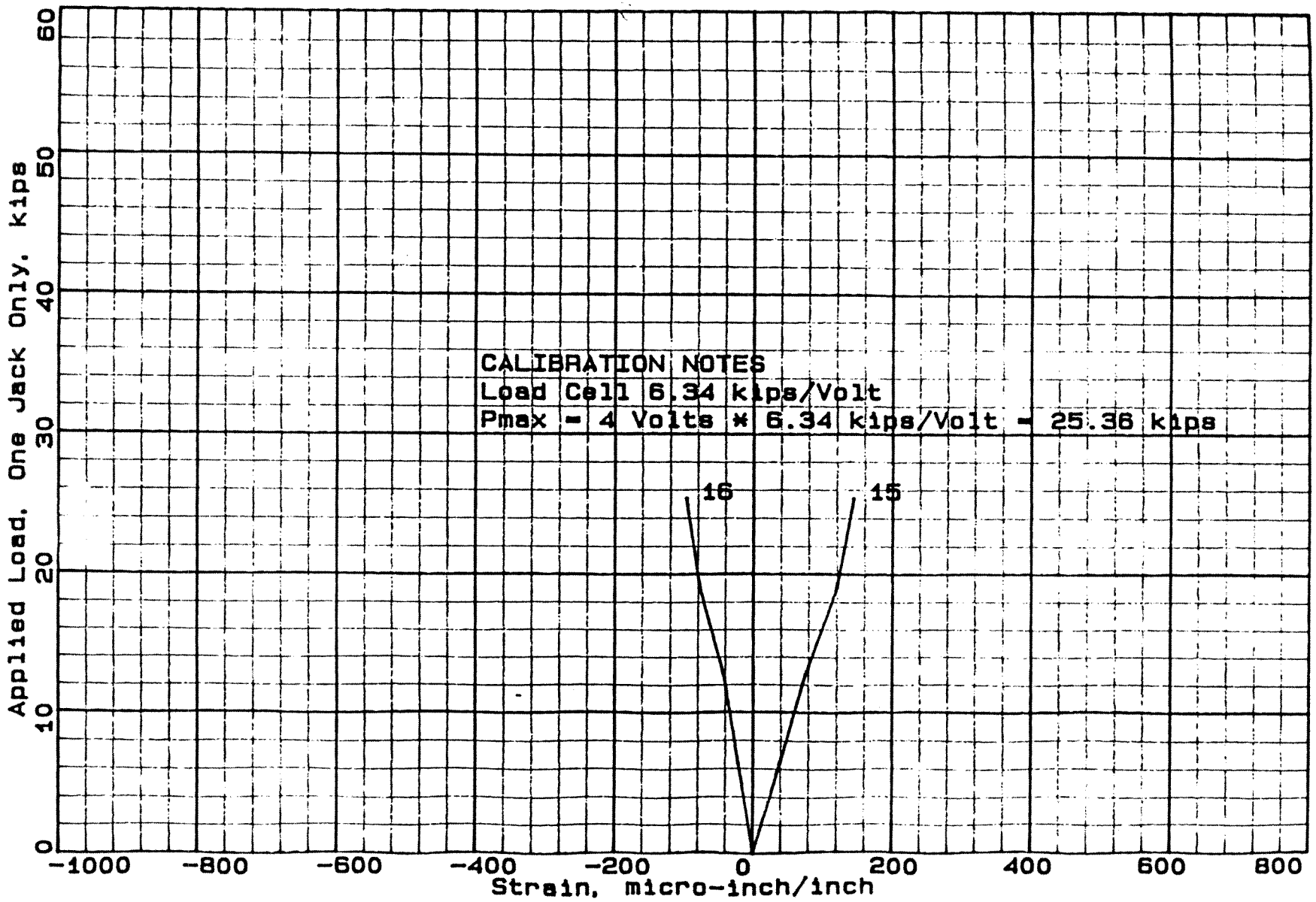

Fig. C-13 - Strain vs Load For Center Support Steel Gages 15 And 16
At 0 Fatigue Cycles (Test #3, Run 4)

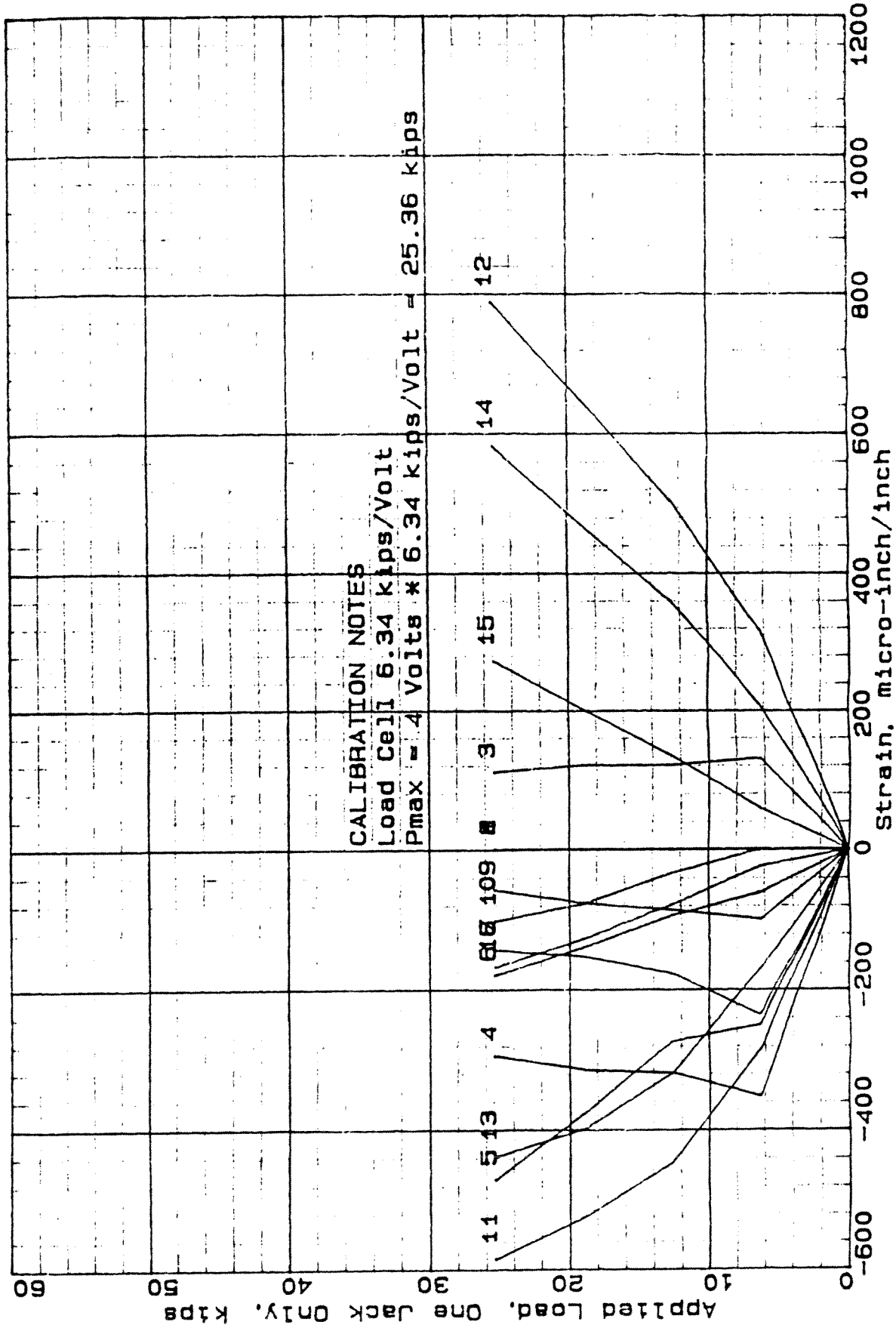

Fig. C-14 - Strain vs Load For All Concrete And Steel Gages At 1,489,930 Fatigue Cycles (Test #3)

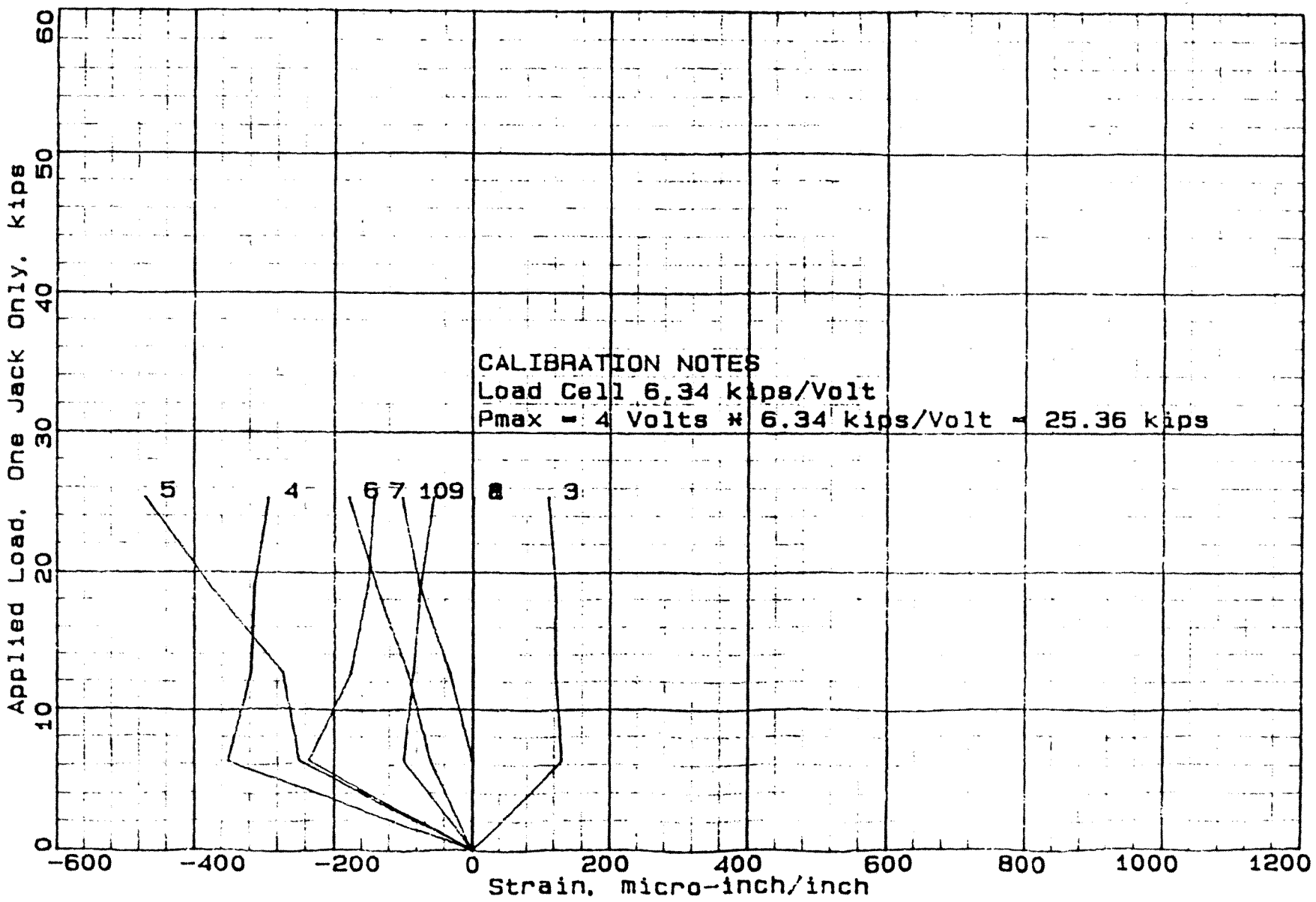

Fig. C-15 - Strain vs Load For All Concrete Gages 1 through 10
At 1,489,930 Fatigue Cycles (Test #3)

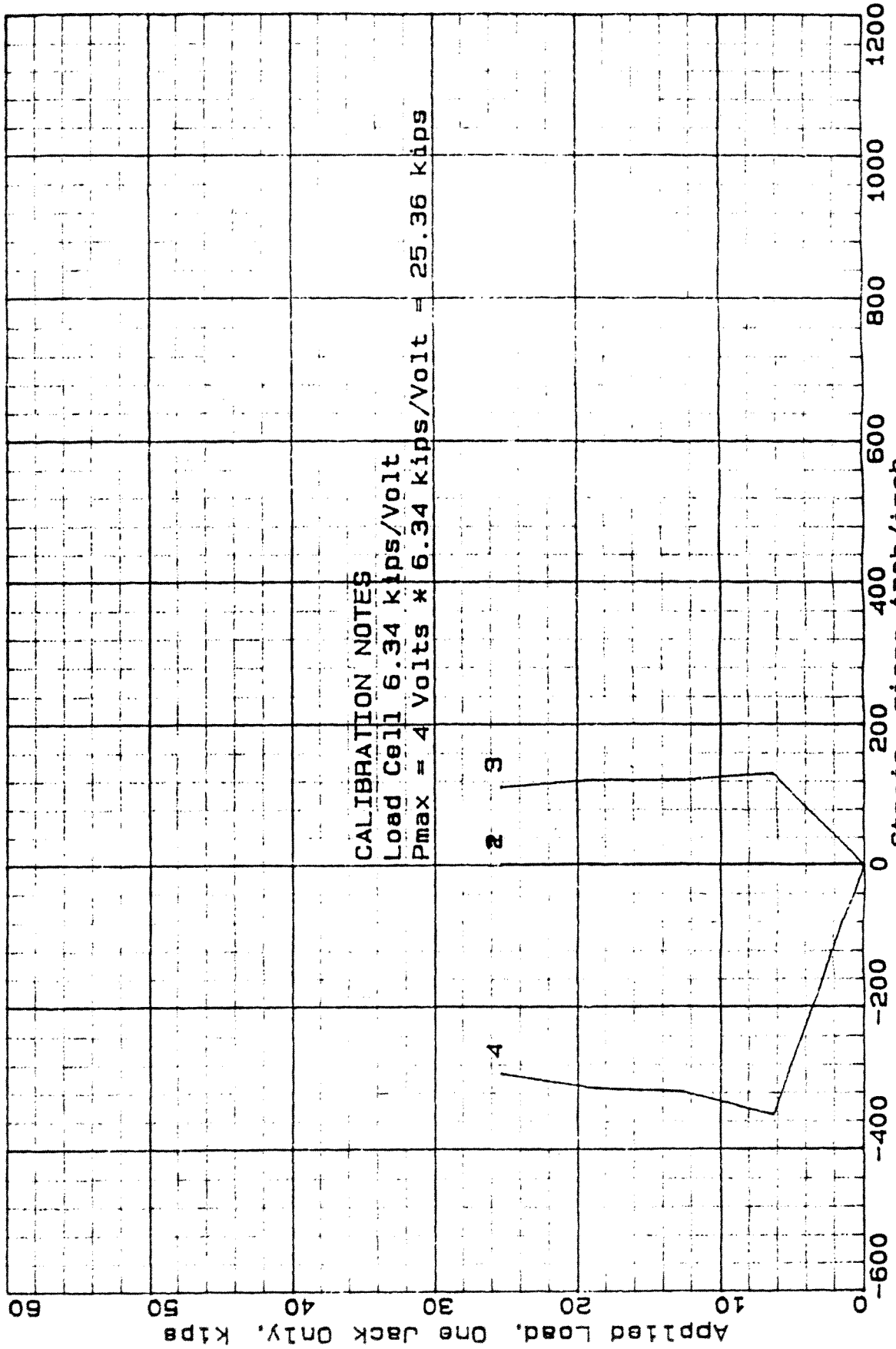

Fig. C-16 - Strain vs Load For West Span Below-Load Concrete Gages 1 Through 4 At 1,489,930 Fatigue Cycles (Test #3)

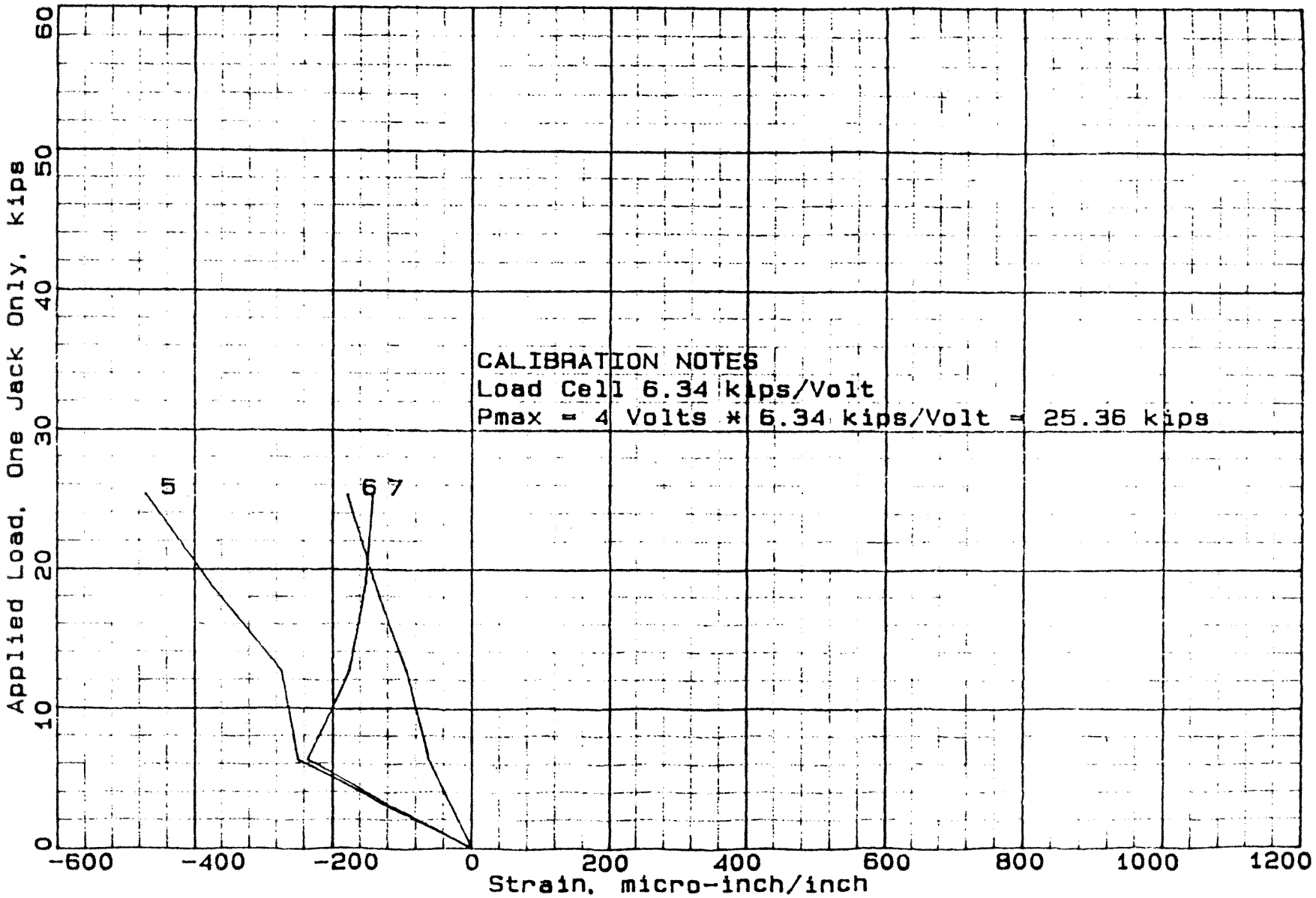

Fig. C-17 - Strain vs Load For West Span Off-Load Concrete Gages 5 Through 7 At 1,489,930 Fatigue Cycles (Test #3)

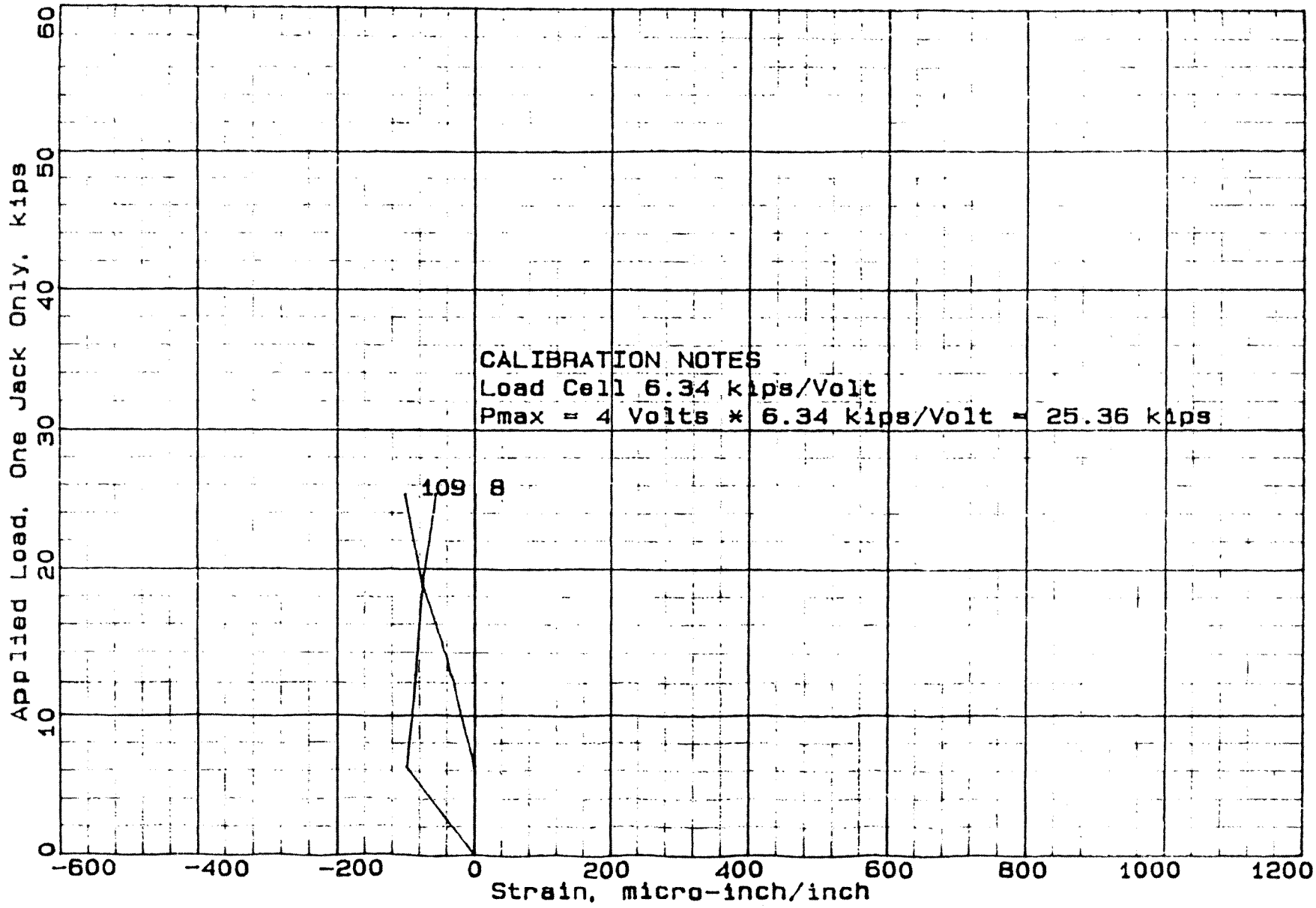

Fig. C-18 - Strain vs Load For Center Support Concrete
Gages 8 Through 10 At 1,489,930 Fatigue Cycles (Test #3)

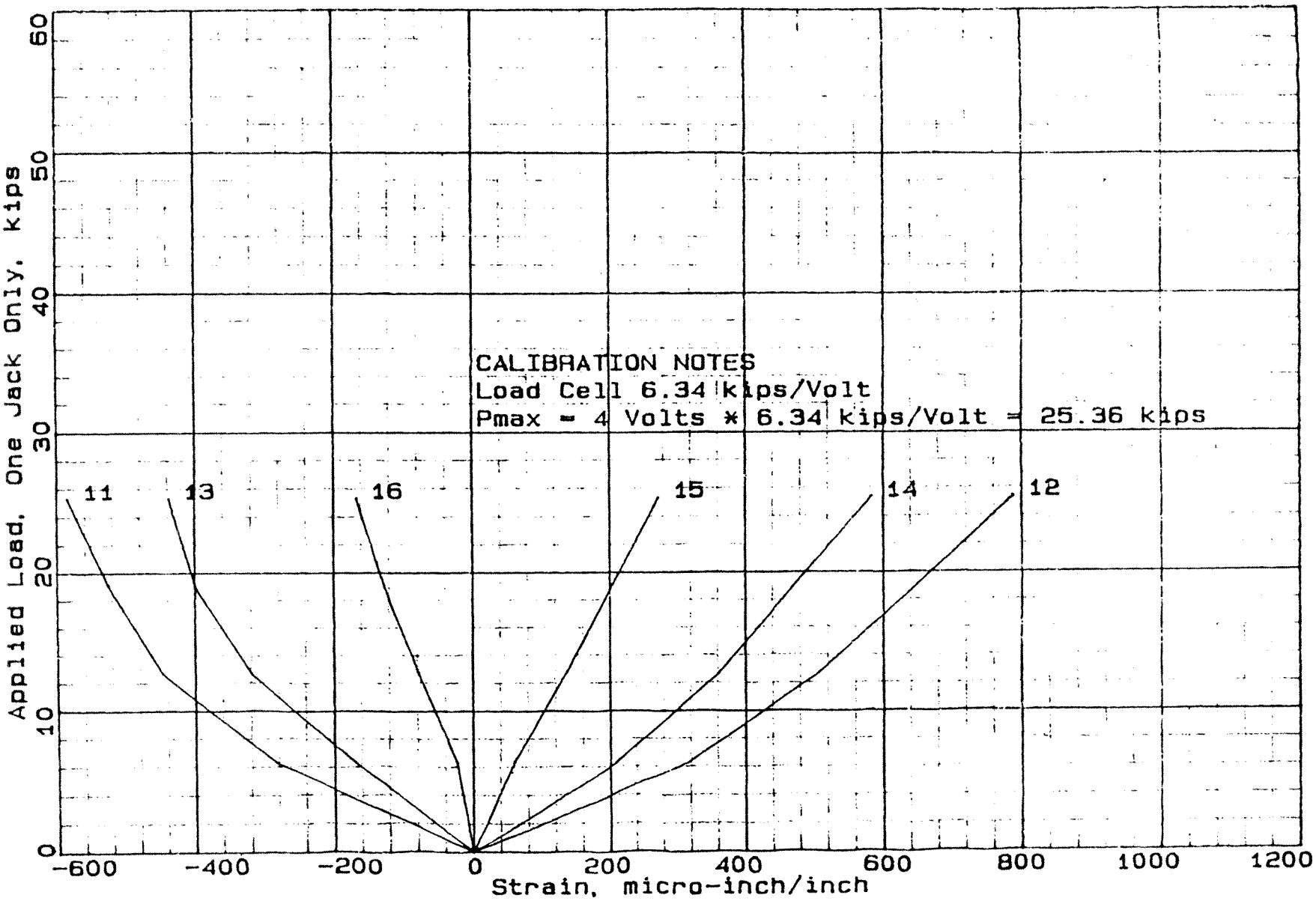

Fig. C-19 - Strain vs Load For All Steel Gages 11 through 16 At 1,489,930 Fatigue Cycles (Test #3)

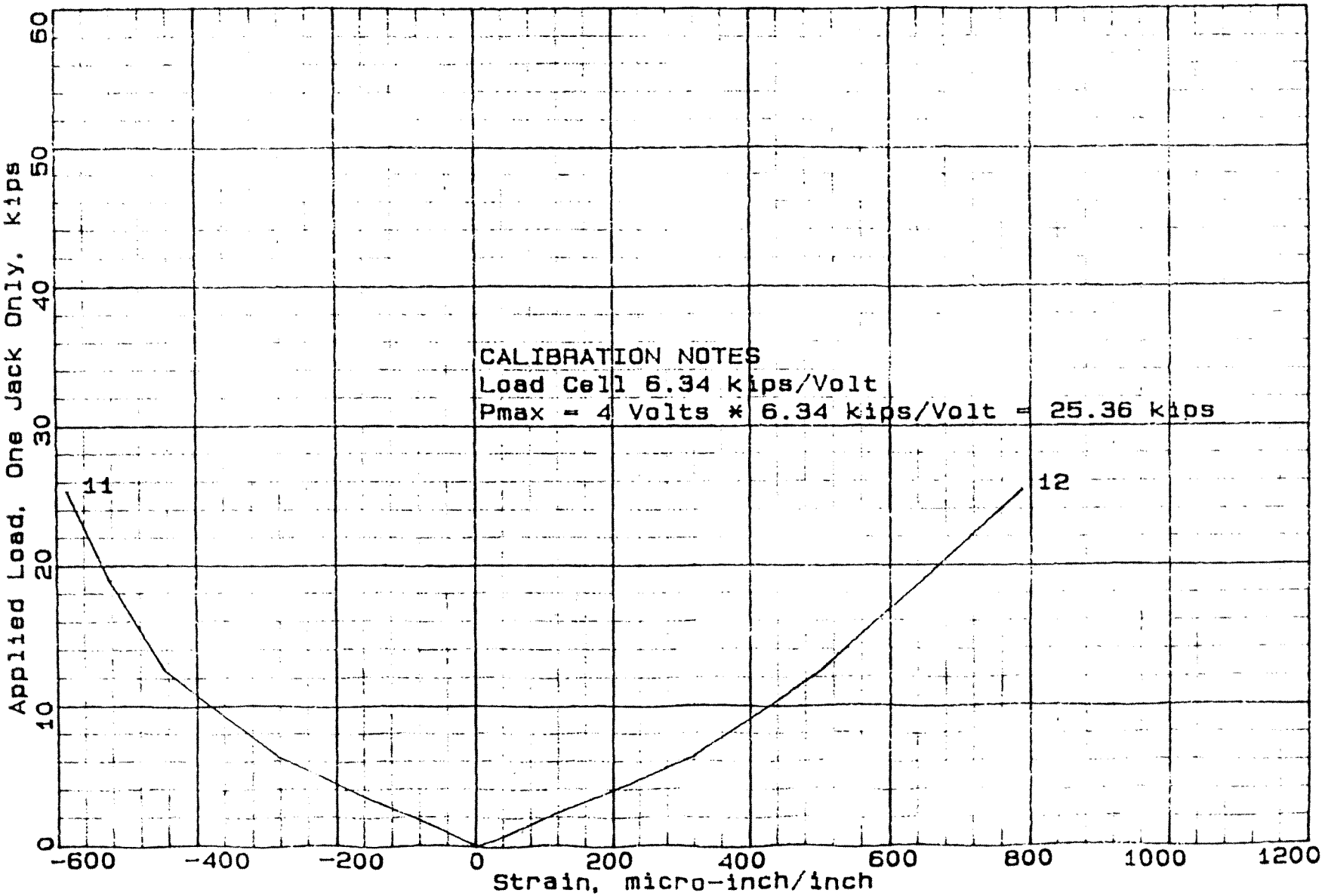

Fig. C-20 - Strain vs Load For West Span Below-Load Steel Gages 11 And 12 At 1,489,930 Fatigue Cycles (Test #3)

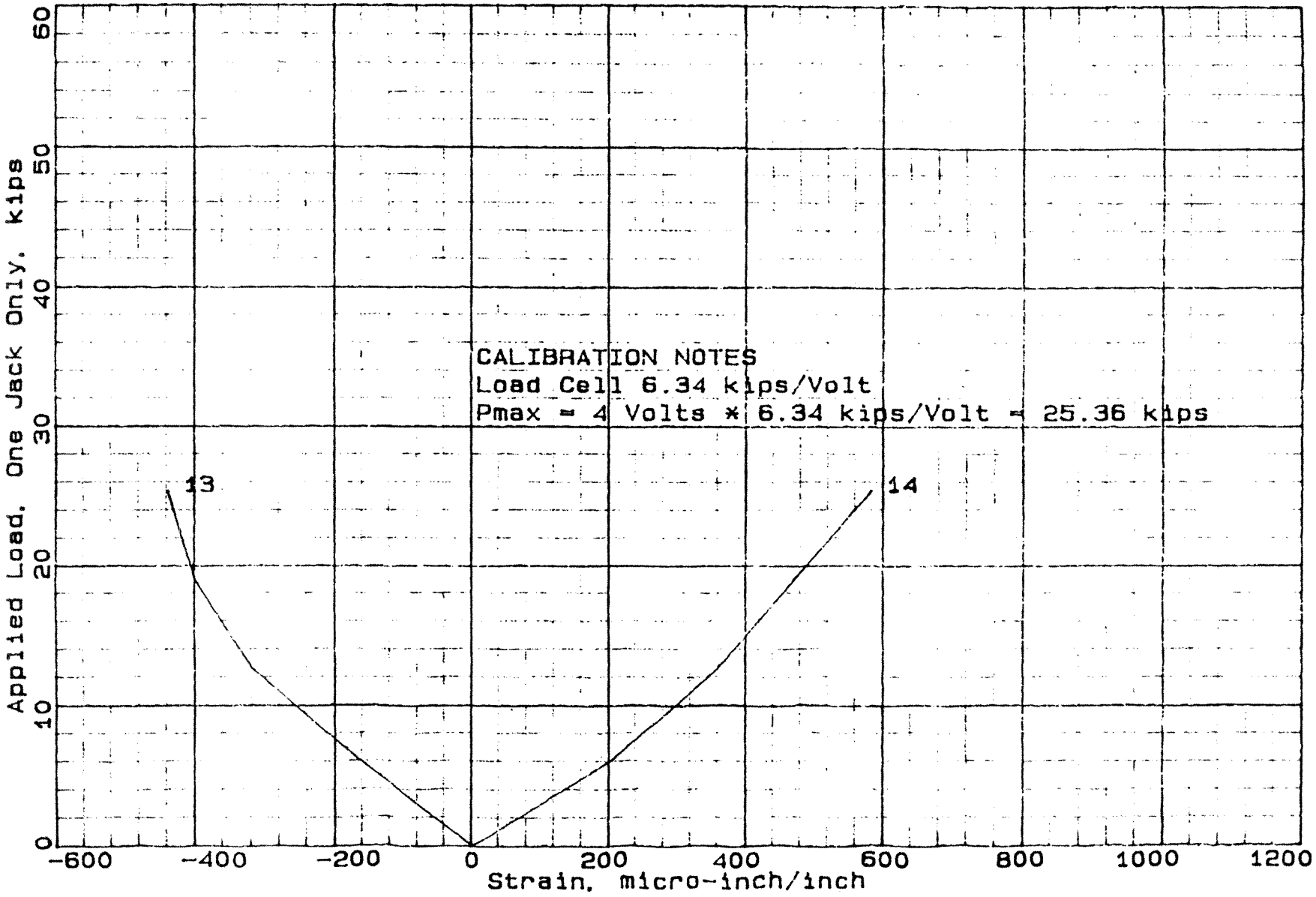

Fig. C-21 - Strain vs Load For West Span Off-Load Steel Gages 13 And 14 At 1,489,930 Fatigue Cycles (Test #3)

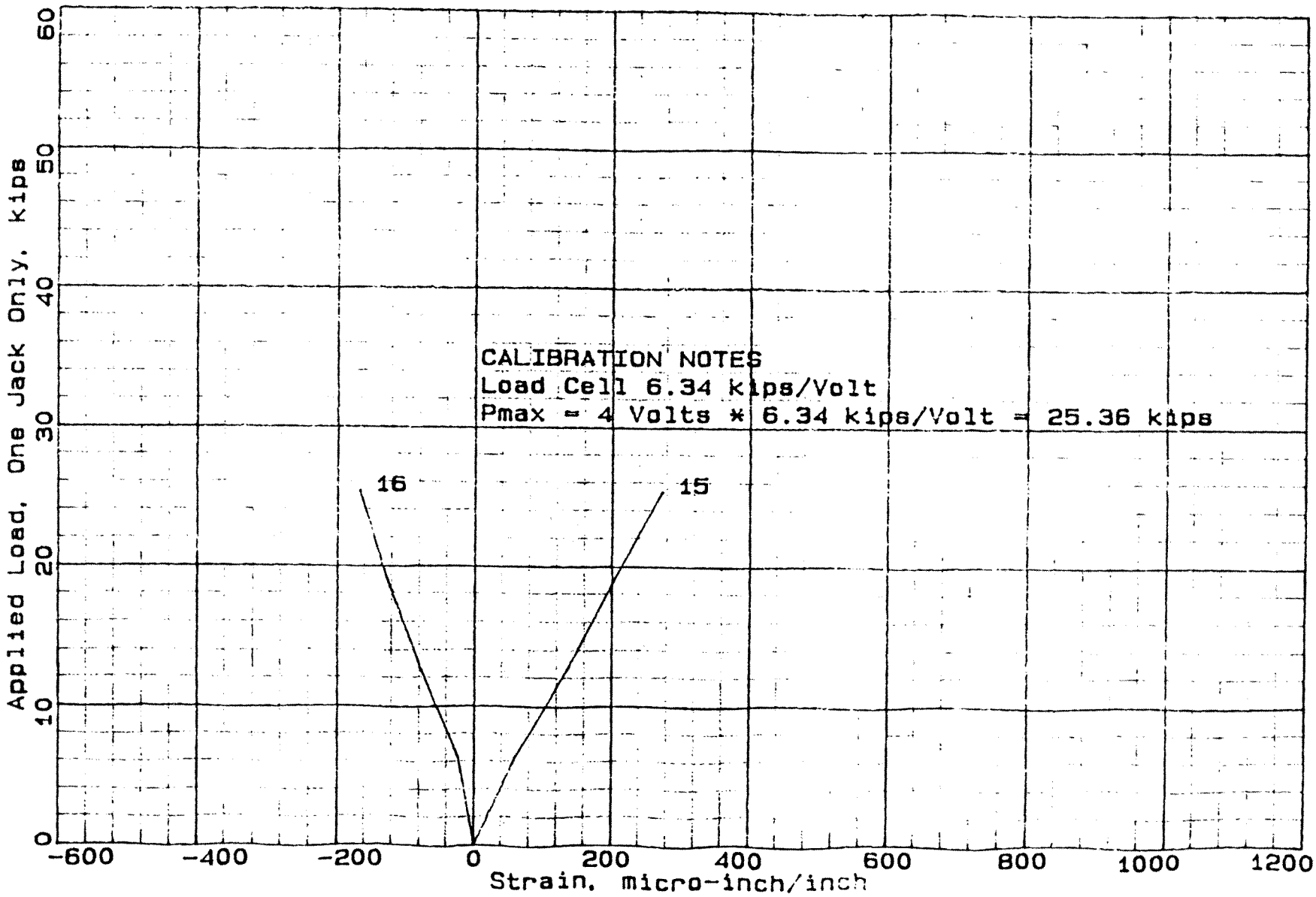

Fig. C-22 - Strain vs Load For Center Support Steel Gages 15 And 16
At 1,489,930 Fatigue Cycles (Test #3)

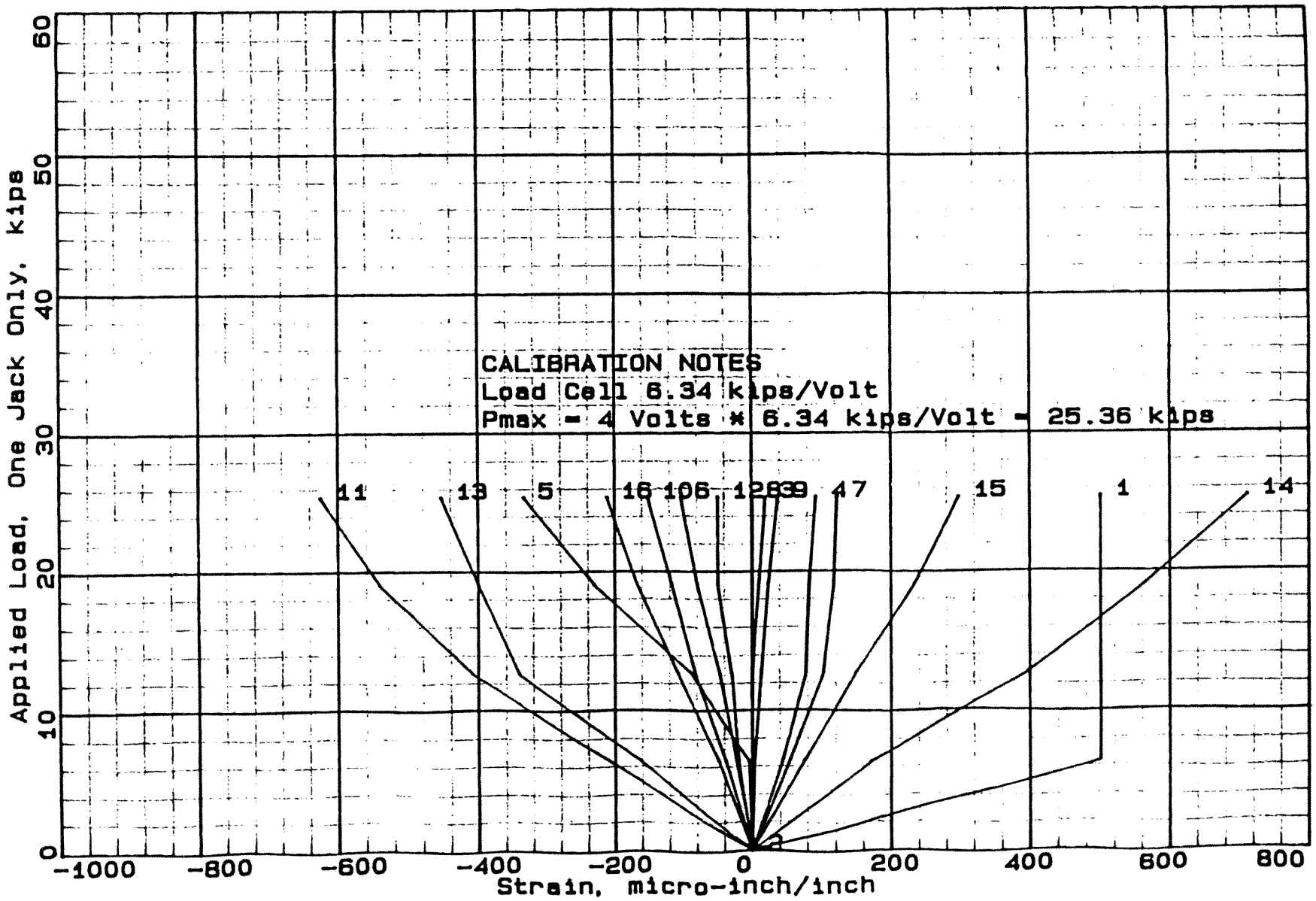

Fig. C-23 - Strain vs Load For All Concrete And Steel Gages
At 4,278,610 Fatigue Cycles (Test #3)

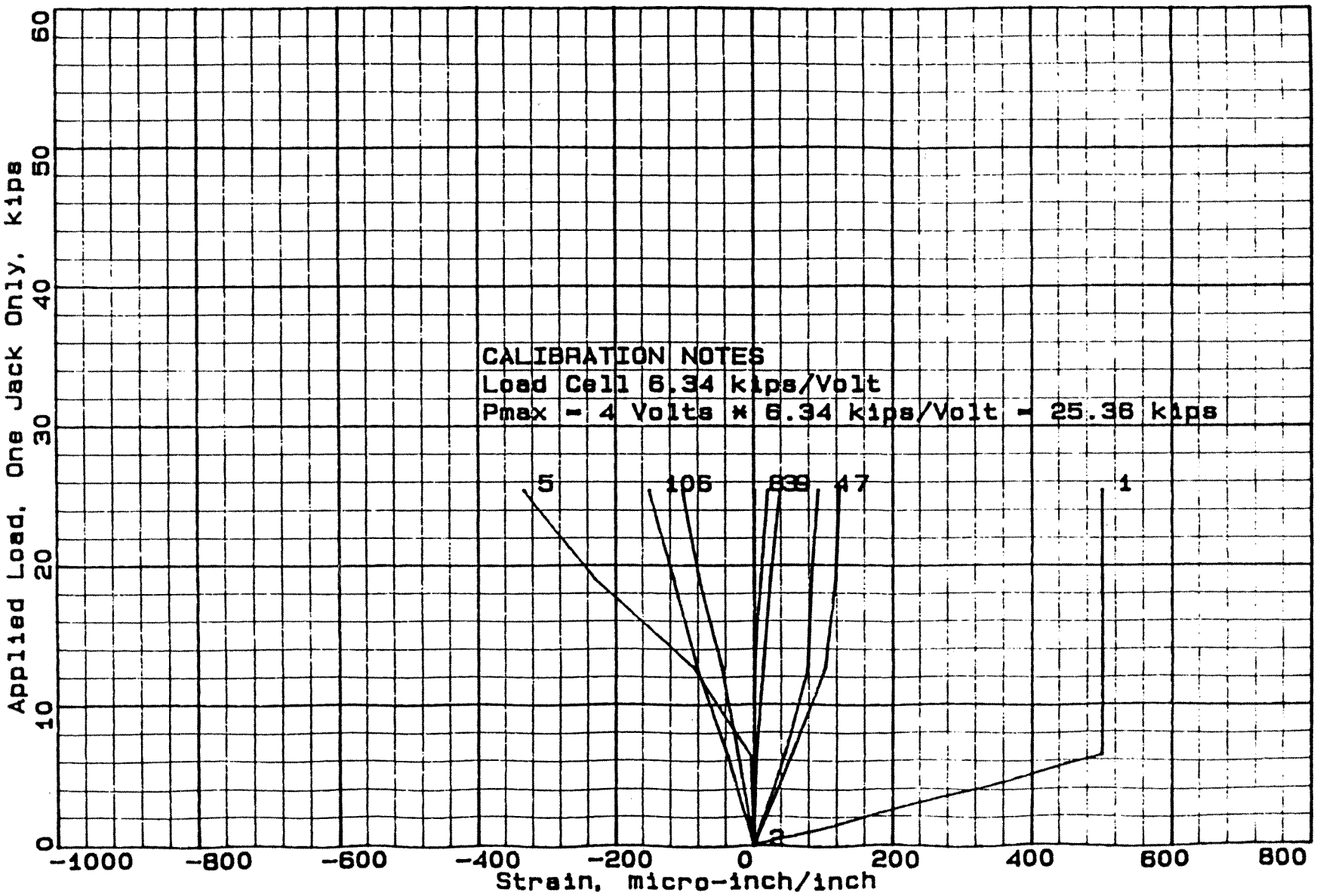

Fig. C-24 - Strain vs Load For All Concrete Gages 1 through 10
At 4,278,610 Fatigue Cycles (Test #3)

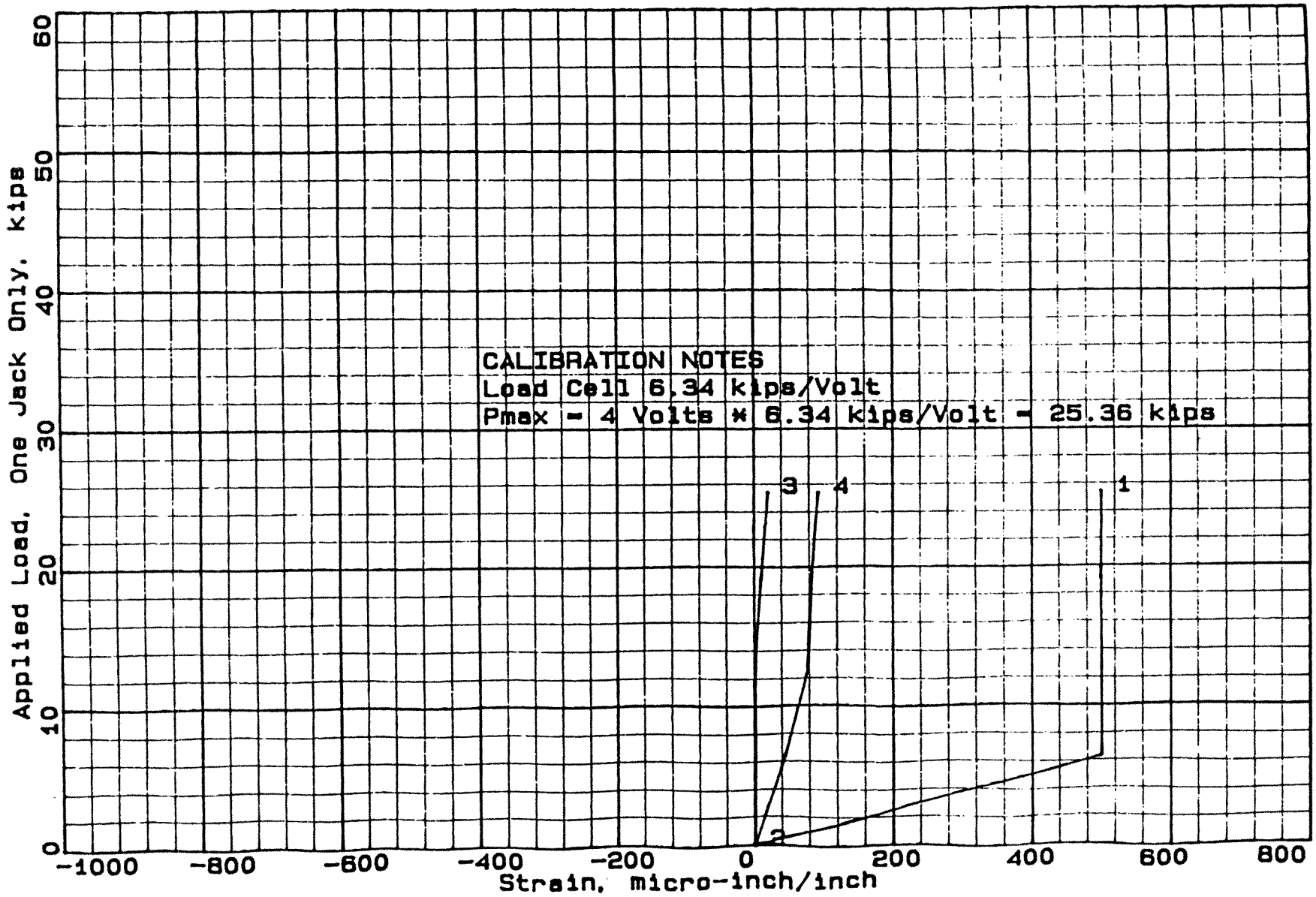

Fig. C-25 - Strain vs Load For West Span Below-Load Concrete Gages 1 Through 4 At 4,278,610 Fatigue Cycles (Test #3)

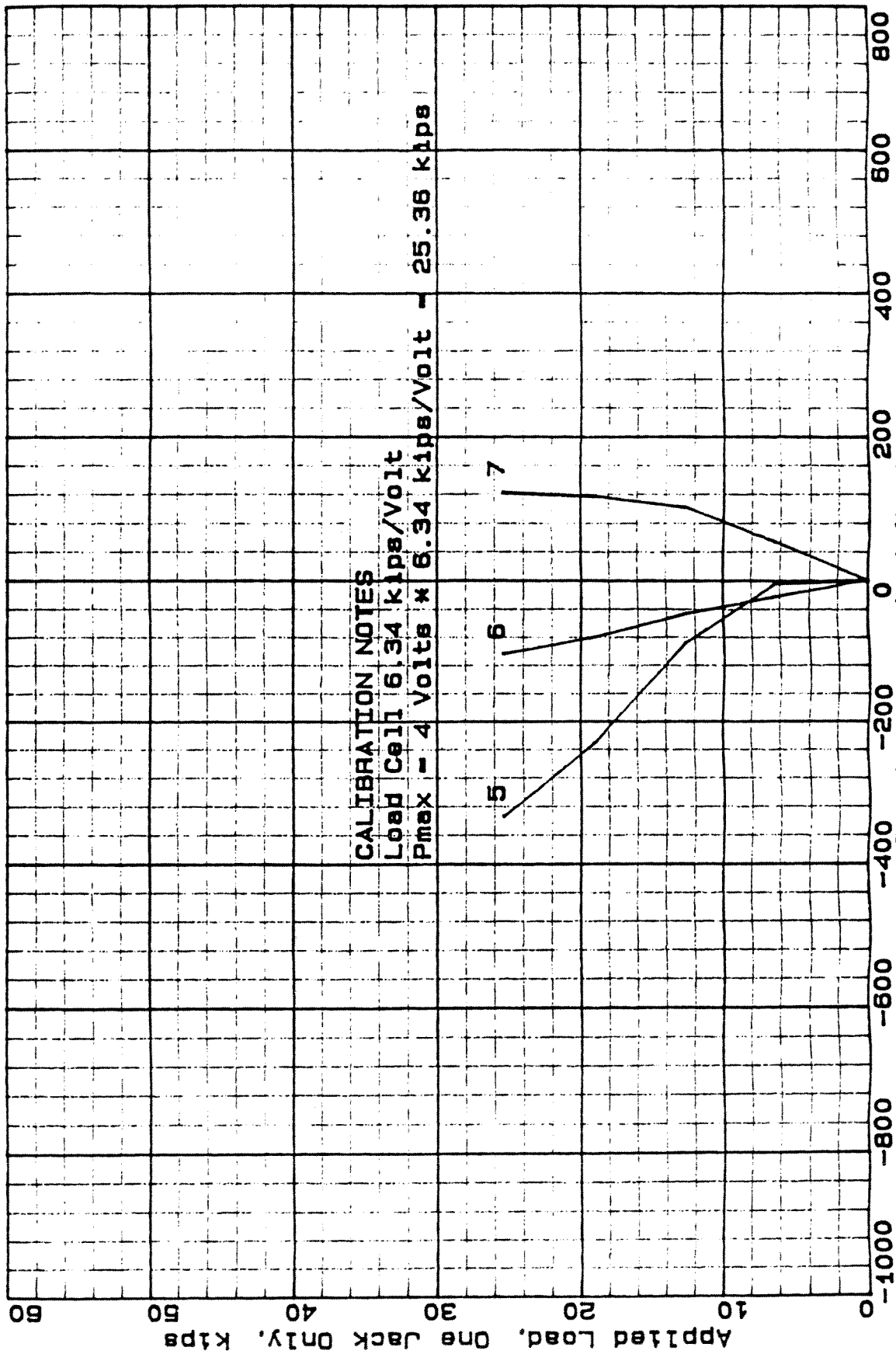

Fig. C-26 - Strain vs Load For West Span Off-Load Concrete Gages 5 Through 7 At 4,278,610 Fatigue Cycles (Test #3)

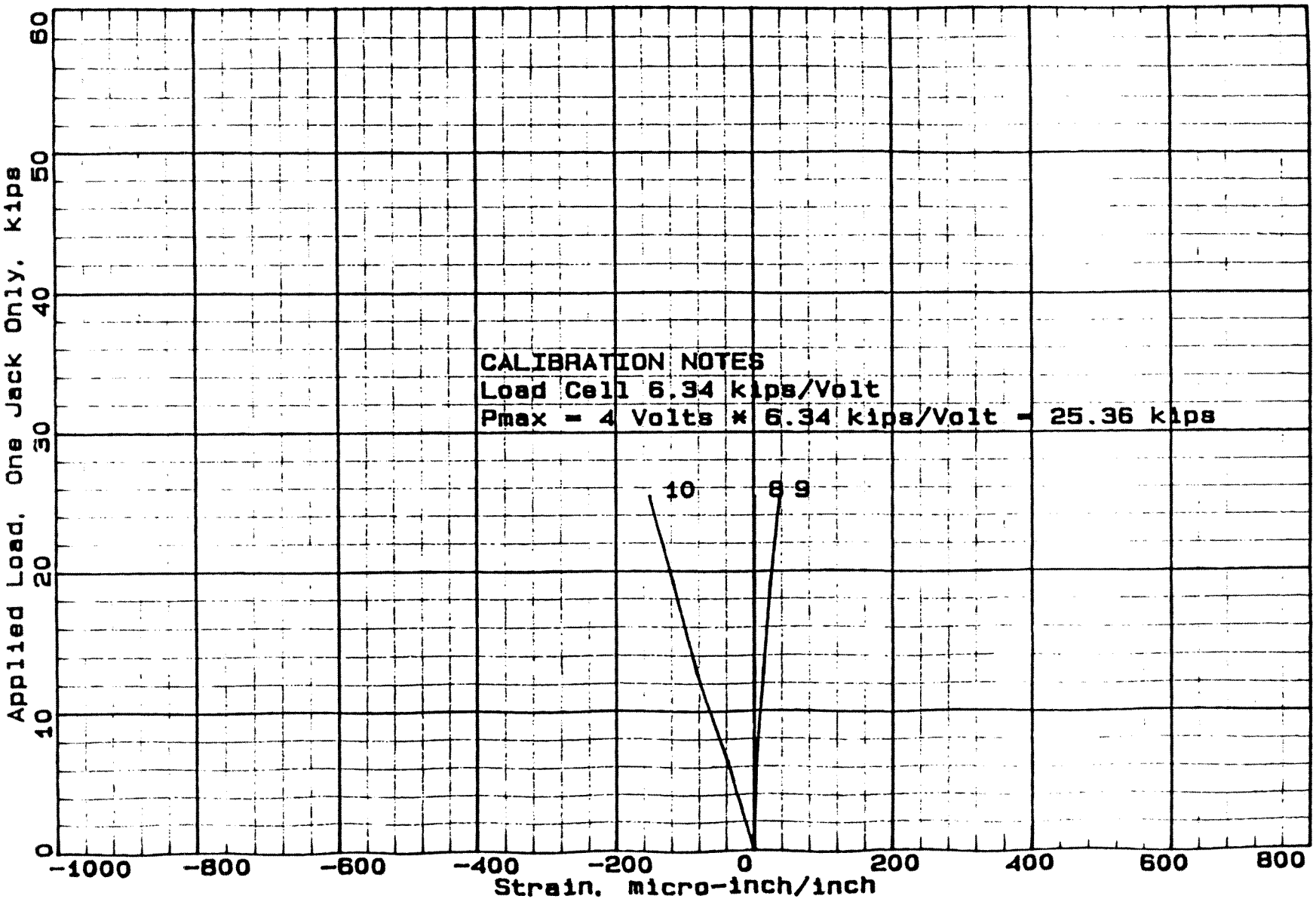

Fig. C-27 - Strain vs Load For Center Support Concrete
Gages 8 Through 10 At 4,278,610 Fatigue Cycles (Test #3)

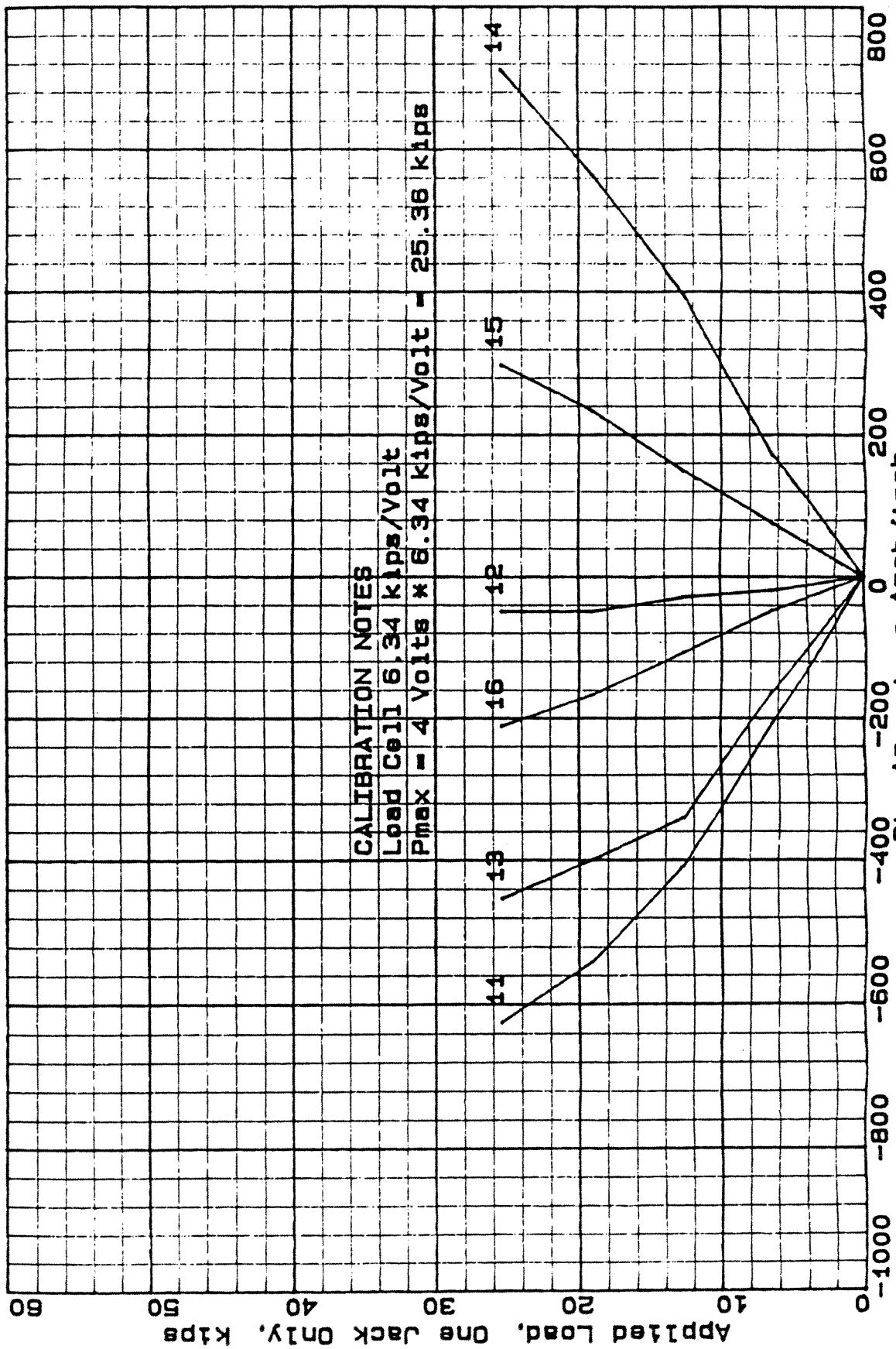

Fig. C-28 - Strain vs Load For All Steel Gages 11 through 16
At 4,278,610 Fatigue Cycles (Test #3)

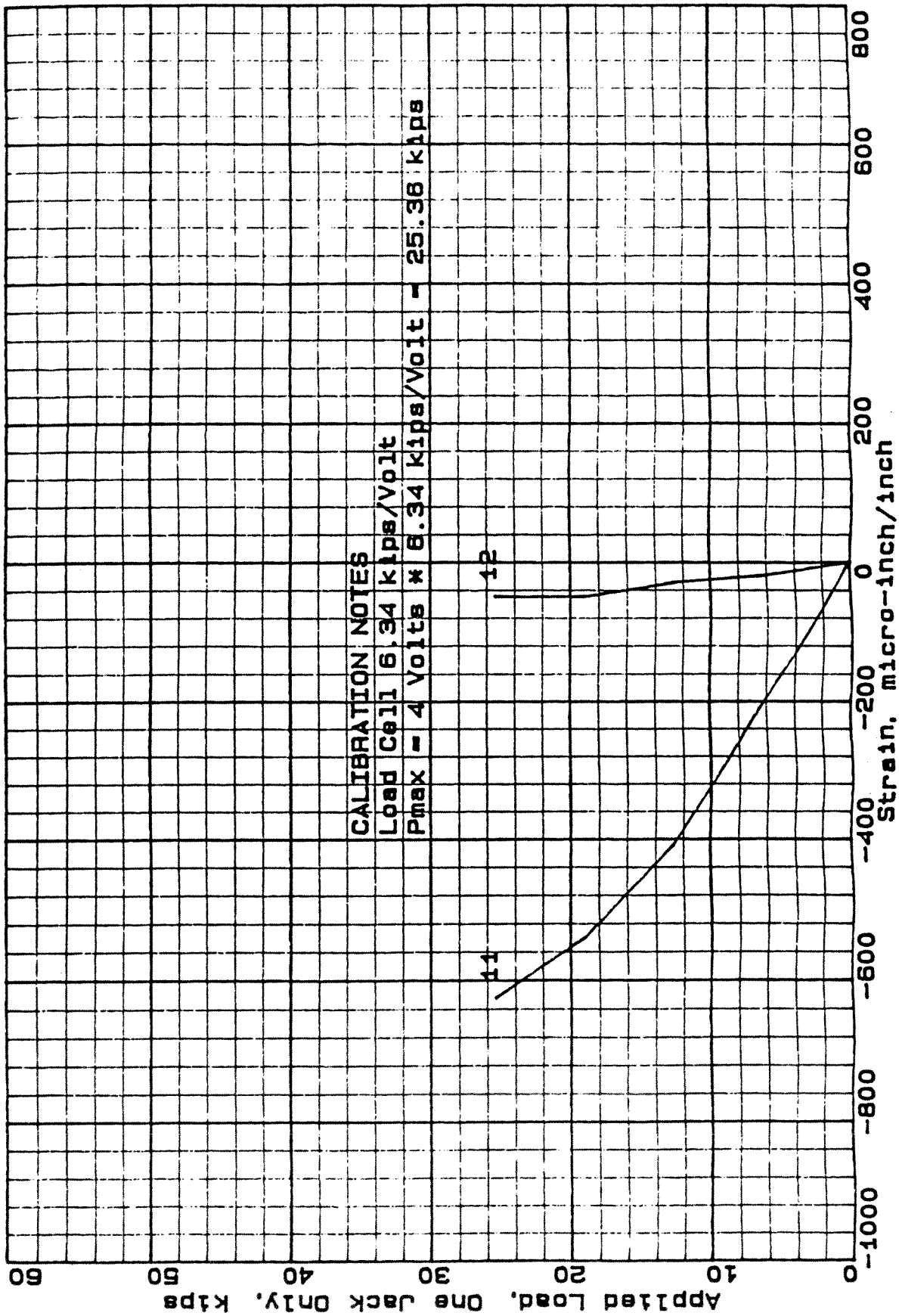

Fig. C-29 - Strain vs Load For West Span Below-Load Steel Gages 11 And 12 At 4,278,610 Fatigue Cycles (Test #3)

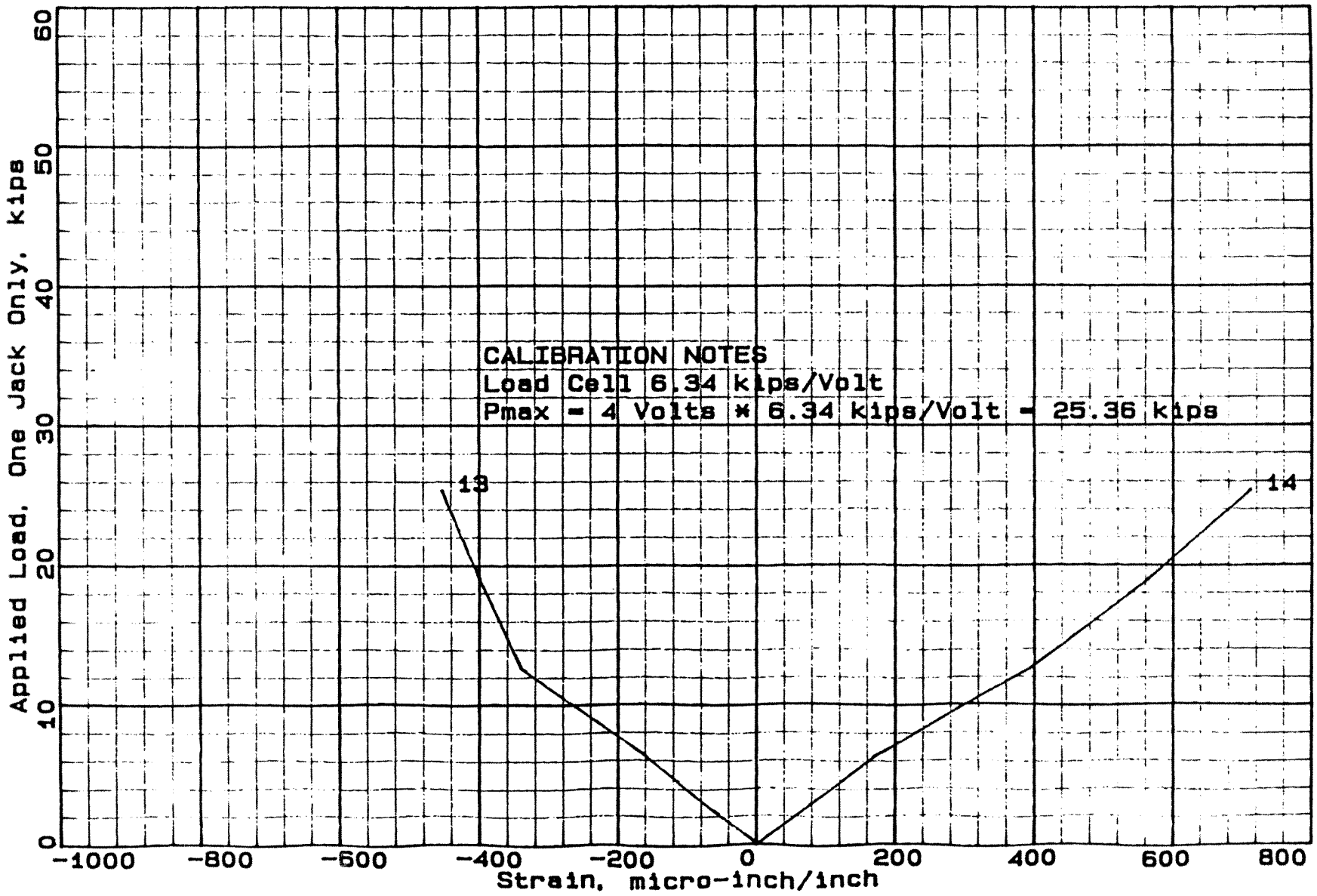

Fig. C-30 - Strain vs Load For West Span Off-Load Steel Gages 13 And 14 At 4,278,610 Fatigue Cycles (Test #3)

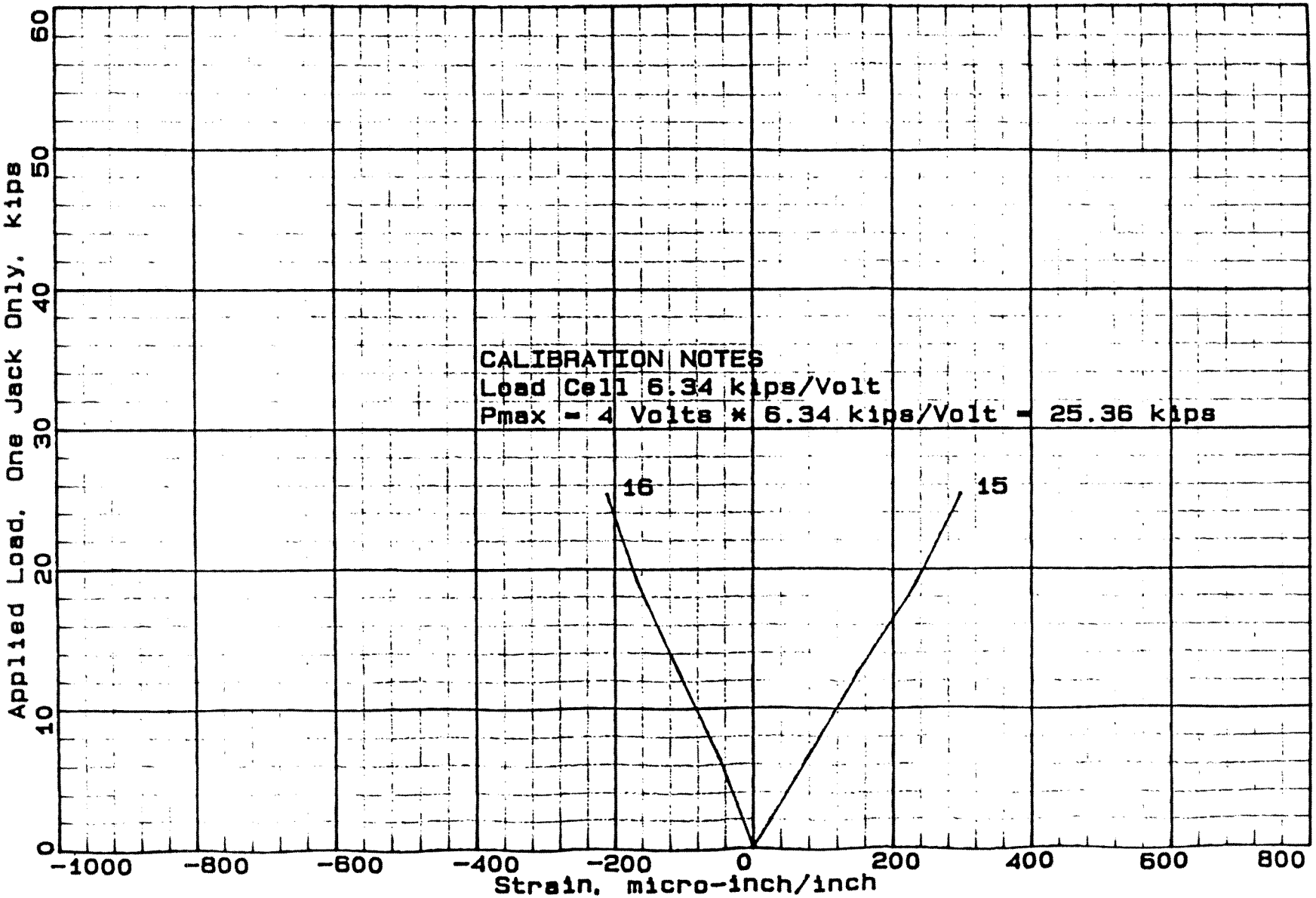

Fig. C-31 - Strain vs Load For Center Support Steel Gages 15 And 16
At 4,278,610 Fatigue Cycles (Test #3)

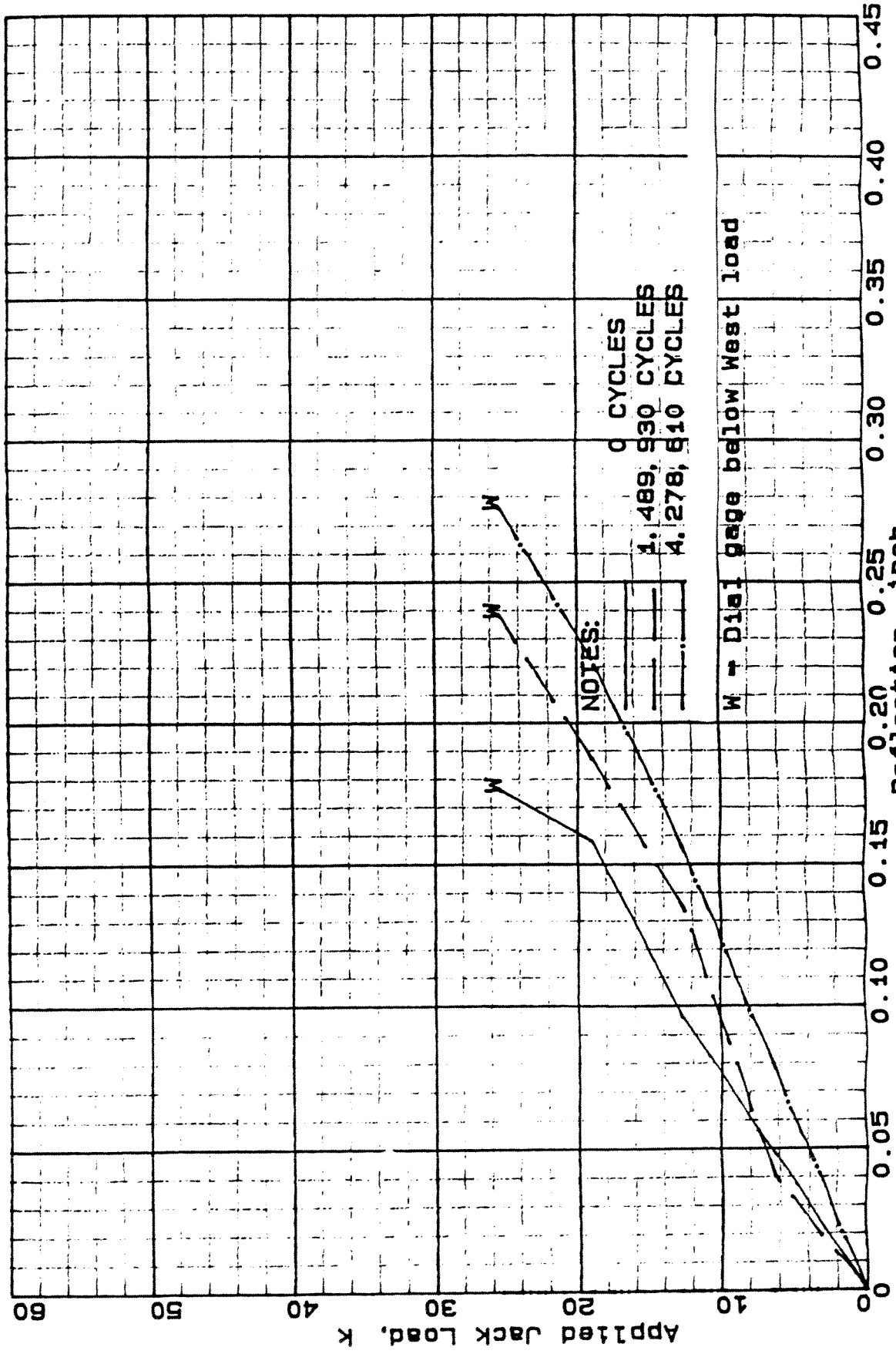

Fig. C-32 - Deflection vs Load In West Span At 0; 1,489,930; And 4,278,610 Fatigue Cycles (Test #3)

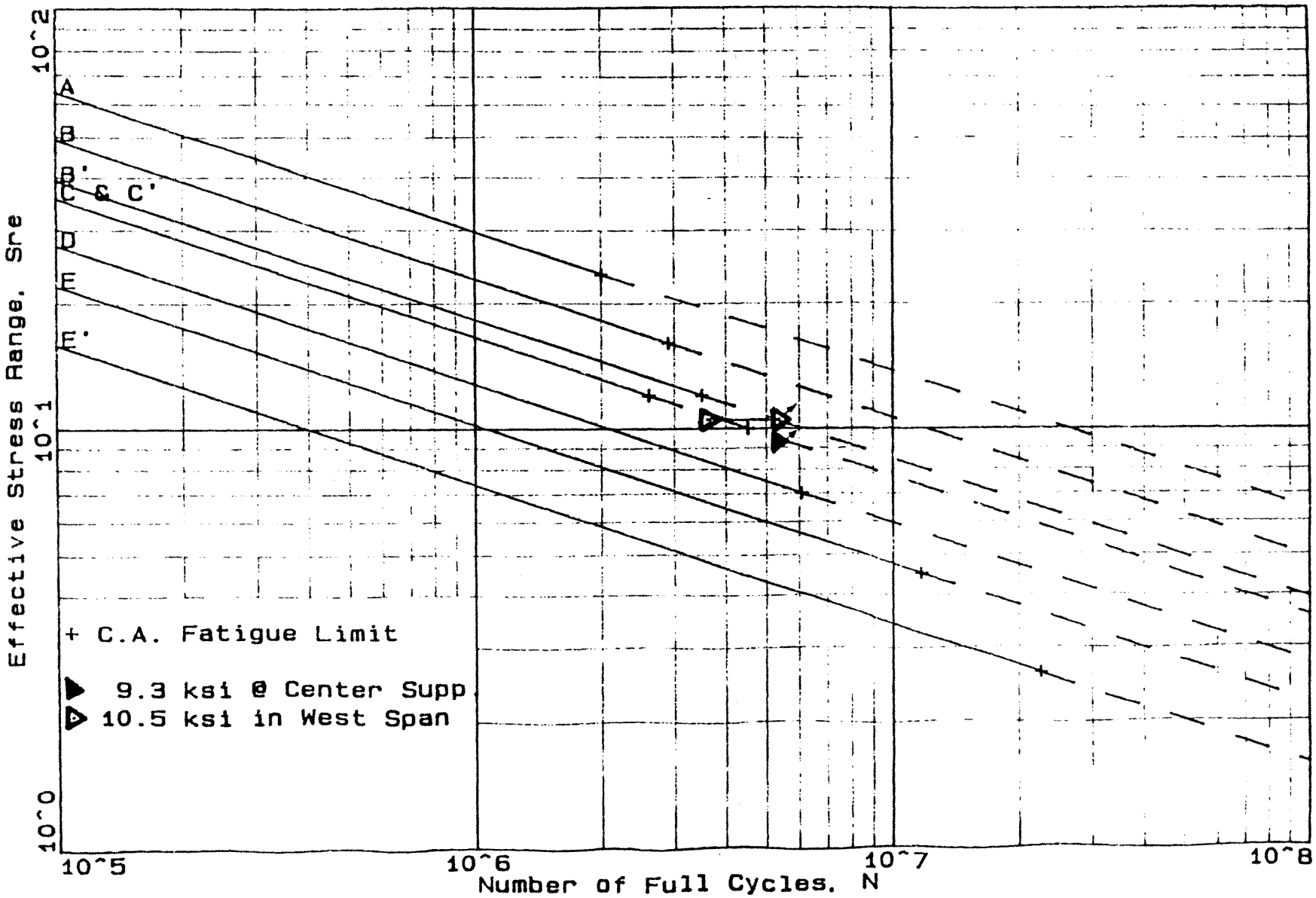

Fig. C-33 - Fatigue Failures Of Main Steel Bars In Test #3 Compared With 1991 AASHTO Fatigue Categories

APPENDIX D - FINITE ELEMENT ANALYSIS FOR TEST #3

D-1 INTRODUCTION

The load/moment/deflection relationships for all tests were confirmed by approximate hand and spread sheet calculations, and/or finite-difference analysis.[1] Although the finite difference calculations provided considerably improved correlation with the test results, it was felt that a finite element analysis should also be performed for Test #3. This appendix discusses the results of the finite element analysis conducted for the Test #3 specimen.

Commonly, the computation of stresses in concrete-filled steel-grid bridge deck is based on the transformed area-method, and specifically on AASHTO specification sections 3.24 and 3.27.[4] Tests that have been performed on different concrete filled panels have shown that the specified loads and analysis methods are conservative for the determination of section properties and load distribution. Specifically, this was shown in the tests conducted under Phase I and II of this project. Since computation of section properties and the determination of moment resistances by tests involves significant efforts, time, and money, other methods such as the finite difference, finite strip, or finite element methods should be utilized for a more precise analysis. However, some initial tests are required to confirm the proper development of a valid geometrical models, which in turn can be used for the analysis of many other different concrete-filled steel-grid products.

D-2 OBJECTIVES

A finite element analysis of Panel #3 was conducted with the objective to compare the test results with analytically derived results, especially for the steel stresses/strains. This test panel had been strain gaged for strains/stresses in the positive and negative bending moment regions along the longitudinal centerline of the specimen, and off

center. Also, deflection measurements had been taken below the main wheel load before the fatigue test commenced.

D-3 FEA DETAILS AND PROCEDURE

Some finite element analysis (FEA) details related to the geometry of the specimen analyzed are highlighted below. For further details reference is made to Appendix C. In this appendix, more emphasis is placed on the procedure used to develop the finite element model, to describe the model, to describe the FEA results, and to make a comparison with the stresses/strains measured prior to starting the fatigue test, .

D-3.1 Panel Geometry

As described in more detail in Appendix C, the Test #3 specimen consisted of a 4-1/2-inch-deep steel grid filled with concrete. The main bars were spaced at 6 inch on center, connected by cross-bars at 4 inch center to center, supplemented by #5 steel reinforcing bars. The deck was filled with concrete having a 1-5/8 inch overfill. The panel was 20 foot long and 6'-6" wide, and was supported in a manner that resulted in two continuous spans, 9'-9" each.

D-3.2 Static Calibration Load

A maximum hydraulic actuator load of P = 25.4 kips (equivalent to 4 volt @ 6.35 kip/volt) was statically applied to the panel through a 4-wheel truck axle with a hollow rectangular cross section. The load was situated such that it resulted in two wheel-pair loads of P_w = 19.76 kip and P_e = 5.64 kip below the west and east wheel pairs, respectively. For further reference and details please see Figure C-3.

D-3.3 Load Location

The 19.76-kip west wheel-pair load was applied near the center of the west span. Since the center-to-center dimension between the two pairs of wheels was 6 feet, the center of the 5.64-kip east wheel-pair load was located 10 inches to the east side of the center support. The load locations are also shown in Figure C-3.

D-4 MEASURED STRESSES

The static stresses resulting from the applied load were measured before the fatigue test commenced. During Run 4, the strains measured under the maximum load applied resulted in the following stresses in the top and bottom steel fibers of main longitudinal Bar 6, which was located along the longitudinal centerline of the test specimen.

In the positive moment region below the wheel in the west span the stresses based on the measured strains were:

8.8 ksi compression in the top fiber,

11.8 ksi tension in the bottom fiber.

In the negative moment region at the center support the stresses based on the measured strains were:

2.6 ksi compression in the bottom fiber,

4.7 ksi tension in the top fiber.

D-5 FINITE ELEMENT MODELS AND ANALYTICAL RESULTS

As shown in Figure D-1, the test slab was modeled by using 6"-by-6" plate elements, except that at the both sides of the center support 6"-by-3" elements were used. Thus, the model had a total of 574 nodes and 520 elements. Each wheel load was distributed over a 18"-by-6" area, where the 18-inch dimension is parallel to the direction of the span, along the longitudinal centerline. The loads were applied as a pressure load over the surface of the plate elements.

Computer program Super SAP was utilized to analyze the specimen. With this computer program, three different models with varying section properties were executed. The models and the resulting moments and stresses are more closely described below.

D-5.1 Isotropic Model With Constant Plate Thickness

The first model analyzed had a constant plate thickness of 5-7/8 inch, both in the positive and the negative moment regions. Thus, for this model, it was assumed

that no concrete cracks or reductions of section properties had occurred in the negative or positive bending moment regions of the panel. Concrete cracks observed immediately during the static test process indicate that this is not a correct assumption. Therefore, the resulting stresses in the negative moment region are high as compared with the stresses derived for the positive moment region.

Since section properties were not available from static tests, the section properties for this panel were computed by utilizing the transformed area method. Thus, the following section properties were used.

For the positive moment region:

moment of inertia = 18.860 in.^4/ft,

section modulus for the top fiber = 28.490 in.^3/ft,

section modulus for the bottom fiber = 5.255 in.^3/ft.

For the negative moment region:

moment of inertia = 8.730 in.^4/ft,

section modulus for the top fiber = 3.055 in.^3/ft,

section modulus for the bottom fiber = 6.261 in.^3/ft.

Utilizing these section properties the resulting stresses are summarized as follows.

For the positive moment region:

maximum moment = 38.455 in.-k/ft

1.4 ksi compression in the top fiber,

7.5 ksi tension in the bottom fiber.

For the negative moment region:

maximum moment = 39.423 in.-k/ft

12.9 ksi tension in the top fiber,

6.3 ksi compression in the bottom fiber.

D-5.2 Isotropic Model With Varying Plate Thickness

The second model utilized varying plate thicknesses such as 5-7/8 inch in the positive and 3.40 inch in the negative moment regions. The ratio of these two

thicknesses is equal to the ratio of the tensile section moduli of the two moment regions determined to account for the fact that under the initially applied loads the concrete overfill in the negative bending moment region had cracked. The negative bending moment region was assumed to extend from the center support line to parallel lines on either side at a distance derived from the inflection points of a continuous beam over two spans.

Using these thicknesses the computed bending moments and stresses were as follows.

For the positive bending moment region:

maximum bending moment = 85.530 in.-k/ft,

3.0 ksi compression in the top fiber,

16.3 ksi tension in the bottom fiber.

For the negative bending moment region:

maximum bending moment = 22.950 in.-k/ft

7.5 ksi tension in the top fiber,

3.7 ksi compression in the bottom fiber.

The stresses at the top and bottom of the slab were also plotted in form of stress contour plots shown in Figure D-2 and D-3. The stress magnitudes shown in the plots are irrelevant because the finite element calculates them on the basis of the overall slab thicknesses that were input for each element. However, the plots due give an indication where high stresses occur. As expected, the highest stressed regions are found below the wheel load in the west span and at the interior support, both straddling the longitudinal centerline.

D-5.3 Orthotropic Model

The third model utilized plate elements with different section properties in each of the major in-slab-plane directions (X and Y), and different properties in the positive and negative bending moment regions. The plate coefficients utilized in this model were plate stiffness coefficients tested and derived for Panel 3 of the Phase I tests conducted for this project. Panel 3 of the work conducted under Phase I of this project

had a 4-1/4-inch-deep main bar spacing of 6 inch on center, while the main bar spacing of fatigue Test #3 described in this report had a main bar spacing of 8 inch. Despite this difference, the chosen plate stiffness values D_x, D_y, and D_{xy}, and the resulting coefficients C_{xx}, C_{yy}, C_{xy}, and G utilized were the most realistic values that could be chosen for the subsequent calculations. The coefficients determined for the deck are as follows.

For the positive bending moment region:

C_{xx} = 3,195 ksi; C_{yy} = 1,538 ksi; C_{xy} = 0 ksi; G = 710 ksi.

For the negative bending moment region:

C_{xx} = 4,767 ksi; C_{yy} = 2,501 ksi; C_{xy} = 0 ksi; G = 1,875 ksi.

The above coefficients were computed by using the D-parameters resulting from the static tests, and from equation C = D*(12/t^3). The thicknesses, t, used to determine the C values were 5.875 and 4.25 inch for the positive and negative bending moment regions, respectively. These coefficients were utilized to compute the moments in the moments and stresses in the positive and negative bending moment regions.

Since the static tests of Panel #3 during Phase I did not determine the section properties, the properties resulting from the transformed area method were utilized to compute the stresses as follows.

For the positive bending moment region:

maximum bending moment = 75.506 in.-k/ft,

3.7 ksi compression in the top fiber,

14.4 ksi tension in the bottom fiber.

For the negative bending moment region:

maximum bending moment = 33.020 in.-k/ft

10.8 ksi tension in the top fiber,

5.3 ksi compression in the bottom fiber.

D-5.4 Comparison Of FEA Results With Calibration Measurements

For ease of comparison, the stresses resulting from the FEA analyses described under Section D-5.1 through D-5.3, and the stress results based on strain measurements

taken during the initial static calibration, are summarized in Table D-1. As seen from the table, the correlation between stresses derived from the FEA analysis and from the strains measured before the fatigue test was started, is provided by analysis/test ratios (stress or correlation ratios). For the first finite element model, which used isotropic plate elements with constant thickness as described in Section D-5.1, the correlation ratios are 2.74 for the negative moment region at the top steel fiber of the steel grid, and 0.16 for the positive moment region at the top steel fiber.

The other two models used, and described in Sections D-5.2 and D-5.3, correlate slightly more favorably. The isotropic model with varying plate thickness and correlation ratios ranging from 0.34 through 1.59 provided the best results, while the orthotropic model with ratios ranging from 0.42 through 2.30 was almost as bad as the model with constant plate thickness. Also, as seen from the result shown in Table D-1, the greatest discrepancies for all models utilized are occurring in the top steel fibers, both in the negative as well as in the positive bending moment regions.

D-6 MODIFIED STRESS CALCULATIONS UTILIZING TEST RESULTS

From the results of the above finite element models it is evident that the calculated bending moments are a function of the plate thickness, moments of inertia, and the plate coefficients, and that the stresses are a function of the section modulus of the slab product investigated. To show the sensitivity of the stress results as a function of the section moduli, the neutral axis location for the fatigue Test #3 was determined, using the compression and tension stresses that resulted from the static test calibration.

Since the model with varying plate thickness showed the best correlation with the results based on the test, the bending moments derived for this model were used. Utilizing the test information, the neutral axis location for the Test #3 slab was determined to be located at 2.427 inch and 1.5 inch from the bottom of the test slab for the positive and negative bending moment regions, respectively. For comparative purposes, it should be noted that the neutral axes based on the AASHTO transformed

area method were 3.588 and 1.394 inch from the bottom of the test panel for positive and negative bending, respectively. With this information, the section moduli of the Test #3 deck were computed, using the neutral axes locations derived above. These section moduli were used to determine the stresses. The results were as follows.

For the positive bending moment region:

maximum bending moment = 85.530 in.-k/ft,

8.3 ksi compression in the top fiber,

11.0 ksi tension in the bottom fiber.

For the negative bending moment region:

maximum bending moment = 22.950 in.-k/ft

7.2 ksi tension in the top fiber,

3.9 ksi compression in the bottom fiber.

For ease of comparison, the results are also shown in Table D-2, and are briefly discussed below.

The first line in Table D-2 again shows the stresses at the most important locations in the slab, as derived from the initial calibration procedure of Test #3 (Run 4) and as discussed in Section D-4. The second line of the table repeats the results derived under Section D-5.2 for the model that used different properties for the positive and negative bending moment regions, including the stress ratios derived under Section D-5.4. The section moduli computed for this case were based on the AASHTO transformed area method. The third line in Table D-2 shows the stress results and comparative stress ratios based on the section moduli derived from the AASHTO transformed area method and the neutral axis derived from the test data.

As seen from a comparison between the second and third lines in Table D-2, the range of stress or correlation ratios shown in the second line (0.34 through 1.59) showed significant improvements in the third line (0.93 through 1.53). The major improvements took place in the positive bending moment region, both at the top and at the bottom steel fibers.

D-7 DISCUSSION

Actually, any attempt to model the concrete-filled steel grid as a single material in calculating stress from moment is doomed to failure. In addition to debonding, which allows the concrete and the steel to act independently to some extent, there appear to be significant membrane stresses generated under the concentrated load. This would not normally be of any consequence in small deflection plate theory. These membrane stresses were not apparent in the line-loaded tests conducted in Phase II of this project because this type of loading forced almost every element along any line parallel to the line load or the supports to behave essentially the same way.

In recent work to be reported elsewhere, C. P. Mangelsdorf found out that the integral of the stresses in both the concrete and the steel directly under the concentrated load not only resulted in a bending moment per unit of width less than calculated from plate analysis but also resulted in an unbalanced membrane force in compression. The strain measurements taken away from the load toward one of the free sides lead to a resultant unbalanced membrane force in tension.

It may be construed that the unbalanced tension and compression membrane forces act in concert with each other and provide the necessary equilibrium required across the entire width of the deck. Therefore, precise stress calculations can be expected to be extremely tedious or almost impossible. This should provide and excellent motivation for the development of a more convenient and more accurate approximation method.

D-8 CONCLUSIONS

Based on the above analyses and comparisons, it is perceived that even better correlations could be achieved by iterative computer runs with re-assigned positive or negative bending moment properties on an element-by element bases. This means that the second computer run would utilize the results of the first computer run, i.e. checking each element if it is exposed to positive or negative bending moments, and changing some of the element properties as necessary.

Utilizing this approach, the closest correlation is expected to be achieved with the orthotropic model. However, such attempts are beyond the scope of this study, and do not represent what actually happens in the field where moving wheel loads change the load and stress pattern within a deck with each passage of a truck and the corrosive process provides a mechanism for rebonding as a function of time. Therefore, it is concluded that stresses derived from a finite element analysis of concrete-filled steel-grid decks are not directly obtainable unless refinements of the section properties based on tests are possible.

The results also show the need for establishing a simplified method which would result in more representative moments of inertia and section moduli, which would allow a more accurate stress determination for concrete-filled steel-grid products. Furthermore, such stresses could then be used for a more accurate prediction of the fatigue life of concrete-filled steel-grid products.

Table D-1 - Comparison Of Measured Stresses For Test #3 And Three Different Finite Element Models

	Stresses, ksi				Stress Ratios*			
	+ Moment		- Moment		+ Moment		- Moment	
Source	Top	Bottom	Top	Bottom	Top	Bottom	Top	Bottom
Test	-8.8	11.8	4.7	-2.6	-	-	-	-
D-5.1	-1.4	7.5	12.9	-6.3	0.16	0.64	2.74	2.42
D-5.2	-3.0	16.3	7.5	-3.7	0.34	1.38	1.59	1.42
D-5.3	-3.7	14.4	10.8	-5.3	0.42	1.22	2.30	2.04

*Stresses from indicated report source divided by test values.

Table D-2 - Comparison Of Measured Stresses For Test #3 With Finite Element Model And Modified Stresses

	Stresses, ksi				Stress Ratios*			
	+ Moment		- Moment		+ Moment		- Moment	
Source	Top	Bottom	Top	Bottom	Top	Bottom	Top	Bottom
Test	-8.8	11.8	4.7	-2.6	-	-	-	-
D-5.2	-3.0	16.3	7.5	-3.7	0.34	1.38	1.59	1.42
D-6	-8.3	11.0	7.2	-3.9	0.94	0.93	1.53	1.50

*Stresses from indicated report source divided by test values.

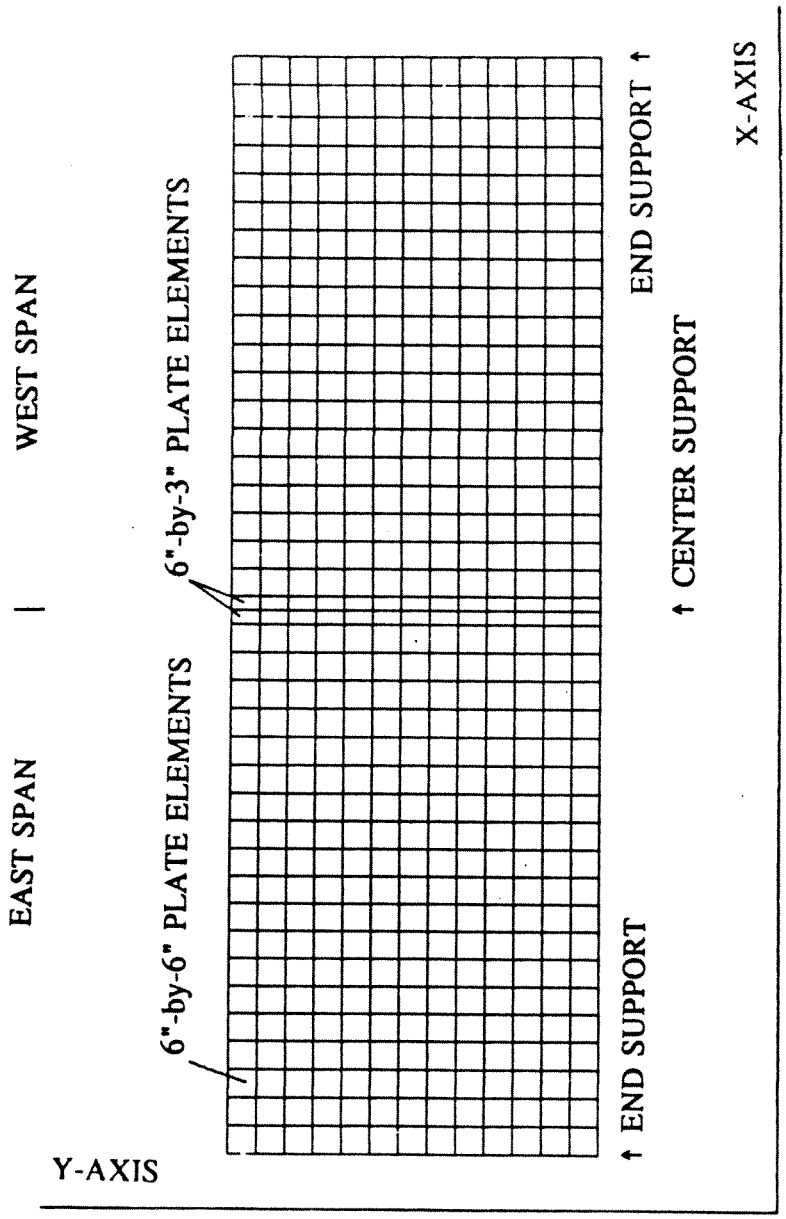

Fig. D-1 - Finite Element Layout For Test #3 Fatigue Test Deck

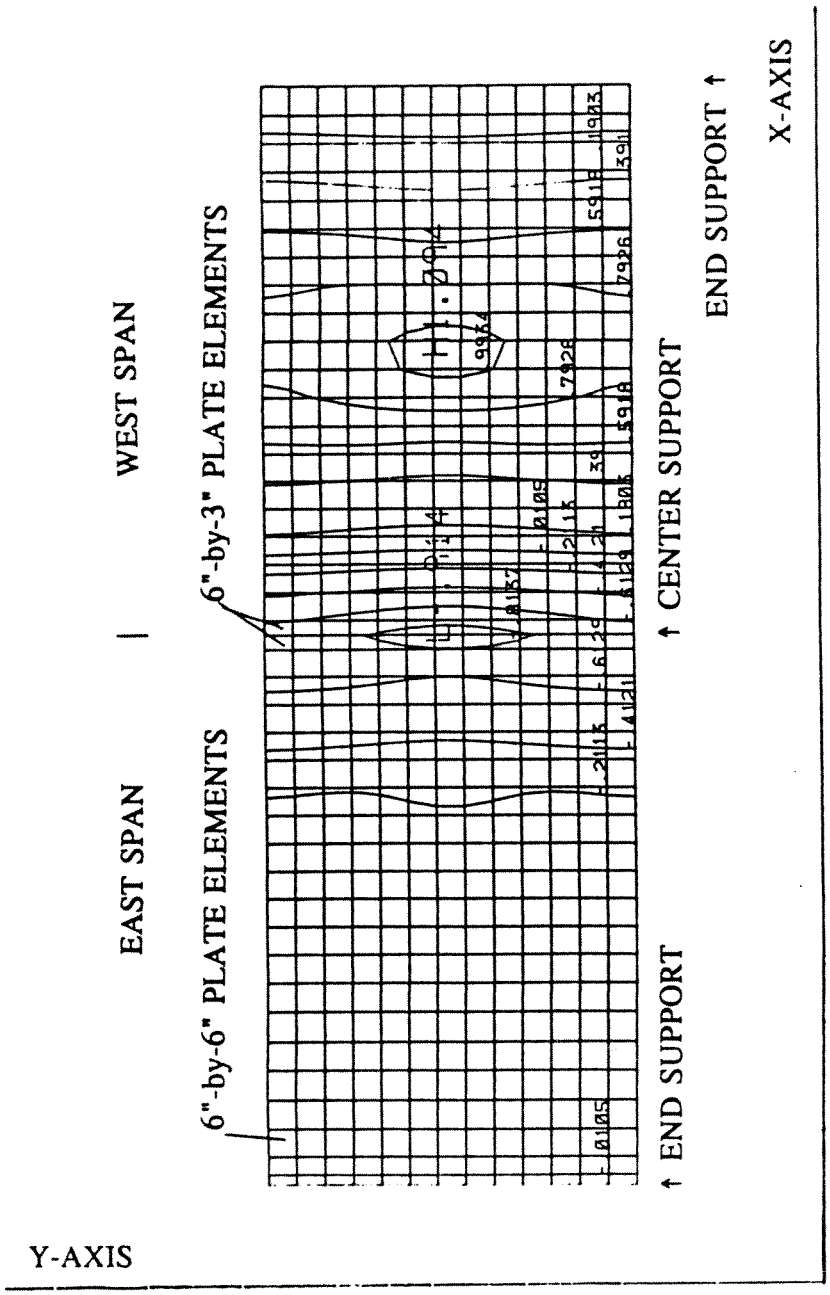

Fig. D-2 - Representative Bottom-Steel Stress Contours, Test #3 Fatigue Test Deck

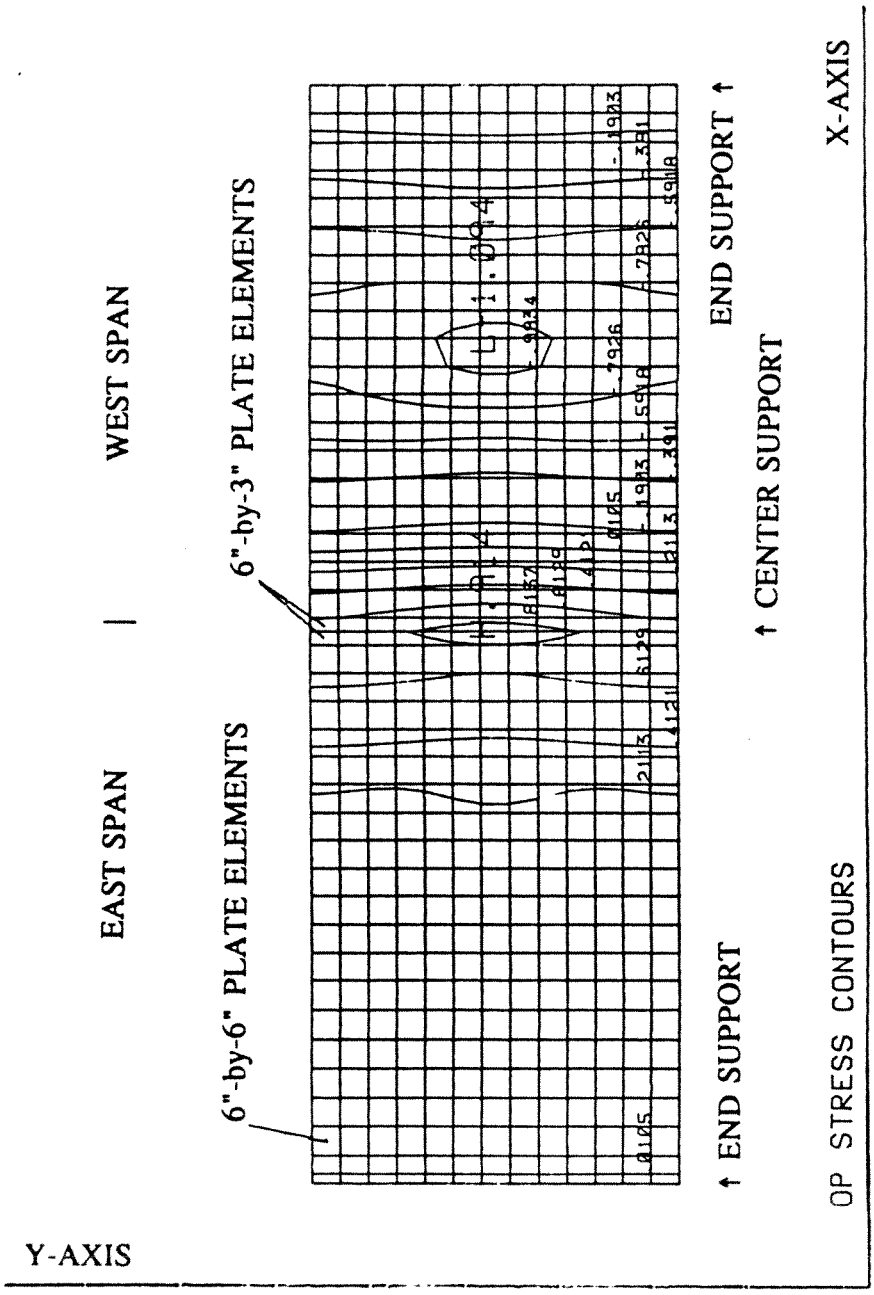

Fig. D-3 - Representative Top-Steel Stress Contours, Test #3 Fatigue Test Deck